CHIRAL DISCRIMINATION OF DICARBOXYLIC ACIDS WITH CINCHONA ALKALOIDS

by

CHRISTELE LYDIA KOMBA

Thesis submitted in fulfilment of the requirements for the degree

Master of Technology**:** Chemistry

in the Faculty of Applied Sciences at the

Cape Peninsula University of Technology

Supervisor: Prof N.B. Báthori

Cape Town
November 2017

The financial assistance of the National Research Foundation (NRF) towards this research is hereby acknowledged. Opinions expressed and conclusions arrived at, are those of the author and are not necessarily to be attributed to the NRF.

DECLARATION

I, Christele Lydia Komba, declare that the contents of this dissertation/thesis represent my own unaided work, and that the dissertation/thesis has not previously been submitted for academic examination towards any qualification. Furthermore, it represents my own opinions and not necessarily those of the Cape Peninsula University of Technology.

Signed **Date**

ABSTRACT

This thesis is aimed at the investigation of the chiral discrimination process during diastereomeric salt formation, when selected cinchona alkaloids are exposed to racemic mixtures of tartaric acid derivatives. This research is based on the use of *(+)*-cinchonine, *(-)*-cinchonidine, *(-)*-quinidine and *(+)*-quinine, which served as chiral bases, in order to resolve racemates of *O,O'*-dibenzoyl-tartaric acid (DBTA) and *O,O'*-di-p-toluoyl-tartaric acid (DTTA). Cinchona alkaloids were selected because of their abilities to form salts with the targeted acids. DBTA and DTTA are commonly used resolving agents to separate racemic bases via diastereomeric salt formation, and they are also commercially available and affordable chiral acids. Results were obtained from all combination but only the experiments with cinchonidine were included in this thesis, namely $[CIND^+][L\text{-}DBTA^-]$, $2[CIND^+][D\text{-}DBTA^{2-}]$, $[CIND^+][L\text{-}DTTA^-]$ and $2[CIND^+][D\text{-}DTTA^{2-}]\cdot 2DMSO\cdot 0.7H_2O$. Experimental analytical techniques, such as thermal analysis, powder X-ray diffraction, and single crystal X-ray diffraction were used to analyze the harvested diastereomeric salts. A correlation of molecular parameters derived from the structures and an investigation of the mechanism, which drives the resolution process were discussed.

The thesis also summarizes the findings on 8 inclusion compounds of *(–)-O,O'*-dibenzoyl-*(2R,3R)*-tartaric acid (*L*-DBTA) and *(–)-O,O'*-di-p-toluoyl-*(2R,3R)*-tartaric acid (*L*-DTTA) or their racemic mixtures, *(rac)*-DBTA and *(rac)*-DTTA, with DMSO and water: *(rac)*-DBTA·H_2O, *(rac)*-DBTA·DMSO, *L*-DBTA·H_2O, *L*-DBTA·DMSO, *(rac)*-DTTA·H_2O, *(rac)*-DTTA·DMSO, *L*-DTTA·H_2O, and *L*-DTTA·DMSO. The discussed inclusion compounds were obtained serendipitously, as a product of the pre-screening of suitable solvents to dissolve both the acids and the cinchona alkaloids during the discrimination experiments. Only few crystal structures of solvates of these two tartaric acid derivatives are known up to now, and fewer of these structures do exist when both the racemic and the enantiopure acid encapsulates the same solvent. The synthesis and structural analysis of these inclusion compounds contribute to the pool of available crystal structures when comparing chiral vs. achiral crystal forms of the same compounds.

ACKNOWLEDGEMENTS

I wish to thank:

- My family, friends and colleagues for their support and encouragement
- My supervisor, Prof N.B. Báthori for her help, advice and support
- The Staff of the Department of Chemistry, Cape Peninsula University Of Technology
- Professor Leonard Barbour, University of Stellenbosch,
- University of Cape Town- Centre for Supramolecular Chemistry Research
- Kelly Shunje for her assistance in the laboratory

The financial assistance of the National Research Foundation towards this research is acknowledged. Opinions expressed in this thesis and the conclusions arrived at, are those of the author, and are not necessarily to be attributed to the National Research Foundation.

DEDICATION

I dedicate this thesis to my family.

TABLE OF CONTENTS

CHAPTER 1: Introduction

CHAPTER 2: Experimental details and materials

CHAPTER 3: Tartaric acid derivatives

CHAPTER 4: Chiral discrimination experiments

CHAPTER 5: Summary and conclusion

LIST OF FIGURES

LIST OF TABLES

List of APPENDICES

GLOSSARY

Term/ Acronyms/ Abbreviations	Definition/Explanation
CSD	Cambridge Structural Database
TGA	Thermogravimetric analysis
DSC	Differential Scanning Calorimetry
PXRD	Powder x-Ray Diffraction
a, b, c	Unit cell axes
α	Angle between b and c unit cell axes
β	Angle between a and c unit cell axes
γ	Angle between a and b unit cell axes
V	Unit cell volume
Z	Number of formula units per cell
ρ	Density
ASU	Asymmetric unit
CINC	Cinchonine
CIND	Cinchonidine
QUIN	Quinine
QUID	Quinidine
DBTA	O,O'-dibenzoyl-tartaric acid
DTTA	O,O'-di-p-toluoyl-tartaric acid
DMSO	Dimethyl sulfoxide

Atom Colours

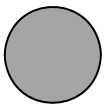

Carbon

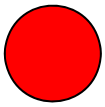

Oxygen

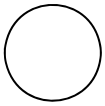

Hydrogen

Nitrogen

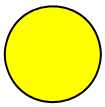

Sulfur

1 Introduction

1.1 Chirality

Isomers are defined as compounds that have the same molecular formula but different molecular structure, and their classification or hierarchy is shown on Figure 1.1. One of the most exciting groups of isomers are the one with stereogenic center. Generally, a stereogenic center (stereo center, chiral center, or asymmetric center) is formed when four different substituents are attached to an sp^3 hybridized atom, which is most often a carbon. (Figure 1.2) If a compound has one stereogenic center, it will take up two different spatial arrangements of the substituents. These two stereogenic isomers are non-superimposable mirror images of each other and are called enantiomers. The compounds presenting this property, i.e. have at least one stereo center and does not have a plane of symmetry, are described as being *chiral*. The property is named chirality; sometimes called enantiomerism, dissymmetry or stereoisomerism. The presence of an asymmetric centre or chiral centre is the most common cause of chirality in molecules. Asymmetric centres are not limited to carbon atoms only; nitrogen and phosphorus can also be asymmetric centres, as long as they have four different groups attached to them.[1]

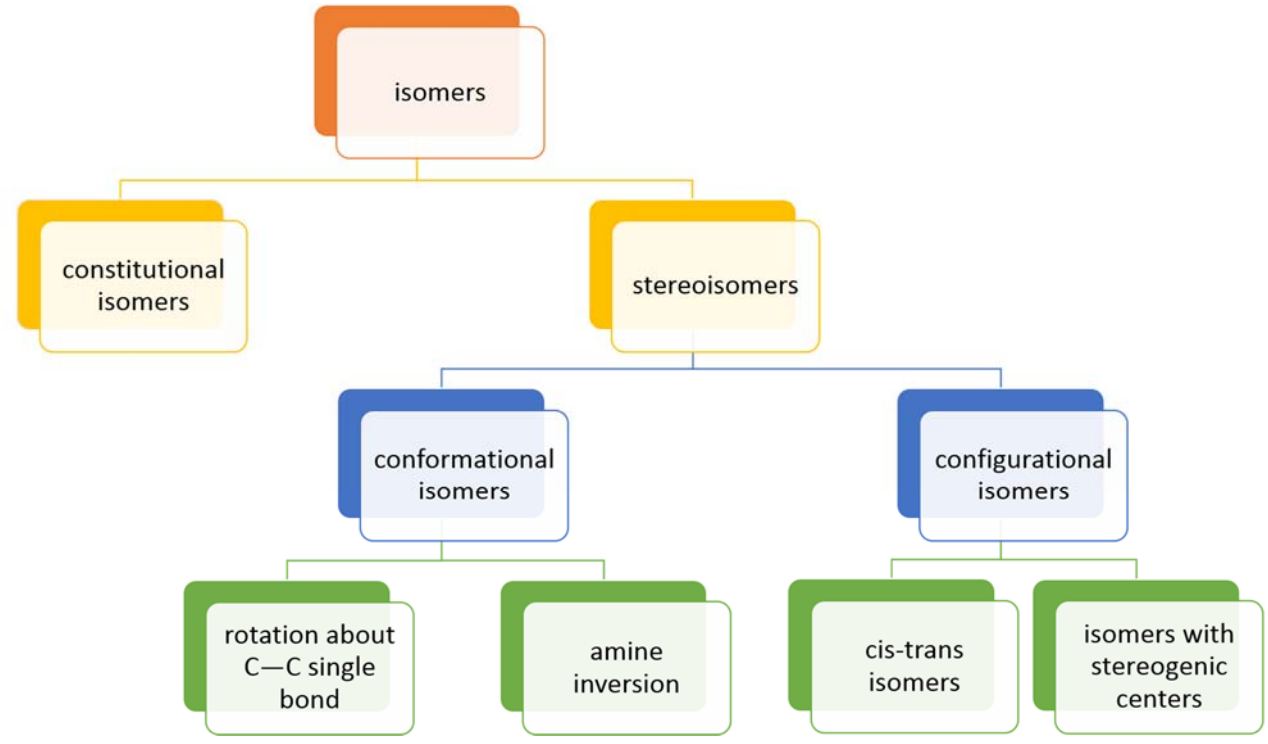

Figure 1.1 Classification of isomers

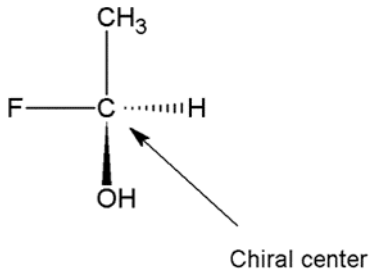

Figure 1.2 Representation of a chiral or stereogenic / stereo center

The terms *chiral* and *chirality* are derived from the Greek word *cheir* for a hand, which is indeed one of the most familiar chiral objects.[2] The French physicist, Jean Baptiste Biot for the first time reported the phenomenon of 'chirality' in a molecule in 1815.[3] Chirality may be applied to molecules, conformations, as well as macroscopic objects, such as crystals.[4] In 1848, Louis Pasteur proved the concept of molecular chirality by the manual separation of the crystals of left-handed and right-handed tartaric acid salts. Chirality can be interpreted as a quality of an individual molecule, or also as a special case of symmetry. On a molecular level, chirality serves as an intrinsic property of the building blocks of life.[5] Several new terms related to chirality, like homochiral or heterochiral, have been introduced.[6]

Chirality plays an important role in the pharmaceutical industry as well as in other chemical industries. Chiral molecules are constituents of a large proportion of therapeutic agents. In pharmaceutical industries about 56 % of the drugs currenly in use are chiral products and 88% of the last ones are marketed as racemic formulations, consisting of an equimolar mixture of two enantiomers.[7]

The phenomena of optical activity played significant role in the development of organic stereochemistry.[8] Chirality and optical activity are historically closely related, however, chemists are prone to use the definitions 'optically active' and 'chiral' mutually. Optical activity is the property of chiral molecules, especially the capacity to rotate the plane of polarized light.[7]

The world market for optically pure products has experienced a marked increase in the last decade which has accelerated the development of novel methods for asymmetric synthetis and chiral separation. Enantiomeric molecular recognition is an essential aspect of supramolecular chemistry. The phenomenon is not only of theoretical interest [9], but is significant in various aspects of biology.

1.2 Enantiomers

Enantiomers are one of the subset of stereoisomers and are most commonly formed when a carbon atom bonds four differents substituents.[3] Enantiomers exist in pairs and represent an important and common case of stereoisomerism, when the two molecules are non-superimposable mirror images of each other. (Figure 1.3) Enantiomer pairs possess identical physical properties, such as boiling points, melting points, or solubilities in a given solvent, but their biological activities and effects can be markedly different. The other difference is upon reflection in a plane polarized light, where they show same magnitude with different signs.[10] The expression 'optical active' substance signifies a pure enantiomer or a mixture containing an excess of one of the two. The composition of a mixture of two enantiomers may be characterised by its optical purity, which may yield the ratio of the two pure enantiomers. The optical purity is generally equal to the enantiomeric purity, which reflects the real composition. A pure enantiomer is often called optically pure.[11]

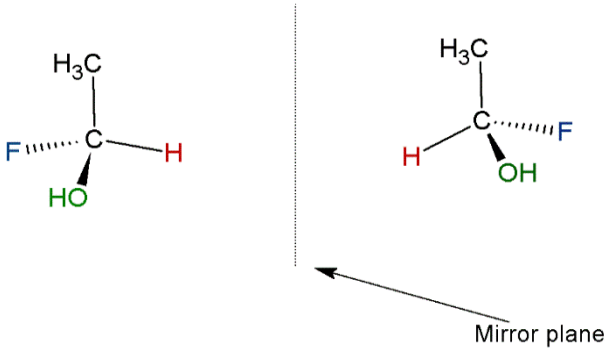

Figure 1.3 A pair of enantiomers

An enantiomer may also be named by the direction in which it rotates the plane of the plane polarized light. If it rotates the light clockwise that enantiomer is labelled *(+)* and thus his mirror-image is labelled *(-)*. The *(+)* and *(-)* isomers have been termed *d* and *l* respectively for *dextrorotary* and *levorotary*.

Despite the fact that they have the same chemical structure, most enantiomers of racemic drugs exhibit signifiant differences in biological activites such as pharmacology, toxicology and pharmacokinetics.[2] Normally in pharmaceutical drugs only one enantiomer gives the desirable response for the appropriate

physiological effect, whereas the other one is passive in that specific function or it might show different significance in its effect on the body which shows side effects.[12]

More recently the isolation and the purification of single enantiomer product has become an important component of manufacturing pharmaceuticals and fine chemicals.[13] The enantiomeric purity of a compound is a key aspect in the analytical, food, pesticide and particularly in the pharmaceutical industries.[14] Chiral discrimination between enantiomers is one of the most predominants fields in analytical chemistry.[15] Conversion of a racemate with a chiral resolving agent and separation of the mixure of diastereomers formed is known as the classical method of resolution.[16] The preparation of enantiopure compounds is one of the most important aims both for industrial practice and research.[17]

1.3 Diastereoisomers

Most chiral organic compounds have more than one chiral centres.[24] Diastereoisomers are configurational isomers that are not enantiomers. Also diastereomers may be defined as any molecules that has two or more chiral centers, chiral axes, or a combination thereof. A diastereoisomer which possesses two chiral carbon, may have a maximum of four stereoisomers. The physical and chemical properties of diastereomers may be different and therefore, their chemical characterization is simple, unlike enantiomers, and their biological activities can often vary.[18] The basic reason for this difference is that enantiomers are 'isometric'; that is for each distance between two given atoms (whether bonded or not) in one isomer there is corresponding identical distance in the other. There is not such 'isometry' in diastereoisomers or in constitutional isomers.[24] The here discussed difference between diastereomers is the basis for derivatization of enantiomers to form diastereoisomeric adducts with selected chiral compounds in chiral separations. The newly formed disatereomeric adducts or salts exibit significant dissimilarity in their physical properties that allow their separation via crystallization.[19]

1.4 Racemate

An equimolar mixture (50/50) of the two enantiomers *(+)* and *(-)*, (*d*- and *l*-) and (*R* and *S*) of a chiral compound is called a racemic mixture or racemic modification. Great interest was presented to understand the chiral discrimination mechanism and hence to develop a rapid and rational way to screen optimal resolving agents for a given target racemate.[20] Racemates, which we generally designate

by the symbol *(±)* are said to be optically inactive by external compensation.[8] This means that be observed inactivity derives from equal propensities to rotate the plane polarized light to the right and to the left direction, arising from the equal amount of each enantiomer in the mixture. When a racemate is dissolved in a non-chiral solvent, then the optical rotation (α) of the solution is 0°. Therefore, the plane polarized light shows no deviation in its rotation. At this stage this chiral mixture can be referred as optically inactive.[21]

A crystalline racemate could be of three different types. The first group is the conglomerate, which is formed as a result of spontaneous resolution of enantiomers into separate crystals, i.e. each and every crystals contains only one of the enantiomers (homochiral) in their structure, the two enantiomers crystallise separately. In the second group, and probably the most common type, the two enantiomers are present in equal quantities within the unit cell of the crystal lattice. The resultant homogenous solid phase corresponds to a true crystalline addition compound called a racemic crystal. The third possibility corresponds to the formation of a solid solution between the two enantiomers. Solid solution is a mixture of two solids that coexist as a single solid phase or crystalline entity. The mixing is usually accomplished by combining the two solids, when they have been melted into liquids at high temperatures, and then cooling them to form the new solid.[8] The obtained crystalline material does contain non-stoichiometric amount of the two enantiomers. The main disadvantage of the formation of solid solutions is that only maximum 50 % of the desired isomer is obtained, and not all the compounds are crystallizable.

1.5 Methods of separations

Even though enantiomers possess the same chemical structure, they often differ considerably in pharmacological activity and pharmacokinetic profile.[2] Therefore the isolation and the purification of the biologically favoured enantiomer from a racemic modification is a crucial element of manufacturing pharmaceuticals or fine chemicals.[22,23] Thus chiral discrimination of enantiomers is one of the critical fields of analytical chemistry and the preparation of enantiopure compounds is one of the most important aims both from the point of applied or basic research.[24'25] The most well studied method of the conversion of a racemate with a chiral resolving agent and separation of the mixure of diastereomers formed is known as the classical method of resolution.[26]

The separation of the two enantiomers that constitue a racemate is called resolution or optical resolution (chiral resolution). Recently it involves crystallization, resolution using resolving agent, chiral chromatographic separations and kinetic resolution. Analytical techniques which have been employed

for enantioseparation involve, diastereomeric crystallization, chromatography techniques, affinity electrokitenic chromatography. When the separation is not complete, an unequal mixture of the two enantiomers is obtained which is often called a partially resolved racemate[8].

The two main approches to attaining chiral compounds are the resolution and the asymmetric synthesis techniques. The resolution of racemic mixtures involves separation methods such as chromatography, polymer-supported liquid menbrane and preferential or diastereomeric crystallization. The existing commercial projects have revealed that sometimes it is more economic to produce single enantiomeric drugs with chromatographic methods, rather than use traditional technologies, such as crystallization or asymmetric synthetis. Besides asymmetric synthetis, crystallization has also been used widely from bench to manufacturing scale for the separation of enantiomers. The principal method for the separation of enantiomers is crystallization.

Resolution of racemic modifications of organic molecules has a considerable importance in the pharmaceutical industry, hence these compounds represents close to ca. 30 % of all drug sales worldwide.[27] Manufacturing racemates is usually more economical than the synthesis of pure enantiomers[28], however occasionally their separation cannot be efficiently performed with high yield and optical purity and the undesired enantiomer utilized or recycled in some manner.[29]

1.5.1 Asymmetric synthesis

Asymmetric synthetis is a reaction or reaction sequence in which one configuration of one or more new stereogenic elements is selectively formed. Generally this technique refers to the production of a chiral product by using many conversion steps starting from an achiral raw material.[30] In an asymmetric synthesis technique, an achiral molecule is enantioselectively converted into a chiral molecule or a chiral molecule can be diastereoselectively converted into a new chiral molecule that contains at least one more chirality element. During an asymmetric synthetic process, the mixture of a substrate and a reagent forms a diastereomeric transition state.

Throughout the reaction, asymmetry will be induced only at the sites of substrate where a chiral element is present. This can be achieved by using many controlled methods which employ (a)substrate, (b) auxilliary, (c) reagent and (d) catalyst.[31]

1.5.2 Enantioselective membrane separations

The method is highly promising but encounters practical problems such as trial and error based chiral selectors for liquid membranes, as well as poor enantioselectivity.[32] Membranes like dense polymers or liquid membranes provide a selective barrier and allow only one of the enantiomers through them. In the case of liquid menbranes a chiral selector, which is non–mixable in the solvent, is used. As a result of the high potential for chiral separation and low operational costs, considerable effort is spent in the membrane based separation process.[33]

1.5.3 Capillary electrophoresis

Capillary electrophoresis (CE) is a recently developed dominant analytical method with a broad range of applications. CE is a process that separates compounds that differ in charge to hydrodynamic size ratio. The procedure is effective for the analysis of polar compounds. The technique is especially suitable for chiral separations. Chiral CE separation is accomplished by adding a chiral selector to the so called background electrolyte. The enantiomers then form fast, reversible equilibria with the selector. More recently the chiral separation of malic acid was accomplished via direct chiral resolution by ligand exchange electrophoresis using Cu(II)-L-tartaric acid as a chiral selector. [34]

1.6 Crystallization techniques

Crystallization must certainly be classified as the earliest process in chemical processing. Besides the fact that crystallization is one of the best and most economical technique for the production of pure solids from impure solutions, it also has the convenience of giving an end product that possesses desirable and well characterised properties.[2] Most chiral compounds can be obtained during crystallization of the desired enantiomer from the racemic mixture. Enantioselective crystallization happens following the seeding of a supersaturated solution of the racemic mixture with a crystal of the desired enantiomer (induced crystallization). Occasionally, enantioselective nucleation and crystal growth can occur without seeding under the proper conditions.[27]

There are two major categories in which enantioseparation via crystallization can be classified: (i) the use of a foreign chiral element to form diastereomers followed by fractional crystallization or the formation of a diastereoselective host-guest inclusion complex[35], (ii) as well as direct crystallization of one enatiomer from a racemic mixture, which includes the most common ‘preferential crystallization’ of pure enantiomers from conglomerate mixtures.[36] In a systematic study, a chiral discrimination

through crystallization has been performed by employing a chiral host, H1:(R,R)-(-)-trans-2,3-bis(hydroxydiphenylmethyl)-1,4-dioxaspiro(4.5)decane, which enclathrated (R)- and (S)-2-butylamine in different proportions. The enantiomeric selectivity of this host for 2-butylamine was measured and the correlation between selectivity, the torsional flexibility of the phenyl moieties of the host, and the concomitant remaining volume that accommodates the guest were found.[37] The mechanism of enantiomeric resolution of 2-butylamine was proved by the way repeated experiments with a structurally related chiral host.

The majority of pharmaceutical manufacturing processes involves a crystallisation process to attain high purity and to make the desired final solid form. The operating condition of crystallization regulates the physical properties of the products; these include the crystal purity, size and shape distribution. Concerning polymorphic or stereomeric pharmaceuticals, the crystallisation technique also directly influences the polymorph produced and the extent of the chiral separation. Improved control of crystallization provides possibilities to reach better crystalline product quality, brief process time, and the reduction or withdrawal of compromised batches.[10]

1.6.1 Racemic crystallization

Enantiomers have identical physiochemical properties except for the sign of optical rotation of plane polarized light, so they cannot be separated directly. Under certain specific conditions enantiomers from a racemic mixture are known to crystallize separately hence caused resolution of the racemic mixture.[10] Most of the time, the separation happens after the preceding conversion of enantiomers into diastereomers. When a chemical reaction is carried out in an achiral environment, it produces a racemate, a mixture consisting of equal amounts of the two enantiomers. However, the separation of an enantiomeric mixture is essential to obtain optically pure species.[38] The method of resolution of racemates can also be applied to non-equimolar mixtures of enantiomers that are normally attained by assymmetric synthesis, since asymmetric synthesis may never possesses a stereoselectivity of 100%. Optical resolution of racemates is one method to acquire pure isomers. Of the various techniques, more chiral compounds are being resolved today using chromatography methods than crystallization.[12] Many factors have an impact on interactions of stereoisomeric molecules in some environment. Theses factors can affect the chromatographic separation of stereoisomers and must be carefully evaluated before developing a separating technique.[12]

1.6.2 Diastereomeric crystallization

Diastereomeric crystallization is a predominant technique used in the resolution of chiral bases and acids. This method of crystallization is based on the formation of diasteremeric salts of the interest of enantiomers, which can be separated easily because of their different physicochemical properties. Even though its image as a 'low-tech' method, diastereomeric crystallisation is universally used today in the separation of racemic mixures, despite the fact that the theoretical yield is only 50%.[38] Research has suggested an approach to choose resolving agents by using the thermal analysis of the diastereomeric salts.[39] It was concluded that when the pair of diastereomeric salts present great dissimilarity in their melting points and heat of fusion, the applied resolving agent would be an ideal separating agent for the formation of the diastereomers with the targeted enantiomers.[18]

1.6.3 Direct crystallization

A substitute to diastereomeric salt formation is direct crystallization of the desired enantiomer, usually iniatiated by seeding with a pure enantiomer.[38] The method is said to be attractive because auxiliaries and reagents other than a solvent are not required. The technique is determined by the occurrence of some substances as crystalline conglomerates. In spite the fact that in a bulk a conglomerate is optically neutral, there are equal amounts of the opposite enantiomers and a given single crystal yields either a (+) or (-) solution when dissolved in an achiral solvent. Conglomerate formation is a prerequisite for resolution by direct crystallization.[40]

1.6.4 Preferential crystallization

Preferential crystallization is a resolution method in which no resolving agent is used. The compound to be resolved must be a conglomerate, which means it crystallises as enantiomeric crystals.[41] Resolution by preferential crystallization was used in the manufacture of chloramphenicol[42], L-Dopa,[43] and (-)-menthol.[44]

Resolution of conglomerates by preferential crystallization or resolution by enzymes has also been applied to large-scale separation of some racemates.[26]

1.7 Kinetic resolution

Kinetic resolution is a substrate selective process in which components of a racemic mixture react at non-identical rates with the resolving agent. This can be an enzyme or microorganism or a simple chiral compound. Pasteur resolved ammonium tartrate by fermentation with Penicillium glaucum mould[45]. Resolutions based on kinetic effects in chemical reactions can be one of several major types, but are typically divided between enzyme and inorganic catalyzed systems. In general, a material capable of enantiomeric differentatiation is used to catalyse a chemical transformation of the two enantiomers at substantially differents rates.

Typically, either enantiomer can be resolved by the suitable selection of the enantiomerically differentiating material. While powerful, beneficial and capable of producing very big enantiomeric excess in some situations, applications are limited due to lenghtly development times, and availability of enantiomerically differentiating materials. Often a high enantiomeric excess in kinetic resolution was found for the enzymatic process when compared to the normal chemical stoichiometric or catalytic processes.[46] This area of research is promising by revealing the potential of chemical catalysts or enzymes in separating the racemates.[47] A good case is the resolution of a 1,4-benzoxazine derivative by reaction with 0.5 eq of (S)-naproxenyl chloride.[48]

1.8 The chiral pool synthesis

Chiral pool synthesis is a method in synthetic organic chemistry to synthesize optically pure product, starting from naturally available starting materials, refered as chiral pool, such as sugars, amino acids. The technique is highly suitable for the synthesis of exclusively one enantiomer of the product, provides the desired product bears a great resemblance to the economic enantiopure natural products that is available. For example, the use of alanine as chiral pool for the synthesis of benzodiazepine derivatives is a well known example. [49]

1.9 Resolution by chromatography

Enantioselective chromatography developed from modest beginnings to a universal technique, especially after the advent of HPLC, and more recently capillary electrophoresis. The most versatile technique to perfom enantioseparation is chromatography.[50] Chiral chromatographic separations

always depend on the difference in the distribution ability of different enantiomers between a stationary phase (chromatographic column) and a mobile phase (either single solvent or mixture of solvent-eluent). In chiral column chromatography the stationary phase is chirally modified with a single enantiomer, rather than being achiral, as in case of general column chromatography. When a racemic analyte passed through the column, both enantiomers differ in affinity to the chiral stationary phase, and therefore they exit the column at different times, causing the separation of the racemate. In order for the separation to be performed, the stationary phases are arranged in columns which are operated mostly in a batch mode. Actually, more refined operation modes replace this typical technology. It has been proven in the last years that the simulated moving bed process is capable of separating in a stable way very different racemic mixtures providing enantiomers of very high purity.[51]

1.10 Resolution of racemates via diastereomeric salt formation

The resolution using salt formation is known as the classical method of resolution. The technique via diastereomeric salt formation has been the most commonly used.[52] The process is known to be based on the interaction of a racemic product with a resolving agent (optically active material) to give two diastereomeric derivatives, which are usually salts. The first separation by diastereomeric salt formation was achieved by Pasteur, when he achieved the separation of (R,R)-tartaric acid from the racemate via the formation of its salt with (R,R)-quinotoxine.[28] Diastereomeric crystallization is used so widely that it provides a measure for judging alternative process[35] and it is a classical technique used in the separation of racemic modification of carboxylic acids and amines.[53] The compounds (salts) formed are diastereomers with different physicochemical properties and can be resolved using different methods, like chromatography; but undoubtedly the most efficient technique of separating such diastereomers is crystallization. Many significant pharmaceuticals are resolved using diastereomeric crystallization.[3] Cephalexin, cefaclor, ampicillin, and amoxicillin are antibiotic products, which are rated on the basis of total sales in the top 10 products sold in single-isomer form.[24]

Diastereomeric crystallization procedure depends on the difference in solubility of the two diastereomeric salts used, so that the least soluble precipitates and is readily separated from the mother liquor.[39] A typical resolution via diastereomeric salt formation was presented when (-)-Cinchonidine was used as a basic resolving agent in the resolution of racemic citronellic acid. The precipitation of the least soluble salt resulted the cinchonidinium-(S)-citronellate monohydrate.[54] Interestingly, when (+)-cinchonine and (–)-cinchonidine have been employed to resolve racemic malic acid, the resulting salts contain the *D*-malate anion in both cases. The cinchoninium and cinchonidinium

L-malates were also crystallised, and the structures of all four salts were analysed in terms of their nonbonding interactions. The final conclusion was that the *D*-malate salts are more efficiently packed in their crystal structures, thus the outcome of the crystallization can be reasoned.[55]

In most of the cases of diastereomeric salt formation, the difference between the solubility of the two diastereomeric salts is not large and the crystals harvested contain both enantiomers. This was observed when crystals of mandelic acid with the resolving agent quinine were harvested. [56] When a series of competition experiments were set, where the resolving agent, quinine was exposed to mixtures of mandelic acid, where the mole fraction of the starting mixture was varied systematically, the outcome of the crystallizations resulted in a series of crystal structures with both R and S-mandelic acids entrapped in the crystal in different ratios. It was concluded that the resolution of mandelic acid by quinine give rise to stable structures of three salt pairs in the crystallographic asymmetric unit containing (R)-, (R)- and (S)-mandelate anions, and dominate a large range of the selectivity profile. This work highlighted the complexity of selecting a suitable resolving agent for a given racemic compound.

To overcome the selection of the suitable resolving agent, the Dutch resolution[57] was developed, whereby structurally related resolving agents are used simultaneously during the resolution process. In this method synchronized addition of several resolving agent shorten the time needed for the hit and miss technique of finding a resolving agent. The Dutch Resolution Method was attempted in a selectivity of 2-butylamine with mixed diol hosts.[58] Moreover the use of various structurally related resolving agent simultaneously resulted in the precipitation of a crystalline diastereomeric salt containing more than one resolving agent in good to high enantiomeric purity and yield.[59] Resolving agent mixtures where developed, were shown to be fast and efficient in resolving a variety of salt forming racemates. The use of resolving agent has been of great impact in the separation of racemates. The perfect resolving agent is selected by depending on the separation factor in the crystallization technique. A list of typical resolving agents are listed in Table 1.1.

Table 1.1: Popular resolving agents[60].

Acids	Bases
*(+)*or*(–)*-Pyroglutamic acid	*(+)* or *(–)*-2-amino-1-butanol
*(+)*or *(–)*-Malic acid	*(+)*-Dehydrobietylamine
(+) or *(–)*-Mandelic acid	*(+)* or *(–)*-1-phenylethylamine
(+) or *(–)*-Camphoric acid	*(+)* or *(–)*-Ephedrine
(+) or *(–)*-1-camphor-10-sulphonic acid	***(–)***-Brucine
(+) or *(–)*-Methoxyphenylacetic acid	*(+)*-Cinchonine
(+) or *(–)*-Methoxy-trifluoromethylphenylactic acid	***(–)***-Cinchonidine
(+) or *(–)*-Tartaric acid	***(–)***-Quinindine
(+) or *(–)*-Dibenzoyl tartaric acid	*(+)*-Quinine

1.11 Aspect of this research

This research is based on the use of *(+)*-cinchonine, *(-)*-cinchonidine, *(-)*-quinidine, *(+)*-quinine, which served as chiral bases[61] (Table 1.2) in order to resolve racemates of O,O'-dibenzoyl-tartaric acid or DBTA, and O,O'-di-p-toluoyl-tartaric acid or DTTA. Cinchona alkaloids were selected because of their abilities to form salts with the targeted acids. In previous studies, *(+)*-quinine was exposed to optically pure (S,S)-tartaric acid and formed the salt quininium-(S,S)-tartrate hemihydrate.[62] Cinchoninium-(L)-tartrate tetrahydrate salt hydrate resulted from the separation of tartaric acid with (+)-cinchonine.[63] Cinchonidine was also used for the resolution of tartaric acid, to give cinchonidinium-(R,R)-tartrate monohydrate salt hydrate.[64]

DBTA and DTTA (Table 1.3) were chosen because of their structural similarity to tartaric acid. Experimental analytical techniques such as thermal analysis, powder X-ray diffraction, single crystal X-ray diffraction were used to analyze the harvested diastereomeric salts, and the process of molecular recognition were studied. A correlation of molecular parameters derived from the structures and an investigation of the mechanism which drives to the resolution process were discussed. Overall, in this thesis 8 crystal structures of DBTA and DTTA with water or DMSO as included solvent, and 4 salts of *(-)*-cinchonidine were analysed and discussed.

Table 1.2: Physical properties and formulas of the base compounds.

Bases	Abbreviations	Formula	Mr ($g.mol^{-1}$)	Mp (°C)
(+)-(Cinchonine)	CINC	$C_{19}H_{22}N_2O$	294.39	258-264
(-)-(Cinchonidine)	CIND	$C_{19}H_{22}N_2O$	294.39	199-202
(-)-(Quinidine)	QUID	$C_{20}H_{24}N_2O_2$	324.42	174-178
(+)-(Quinine)	QUIN	$C_{20}H_{24}N_2O_2$	324.42	173-175

Table 1.3: Physical properties and formulas of the acids compounds.

Acids	Abbreviations	Formula	Mr ($g.mol^{-1}$)	Mp (°C)
(L)-DTTA(*(-)*-Di-P-toluoyl-L-tartaric acid)	(L)-DTTA	$C_{20}H_{18}O_8$	386.35	169-171
(D)-DTTA(*(+)*-Di-P-toluoyl-D-tartaric acid)	(D)-DTTA	$C_{20}H_{18}O_8$	386.35	169-171
(L)-DBTA(*(-)*-O,O'-Dibenzoyl-L-tartaric acid)	(L)-DBTA	$C_{18}H_{14}O_8$	358.30	151-154
(D)-DBTA(*(+)*-Dibenzoyl-D-tartaric acid)	(D)-DBTA	$C_{18}H_{14}O_8$	358.30	151-154

[1] Bruice, P.K. 2007. *Organic chemistry*. 5th edition. 200-250.

[2] Prelog, V. 1976. J .*Molecular catalysis*. 1: 159-172.

[3] Loudon, G.M. 1984. *Organic chemistry*. Massachusetts: Addison-Wesley Publishing co

[4] Nguyen, L.A., He, H. & Pham-huy, C. 2006. Chiral Drugs: *An Overview International Journal of Biomedical science*, 85-100.

[5] Maier, N.M., Franco, P., & Lindner, W. 2001. Separation of enantiomers: needs, challenges, perspectives. *Journal of Chromatography A.,* 906: 3-33.

[6] (a) Mislow, K. & Bickart, P. 1976. An Epistemological Note on Chirality. *Isreal Journal of Chemistry,* 15: 1-6. (b) Mislow, K. 1996. A Commentary on the Topological Chirality and Achirality of Molecules *Croatica Chemical Acta.*, 69: 485-511.

[7] (a) Rentsch, KM. 2002. The importance of stereoselective determination of drugs in the clinical laboratory. *Journal of Biochemical and Biophysical Methods*. 54(1-3): 1-9. (b) Walther, W. & Netscher, T. 1996. Design and development of chiral reagents for the chromatographic determination of chiral alcohols. *Chirality*. 8: 397- 401. (c) Katzung, BG. 2004. *The Nature of Drug In: Basic and Clinical Pharmacology*, 9 thedition.

[8] Dhaneshwar Singh, M. & Biren Singh, Kh. 2012. On the Origin of the Optical Inactivity of meso-Tartaric Acid. *Journal of Chemical and Pharmaceutical Research*. 4(2): 1123-1129.

[9] Guijarro, A., Yus, M. 2009. The origin of chirality in the molecules of life: A revision from awareness the current theories and perspectives of this unsolved problem. *Royal Society of Chemistry*. Cambridge: UK.

[10] Eliel, E.L., Wilen, S.H & Doyle, M.P. 2001. *Basic Organic Stereochemistry*. John Wiley & Sons.

[11] Jacques, J., Collet, A., Wilen, S.H. 1981. *Enantiomers, racemates and resolutions*. Wiley- Interscience.

[12] Kwabe, J. 1989. On the Enantioselectivity of Drugs. *Arzneimittel- Forschung/ Drug research*, 39-2(11): 1379-1384.

[13] Ellie, E.L. & Wilen, S.H. 1994. *The Stereochemistry of Organic Compounds*. Wiley Interscience.

[14] Báthori, N.B., Jacobs, A., Nassimbeni, L.R. & Sebogisi, B.K. 2014. Quininium malates: Partial chiral discrimination via diasteromeric formation. *South African Journal of Chemistry.*, 67: 160-166.

[15] Izake, E. L. 2006. Chiral discrimination and enantioselective analysis of drugs: An Overview. *Journal of Pharmaceutical Sciences.* 96: 1659-1676.

[16] Sheldon, R. A. 1993. *Chirotechnology*, Marcel Dekker, Chapter 6

[17] Challener, CA. 2001. *Overview of Chirality in Chiral Drugs.* 1stedition. Ashgate publisher: England.

[18] Oki, M. 1983.Topics in stereochemistry. 14,1

[19] Jacques, J., Collet, A. Wilen, S.H. 1994. *Enantiomers, racemates and resolutions*. Krieger Publishing Company. Malabar: Florida.

[20] Pasteur, L. C. R. 1853. (*Comptes rendus hebdomadaires des séances de l'academie des sciences*). 37: 162-165.

[21] Mullin, J.W. 2001. *Crystallization*. Reed educational and professional publishing ltd.

[27] Stinson, S.C. 2000. CENEAR. 78: 55–78.
[28] Gu, C.H., Grant, D.J.W. 2003. Physical properties and crystal structures of chiral drugs. *In handbook of experimental pharmacology: Stereochemical Aspects of Drug Action and Disposition*. Springer: Berlin.
[29] Rekoske, J.E. 2001. Chiral separations. AICHE J. 47: 2-5.
[30] Fryzuk, M.D., B.B. 1977. Asymmetric synthesis. Production of optically active amino acids by catalytic hydrogenation. *Journal of the American Chemical Society*. 99: 6262-6267.
[31] Jacobsen, P., Yamamoto. 1999. *Comprehensive Asymmetric* catalysis, Ed: Springer.
[32] Subramanian, G. 2001. Chiral separation techniques. Ed: Wiley-VCH Verlag GmbH: Weinheim.
[33] Tulashie, S., Lorenz, H., Hilfert, L., Eldelmann, F.T., Seidel-Morgenstein, A. 2008. Potential of chiral solvents for enantioselective crystallization.1. Evaluation of Thermodynamic effects. *Crystal Growth & Design*, 8: 3408-3414.
[34] Kodama, S., Yamamoto, A., Matsunaga, A., Soga, T., Hayakawa, K. 2001. Direct chiral resolution of malic acid in apple Juice by ligand-exchange capillary electrophoresis using Cu(II)-L-tartaric acid as a chiral selector. *Electrophoresis*, 22: 3286-3290.
[35] Kozma, D. 2002. CRC *Handbook of optical resolution via diastereomeric salt formation*. CRC Press: FL.
[36] a) Eliel, E., Wilen, S.H.& Mander, L.N. 1994. *Stereochemistry of organic compounds*. Wiley, 297-464.
b) Sakai, K., Hirayama, N. & Tamura, R. 2007. Novel optical resolution technologies. *Topics in Current Chemistry*. Springer-verlag.

[37] Báthori, N. B. & Nassimbeni, L.R. 2010. Selectivity and enantiomer resolution in inclusion chemistry: A systematic study of chiral discrimination through crystallization. *Crystal Growth & Design*., 4: 1782-1787.
[38] Ahuja, S. 1997. Chiral separation application and technology. *American Chemical Society*.

[39] Dyer, U.C., Henderson, D.A, Mitchell, M. B. 1999. Application of automation and thermal analysis to resolving agent selection. *Organic Process Research and Development*, 3: 161 – 165.

[40] Eliel, E.L., Wilen, S.H. 1993. Stereochemistry of Organic Compounds. Wiley-interscience.
[41] Fogassy, E., Nogradi, M., Kozma, D., Egri, G., Palovics, E., Kiss, V. 2006. Optical Resolutions Methods. *Organic & Biomolecular Chemistry*., 4: 3011-3030.
[42] Amiard, G. 1959. *Experientia*., 15:38.
[43] Reinhold, D.F., Firestone, R.A., Gaines, W.A., Chemerda, J.M. & Sletzinger, M. 1968. Synthesis of L-alpha-methyldopa from asymmetric intermediates. *The Journal of Organic Chemistry*., 33: 1209.
[44] Leffingwell, J.C. & Shackelford, R.E. 1974.Laevo-Menthol-Syntheses and organoleptic properties, Cosmetics and Perfumery. *Cosmetics perfumery*., 89(6): 69-89.
[45] Sheldon, R.A. 1993. Chirotechnology. *Industrial synthesis of optically active compounds*. Marcel Dekker: New York.
[46] Collins, A.N., Sheldrake, G.N. & Crosby, J. 1992. *Chirality in Industry: The commercial manufacture and applications of optically active compounds*. Chichester: John Wiley &Sons.
[47] Koeller, K.M. & Wong, C. 2001. Nature. Enzymes for chemical synthesis. *International weekly journal of science*. 409: 232-240.
[48] Charushin, V.N., Krasnov, V.P., Levit, G.L., Korolyova, M.A., Kodess, M.L., Chupakhin, O.N., Kim, M.H., Lee, H.S., Park, Y.J., Kim, K.C. 1999. Kinetic resolution of (±)-2,3-dihydro-3-methyl-4H-1,4-benzoxazines with (S)-naproxen. *Tetrahedron: Assymetry*.,10: 2691-2702.
[49] Fryzuk, M.D. & Bosnich, B. 1977. Asymmetric synthesis. Production of optically active amino acids by catalytic hydrogenation. *Journal of American Chemical Society*. 99: 6262-6267

[50] a) Subraniam, G. 1994. A Practical Approach To chiral separation by liquid chromatography. Ed: VCH: Weincheim. b) Subraniam, G. 2000. Chiral Separation Techniques, A practical Approach. Ed: Wiley-VCH: Weincheim.

[51] Schute, M., Strube, J. 2001. Preparative enantioseparation by simulated moving bed chromatography. *Journal of Chromatography*., 906: 399 – 416.

[52] Eliel, E.L. & Wilen, S.H. 1993. *Stereochemistry of Organic compounds*. Wiley Interscience.

[53] (a) Wilen, S.H. (1971) Resolving Agents and Resolution in Organic Chemistry – Topics in Stereochemistry, Wiley–Interscience, New York, USA, 1971, 6, 107–176. (b) Jacques, J., Collet, A. Wilen, S.H. 1991. *Enantiomers, Racemates and Resolutions*. Krieger Publishing Company. Malabar: Florida. (c) Toda, F. ed., Enantiomer Separation. Fundamentals and Practical Methods, Kluwer Norwell, MA. 2004.

[54] Báthori, N. B., Jacobs, A., Mei, M., Nassimbeni, L.R. 2003. Resolution of *(±)*-Citronellic Acid with *(-)*-Cinchonidine: The crystal structure of Cinchonidinium-(S)-Citronellate Diastereomeric Salt. *Journal of Chemical Crystallography*., 43: 373-376.

[55] Báthori, N. B., Jacobs, A., Mei, M., Nassimbeni, L.R. 2015. Resolution of malic acid by *(+)*-Cinchonine and *(-)*-Cinchonidine. *Canadian Journal of Chemistry*., 93: 858-863.

[56] Báthori, N.B., Nassimbeni, L.R. & Oliver, C.L. 2011. Quininium mandelates- a systematic study of chiral discrimination in crystals of diastereomeric salts. *Chemical Communications*., 47: 2670-2672.

[57] Vries, T., Wynberg, H., Echten, E. 1998. *Angewandte Chemie* International Edititon. 37: 2349-2354.

[58] Báthori, N. B. & Nassimbeni, L.R. 2012. The Dutch resolution method: attempted enhanced selectivity of 2-butylamine with mixed host diols. *Crystal Growth & Design*., 12: 2501-2507.

[59] (a) Vries, T., Wynberg, H., Echten, E. 1998. *Angewandte Chemie* International Edititon. 37: 2349-2354. (b) Kaptein, B., Vries, T.R.,Nieuwenhuyzen, J.W., Kellogg, R.M., Grimbergen, R.F.P., Broxterman, Q.B. 2005. New Developments in Crystallization-Induced resolution. *In Handbook of chiral chemicals.,2nd edition.*

[60] Vaidya, N.A. 2001, Diastereomeric crystallisation-''the classical''chiral technology. *Innovations in pharmaceutical Technology., 82-85.*

[61] Kolb, H.C., Van Nienwenhze, M.S. & Sharples, K.B. 1994. Catalytic Asymmetric Dihydroxylation. *Chemical Reviews*., 94: 2483-2547.

[62] Ryttersgard, C., Larsen, S. 1998. Quininium hydrogen(S,S)-tartrate hemihydrate, a salt with a unique conformation of the hydrogen tartrate ion. *Acta Crystallographica*., C54: 1698-1701.

[63] Puliti, R, Maltia, C.A., De Fazio, A., Ghiora, M.R., & Mazzarella, L. 2001. Cinchoninium-L-tartrate tetrahydrate*. Acta Crystallographica*., C57: 1447-1449

[64] Ryttersgard, C., Larsen, S. 2003. Cinchonidinium (R,R)-tartrate monohydrate. *Acta Crystallographica*., E59: 1715-1716.

2. EXPERIMENTAL DETAILS AND MATERIALS

2.1 Experimental details

2.1.1 Crystal Growth

Inclusion compounds and salts were obtained by dissolving and stirring a racemic acid with one of the cinchona alkaloids (base) in a suitable solvent at 60°C on a hot plate until the solution became clear. Then the solution was sealed with a pierced parafilm and left to crystallize at room temperature. A sequence of solvents were employed including ethanol, methanol, water, dimethyl sulfoxide, tetrahydrofuran. Grinding experiments were carried out to investigate the formation of the selected compounds with minimal amount of solvent present. The selected acids were exposed to a few drops of dimethyl sulfoxide or water as solvent then ground for 10 mins.

2.1.2 Thermal analysis (TA)

Thermal analysis includes Thermogravimetry (TG) and Differential Scanning Calorimetry (DSC). Thermogravimetry and Differential Scanning Calorimetry were performed on a PerkinElmer Pyris 6 TA instrument and a PerkinElmer DSC 6000 system under dry N2 purge gas with a flow rate of 30 $ml.min^{-1}$ with a constant scanning rate of 10 $°C.min^{-1}$. Crystals were removed from their mother liquor, carefully dried with a filter paper, crushed to a fine powder and placed in an open pan for TG analysis and vented pans for DSC analysis.

2.1.3 Thermogravimetric analysis (TGA)

Thermogravimetric analysis (TG) is an experimental technique used in a complete evaluation and interpretation of results when it is known as Thermogravimetric Analysis (TGA).[1] The method has been defined by the International Confederation for Thermal Analysis and Calorimetry as a method in which the mass change of a substance is measured as a function of temperature, whilst the substance is subjected to a controlled temperature programme.[2] The temperature programme has to be taken to include holding the sample at a constant temperature other than ambient, when the mass change is measured against time.[1] A mass loss is only observed if a process occurs where a volatile component is lost. Thermogravimetric analysis depends on a high degree of precision in three measurements: mass changes, temperature and temperature change.

The typical instrumental requirements for TGA are a precision balance with a pan loaded with the sample, and a programmable furnace. A classic operating range for the furnace is from room temperature to 1000°C, with

a heating rate up to 100 °C/min. A thermocouple is placed close to the sample to indicate the sample temperature.

Thermogravimetric curves are referred to as mass loss curves (more rarely mass gain curves, as occur in oxidation reactions where the carrier gas in oxygen). Thermogravimetric curves can be used to evaluate the temperatures ranges, the number of decomposition stages, and fractional weight loss of each stage.[3] The technique is quantitative and a well-established method for the characterization of materials. TGA can give information about physical phenomena and chemical phenomena, including vaporization, absorption; and also chemisorption or desolvation.[4]

2.1.4 Differential scanning calorimetry (DSC)

DSC is the measurement of the change of the difference in the heat flow rate to the sample and to a reference, while they are subjected to a controlled temperature program.[5] The method is the most widely used for all the thermal analysis techniques. The gas atmosphere is well defined at all times during the experiment and the change in the temperature follows a pre-defined program. Unlike thermogravimetry, the technique is not dependent on the sample undergoing a change in mass.[2] Differential scanning calorimetry was used to determine the onset temperatures as well as the enthalpy change through the departure of a volatile compound from the solid material. Two identical measuring sensors were used, one for the reference and one for the sample. The signal from the instrument depends on the difference between the responses of the two sensors[2]. The temperature of both pans is increased at a constant rate.[6]

Different properties, such the heat capacity or glass transition, can be determined from DSC data collection. The sample can undergo endothermic or exothermic procedures that would result in a curve of heat flux temperature or versus time. In DSC, the temperature calibration is done by running standard materials, such as indium and zinc.

There are two main type of DSC exists

- Heat-flux DSC: is a technique in which the temperature of the sample unit, formed by a sample and reference material, is varied in a specified program, and the temperature difference between the sample and the reference material is measured as a function of temperature.
- Power compensated DSC: The difference of thermal energy that is applied to the sample and the reference material per unit of time is measured as a function of the temperature to equalize their

temperature, while temperature of the sample unit, formed by the sample and reference material, is varied in a specified program.

Both types of differential scanning calorimeters make use of a crucible to contain the sample. The reference is either an inert material in a crucible of the same type as that used for the sample, or simply the empty crucible. Crucibles commonly measure 5-6 mm in diameter, which gives some idea of the overall dimensions of the DSC cell. TGA and DSC results are influenced by the sample size; flow rate and heating rate of the N_2 gas.[3] Melting point of *(rac)*-DBTA·H_2O, *(rac)*-DBTA·DMSO, *L*-DBTA·H_2O, *(rac)*-DTTA·H_2O *(rac)*-DTTA·DMSO, *L*-DTTA·H_2O, *L*-DTTA·DMSO, [$CIND^+$][*L*-$DBTA^-$], 2[$CIND^+$][*D*-$DBTA^{2-}$], [$CIND^+$][*L*-$DTTA^-$], 2[$CIND^+$][*D*-$DTTA^{2-}$] 2DMSO·0.7H_2O were measured using a PerkinElmer Pyris 6000 series instrument.

2.1.5 Powder X-ray diffraction (PXRD)

X-ray powder diffraction is a rapid analytical technique primarily used for phase identification of a crystalline material, and can provide information on unit cell dimensions. The analysed material is homogenized and is ground to a fine powder. In this technique the diffraction pattern is obtained from a powder of the material, rather than a single crystal. Powder diffraction is more convenient than single crystal diffraction, because the method does not require individual large enough crystals to be obtained. A diffraction pattern plots intensity against the angle of the detector measured in 2Θ where Θ is the Bragg angle. All compounds were collected on a Bruker D2 phaser diffractometer with a graphite-monochromated Cu Kα radiation ($\lambda = 1.5418$ Å) at room temperature[7] to determine the diffraction data. The diffractograms were obtained under ambient conditions at a power setting of 40 kV and 20 mA in adsorption mode. The sample rotates on a horizontal plane while the incoming and outgoing beams are synchronized to move at a preselected angular velocity from 4° to 60° in 2Θ.[6]

2.1.6 Single crystal X-ray diffraction

Historically X–rays were discovered in 1895 by William Roentgen. In 1912, the German physicist Max von Laue suggested that because the wavelength of X-rays is comparable in magnitude to the distances between lattice points in a crystal, the lattice should be able to diffract X-rays. X-ray diffraction refers to the scattering of X-rays by the units of a crystalline solid. The scattering, or diffraction, patterns produced are used to deduce the arrangement of particles in the solid lattice.[8] X –ray diffraction is actually a common technique for the study of crystal structures and atomic spacing.[9] Single crystal X-ray diffraction is a non-destructive analytical technique, which provides detailed information about the internal lattice of crystalline substances, such as unit cell dimensions, bond lengths, bond angles, and details of site ordering. It is the most popular analytical method to

solve the three dimension structure of a molecule.[4] The technique is considered to be the most dominant technique for elucidating crystal structures.[10] The method requires three main steps: (i) data collection, (ii) structure solution and (iii) refinement.

Diffraction data for all compounds were collected on a Bruxer APEX II diffractometer with a graphite-monochromated MoKα (λ= 0.71073 Å) at 173 K using an Oxford Crysostream 700.[11] Structures were solved and refined by using SHELXS and SHELXL [12] which was run under a graphical user interface, X-seed.[13] The space groups were determined by using the collected intensites and pre-determined cell parameters as inputs to the program XPREP.[14] SHELXS-97[12] was used to solve all structures by direct methods and refinement was carried out with SHELXL-97 [12] by employing full- matrix least-squares against F^2 for unique reflections :

$$\sum W(F_o^2 - kF_c^2)^2 \qquad \text{(eq.1)}$$

The agreement between the observed structure factors (F_0) and the calculated structure factors (F_c) were monitored by assessing the residual index R. The residual index R_1 is the agreement between the observed and calculated structure based on F, while the residual index, R_2 is the agreement based on F^2.

$$R_1 = \frac{\sum||F_o| - |F_c||}{\sum|F_o|} \qquad \text{(eq.2)}$$

$$R_2 = \left[\frac{\sum w(F_o^2 - F_c^2)^2}{\sum w(F_o^2)^2}\right]^{\frac{1}{2}} \qquad \text{(eq.3)}$$

The weighting scheme *w* was used to yield a constant distribution in terms of *a* and *b*, and further refined in the final cycles of structure refinement.

$$w = \frac{1}{\sigma^2(F_o^2) + (aP)^2 + bP} \qquad \text{(eq.4)}$$

$$P = \frac{max(0, F_0^2) + 2F_c^2}{3} \qquad \text{(eq.5)}$$

Where SHELXL-97[12] refines against F^2, which leads to a greater deviations of the Goodness of fit (S) from unity than the refinement against F. The Goodness of fit expression is:

$$S = \left[\frac{\sum w(|F_o|^2 - |F_c|^2)^2}{(N - n_P)}\right]^{\frac{1}{2}} \quad \text{(eq.6)}$$

Where N is the number of reflections and n_p is the total number of parameters refined.

The hydrogen atoms bound to carbon atoms were placed at idealized positions and refined as riding atoms with U_{iso}(H)= 1.2 U_{eq} (Ar-H, CH_2) or 1.5 U_{eq} (CH_3) of the atom to which the H is bound. H atoms bonded to the carboxylic acid, amine or amide groups were located in the difference electron density map and their coordinates refined freely but their isotropic displacement parameters were fixed (Uiso (H)=1.2 Ueq(O) or Ueq(N)) if it was necessary.

X-ray powder patterns were calculated using LAZY PULVERIX[15] and compared to experimental powder patterns for characterization. All the crystal packing diagrams were generated with Pov-Ray[16]. The program LAYER[17] was utilized to test systematic absences and space group symmetry. For verification of types of voids occupied by guest molecules, the program SECTION[18] was used to slice through cross sections of the unit cell. X-seed were used as a graphical interface for the programs SHELXS-97, SHELXS-97, LAZY PULVERIX, Pov-ray, LAYER and SECTION.

Others programs used in addition to X-seed:

- Platon[19]
    - A multipurpose analytical tool for crystal structure analysis; calculates all molecular parameters for the structures
- ConQuest[20]
    - Search engine using the Cambridge Structural Database (CSD) for informative and comparative structure details.

2.1.7 Crystal Structure Analysis

Diagrams and publication material were generated using PLATON, X-seed and Mercury[22].

2.1.8 Computing components

ConQuest: is the primary program for searching and retrieving information from the Cambridge Structural Database (CSD).[17]

SADABS: (Siemens Area Detector Absorption Corrections): an application in the APEX suite used to scale and correct data for absorption collected on a Bruker AXS area detector.[21] The program is designed to exploit data redundancy, corrects for errors resulting from the variation in the volume of the crystal, absorption by the crystal support and crystal decay during the measurement.

XPREP: This program determines the space group , reads the raw data file (.raw) and the parameter file (.p4p) written by the diffractometer control program, also writes the instruction file (.ins) and reflection data file (.hkl).[20]

X-Seed: Graphical User Interface for crystallography and graphical programs.[11]

Layer: is a component of X-seed. It displays simulated precession photographs of the reciprocal lattice levels using the intensity data.[15]

LAZY Pulverix: software which calculates the theoretical powder X-ray diffraction pattern from single crystal X-ray diffraction data.[13]

Pov-Ray: program which generated graphics.[14]

Pov-Label: allows controlling the atom labels on an image rendered using Pov-Ray.[14]

Mercury: Analysis software which provides options to aid the investigation and analysis of crystal structures. It can import chemical bond types, 2D connection tables and present them in 3D illustration, generates packing diagrams, defines and visualises Miller planes, and take a slice through a crystal in any directions. Also, it displays space group symmetry elements, calculates voids based either on contact surface or solvent accessible surface and intermolecular potentials; also it performs basic gas phase calculations.[22]

2.1.9 CrystalExplorer

CrystalExplorer is a computer package that utilizes calculated Hirshfeld surfaces[23] of molecules within a crystal structure, to determine the intermolecular interactions between particular molecules and their surrounding environment. Hirshfeld surfaces are created by an extension of the weight function describing an atom in a molecule, to include the function of a molecule in a crystal.[24] The isosurfaces generated from these calculations,

with a specified weight function *w* (r) = 0.5, surrounds the molecule and by partitioning the electron density of the molecular fragments, delineates the space occupied by a molecule in a crystal.[25] Hirshfeld surfaces can provide information about intermolecular interactions in the crystal as the surface is determined by both the enclosed molecule and its closest neighbours. Fused sphere van der Waals (or CPK), smoothed Connelly surfaces or other molecular surfaces can be used to visualise and quantify molecular geometries and designated only by the molecule itself.[25] The only surfaces is that the crystal structures imported into the program are well-characterised with all hydrogen atoms located accurately. The equation used to define a Hirshfeld surface is *w* (r) = 0.5 where *w* (r) is the weight function[25] describe as

$$w(r) = \sum_{i \in molecule} \rho_i(r) / \sum_{i \in crystal} \rho_i(r) \qquad \text{(eq.7)}$$

where ρ is a spherical atomic electron distribution located at the i^{th}nucleus. The surfaces incorporated in this study are all calculated using the d_{norm} function so that the contact distance is normalised according to the formula

$$d_{norm} = \frac{d_{i-r_i^{vdw}}}{r_i^{vdw}} + \frac{d_{e-r_e^{vdw}}}{r_e^{vdw}} \qquad \text{(eq.8)}$$

d_i is the distance from the surface to the nearest atom interior to the surface ; d_e is the distance from the surface to the nearest atom exterior to the surface. The sum of the distances would give an approximate contact distance.

2.2 Materials

2.2.1 Acids

O,O'-di-p-toluoyl-tartaric acid and O,O'-dibenzoyl-tartaric acid were used in this project. **Table 1.3** summarizes their physical properties and figure **2.1** shows their structures illustrated with line diagrams.

DBTA

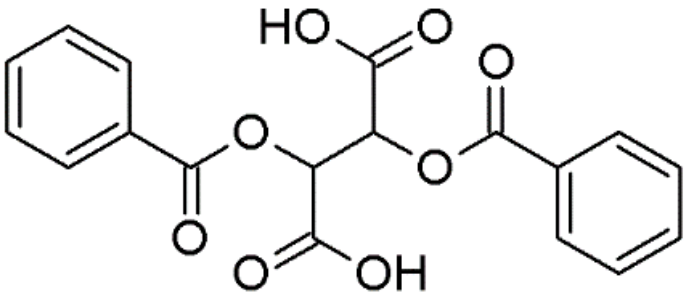

DTTA

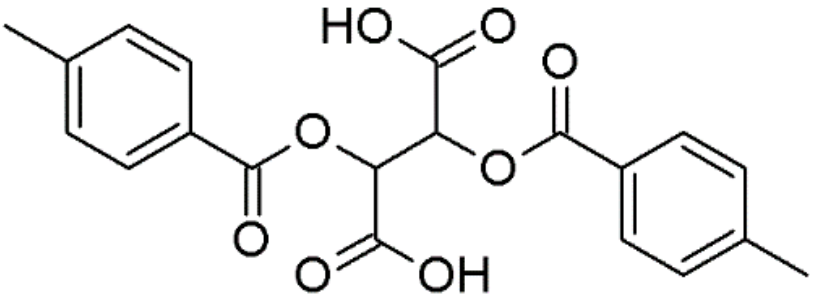

Figure 2.1: Chemical structures and abbreviations of acids.

2.2.2 Bases

Cinchona alkaloids used as base for this project, *(+)*-Cinchonine, *(-)*-Cinchonidine, *(+)*-Quinidine, *(-)*-Quinine, were purchased from Sigma-Aldrich. The physical properties of the cinchona alkaloids with their chemical formula and molecular weights are given in **table 1.2** while their structures are illustrated with line diagrams in **Figure 2.2.**

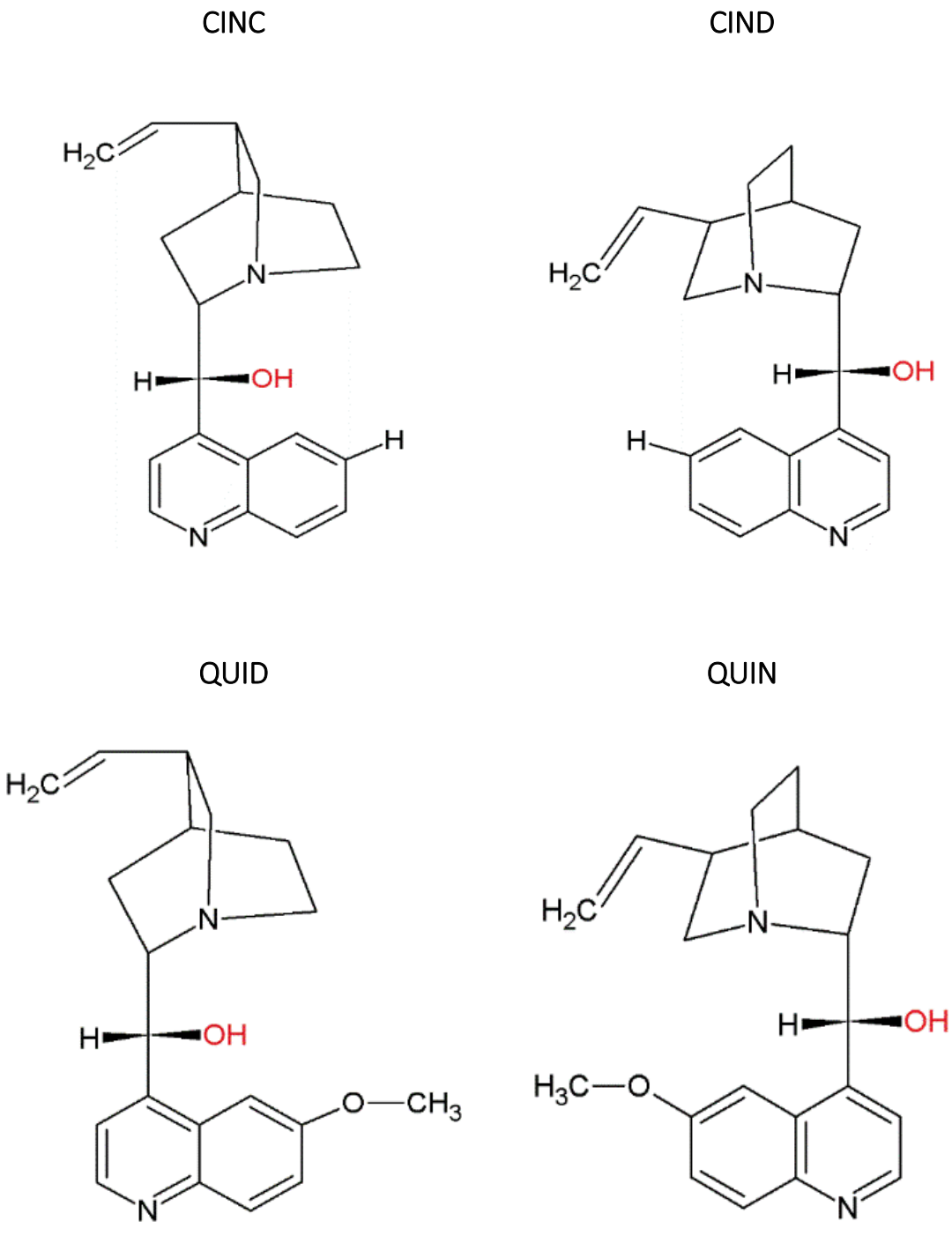

Figure 2.2: Chemical structures and abbreviations of bases.

[1] Haines, P.J. 2002. *Principles of Thermal Analysis and Calorimetry.* The Royal Society of Chemistry (Cambridge).
[2] Mackenzie, R.C., Elving, P.J. & Kolthoff, I.M. 1983. *Nomenclatures in Thermal analysis in Treatise on Analytical Chemistry*. John Wiley& Sons, New York.
[3] Brown, M.E. 1998. Introduction to Thermal Analysis. Chapman & Hall, London.
[4] Coats, A.W. & Redfern, J.P. 1963. *Thermogravimetric Analysis. A review.* The Analyst, 88: 906-924.
[5] Hohne, G., Hemminger,W.F. & Flammershein, H.J. 2003. *Differential scanning calorimetry*. Springer, Second Edition, New York.
[6] Caira, M.R. & Nassimbeni, L.R. 1996. *Phase Transformations in inclusion compounds, kinetics and thermodynamics of enclathration*. In Comprehensive Supramolecular Chemistry, MacNicol, D.D., Toda, F., Bishop, R., Eds; Pergamon: Oxford; Vol 6, Chapter 5.
[7] Bruker 2010. D2 PHASER. Version 3-07. Bruker AXS GmbH, Karlsruhe, Germany.
[8] Skoog, D.A. 1985. Principes of instrumental analysis. Saunders College Publishing- International Edition.
[9] Hasegawa, K. 2012. The Rigaku Journal. 28.1.
[10] Harris, K.D.M., Treymane, M. & Kariuki, B.M. 2001. *Contemporary advances in the use of powder X-ray diffraction for structure determination*. Angewandte Chemie International Edition, 40: 1626-1651.
[11] Bruker 2005. *APEX2*. Version 1.0-27.Bruxer AXS Inc., Madison, Wisconsin, USA.
[12] Sheldrick, G.M. and Schneider, T .R. 1997. SHELXL: High resolution refinement. *Macromolecular Crystallography*, 277: 319-343.
[13] Barbour, L.J. 2003. X-seed: Graphical interface for SHELX program. *Journal of Supramolecular Chemistry*, 1: 189-191.
[14] XPREP, Data Preparation and Reciprocal Space Exploration, Version 5.1/NT © 1997, Bruker Analytical X-ray Systems.
[15] Yvon, K., Jeitschko, W.and Parthe, E.J. 1997. LAZY PULVERIX, a computer program, for calculating X-ray and neutron diffraction powder patterns. *Journal of Applied Crystallography*.,10:73-74.
[16] POV-Ray - The Persistence of Vision Raytracer by David K. Buck, Aaron A. Collins.
[17] Barbour, L.J. 1999. LAYER, A computer program for the graphite display of intensity data as simulated precession photographs. *Journal of Applied Crystallography*., 32: 351
[18] Barbour, L.J. 1999. Section, A computer program for the graphic display of cross sections through a unit cell. *Journal of Applied Crystallography*, 32: 351.
[19] Spek, A.L. PLATON, A multipurpose crystallographic tool, Version 10500, © 1980-2000
[20] ConQuest, A program for the search of CSD, Version 1.7, © 2001.
[21] G.M. Sheldrick. University of Göttingen, 2002, Germany.
[22] Allen, F.H. & Lipscomb, K.J. 2004. The Cambridge Structural Database. *Encyclopaedia of Supramolecular Chemistry*, 1: 161-168.
[23] Hirshfeld, F.L. 1977. Bonded atom fragments for describing molecular charge densities. *Theoretica Chimica*. *Acta*, 44: 129-138.
[24] Spackman, M.A. & Jayatilaka, D. 2009. Hirshfeld Surface Analysis. *CrystEngComm*, 11: 19-32.
[25] The CrystalExplorer Manual. http://hirshfieldsurface.net/wiki/index.php/Surface_Properties. Accessed 15 February 2014.

3. Crystal structures of tartaric acid derivatives

In the following chapters, inclusion compounds of *(–)-O,O'*-dibenzoyl-*(2R,3R)*-tartaric acid (or *L*-DBTA) and *(–)-O,O'*-di-p-toluoyl-*(2R,3R)*-tartaric acid (*L*-DTTA) or their racemic mixtures, *(rac)*-DBTA and *(rac)*-DTTA with achiral common solvents are discussed. DBTA and DTTA are commonly used resolving agents to separate racemic bases via diastereomeric salt formation. These compounds were selected as our targets of chiral discrimination experiments (see Chapter 4) because of their structural similarity to tartaric acid and also because of their likeliness to form salts with the selected cinchona alkaloids.

During the pre-screening of suitable solvents to dissolve both the acids and the cinchona alkaloids, a wide variety of solvents were tested and in some occasions suitable crystals were harvested. These crystals were inclusion compounds of DBTA or DTTA and did not contain the cinchona alkaloid. A Cambridge Structural Database search were carried out to target DBTA or DTTA structures (CSD version 5.38 updates, Feb 2017; focused on only organic compounds with 3D coordinates available) and resulted in 118 hits. It was concluded that only few crystal structures of solvates of these two tartaric acid derivatives are known or published, and significantly less of these structures do exist when both the racemic and the enantiopure acid encapsulates the same solvent.[1]

To contribute to the pool of available crystal structures when comparing chiral vs. achiral crystal forms of the same compounds, 8 crystal structures of DBTA and DTTA with water or DMSO as included solvent were analysed and discussed in details.

3.1 DBTA solvates

In this chapter the crystal structures of the hydrates and DMSO solvates of O,O'-dibenzoyl-tartaric acid (DBTA) will be discussed. The racemic mixtures of DBTA were formed by mixing the *L* or *(-)-R,R* and the *D* or *(+)-S,S* enantiomers in an equal amount and dissolved them in water or DMSO. The structural data of *L*-DBTA·DMSO was already published[2] thus that 3D data was used for comparison. Table 3.1 contains crystallographic data for the structures and Table 3.2 summarizes their most prominent hydrogen bonds.

[1] Z. Kovari, Z. Bocskei, C. Kassai, E. Fogassy, D. Kozma, *Chirality* (2004), 16, S23-S27.
[2] D. Eissmann, E. Weber, *Struct. Chem. Comms.* (2010), **1**, 40. Structure is published under the code ILEZEF.

Table 3.1 Crystallography data for hydrates and DMSO solvates of DBTA.

Compounds	***(rac)*-DBTA·H_2O**	***(rac)*-DBTA·DMSO**	***L*-DBTA·H_2O**	***L*-DBTA·DMSO (ILEZEF)***
Molecular formula	$C_{18}H_{18}O_{10}$	$C_{22}H_{26}O_{10}S_2$	$C_{18}H_{16}O_9$	$C_{22}H_{26}O_{10}S_2$
Formula Weight ($g.mol^{-1}$)	394.32	514.55	376.31	514.55
Crystal system	tetragonal	tetragonal	monoclinic	monoclinic
Space group (No.)	$I4_1/a$ (88)	$I4_1/a$ (88)	$P2_1$ (4)	$C2$ (5)
a (Å)	16.926 (2)	17.334(3)	8.9778(18)	20.3106(5)
b (Å)	16.926(2)	17.334(3)	8.1128(16)	5.7460(1)
c (Å)	13.029(3)	16.521(3)	24.753(5)	12.1708(3)
α (°)	90	90	90	90
β (°)	90	90	99.55(3)	119.277(1)
γ (°)	90	90	90	90
V ($Å^3$)	3732.7(13)	4964(2)	1777.9(6)	1238.96
Z	8	8	4	2
ρ_{calc} ($g.cm^{-3}$)	1.403	1.377	1.406	1.379
μ (MoKα) (mm^{-1})	0.116	0.267	0.115	n/a
F (000)	1648	2160	784	n/a
Crystal Size (mm)	0.10×0.10×0.10	0.14×0.30×0.38	0.11×0.20×0.32	n/a
Temperature (K)	173(2)	173(2)	173(2)	n/a
Radiation (Å)	MoKα, 0.71073	MoKα, 0.71073	MoKα, 0.71073	n/a
Theta min-max (°)	1.97; 28.51	2.35; 28.30	1.66; 27.62	n/a
Dataset (±h; ±k; ±l)	-22:22; -22:22; -17:17	-23:23; -21:23; -11:22	-11:11; -10:10; -32:32	n/a
Final R indices [I>2σ(I)]	0.0502; 0.1221	0.0317; 0.0814	0.0712; 0.1722	0.021
R indices [all data]	0.0626; 0.1324	0.0386; 0.0861	0.1314; 0.2025	n/a
Tot., uniq. data, R (int)	2368; 1905; 0.0452	3083; 2677; 0.0378	8161; 4742; 0.0513	n/a
N_{ref}, N_{par}	2368;130	3083;157	8161;490	n/a
S	1.054	1.053	1.035	n/a
Max. and av. Shift/error	0.000/0.000	0.000/0.001	0.000/0.000	n/a
Min. and max. resd. dens.($Å^3$)	-0.565; 0.762	-0.297; 0.261	-0.323 ;0.548	n/a

** Previoulsy published (CSD Ref. code: ILEZEF)-see page 36.*

Table 3.2 Hydrogen bond details for hydrates and DMSO solvates of DBTA.

D-H···A	d(D-H) (Å)	d(H···A) (Å)	d(D···A) (Å)	D-H···A (°)	Symmetry Operators
(rac)-DBTA·H₂O					
C1-H1···O4	1.000	2.486	3.407	152.78	*y-1/4, -x+1/4, -z+5/4*
O4-H4···O14	0.840	1.733	2.527	156.84	
O14-H14B···O17	0.849	2.112	2.910	156.62	*-x, -y, -z+1*
(rac)-DBTA·DMSO					
O4-H4···O14	0.840	1.707	2.537	168.97	
O4-H4···S15	0.840	2.795	3.605	162.56	
C17-H17A···O7	0.980	2.510	3.225	129.63	*-x+1/2, -y+1/2, -z+1/2*
L-DBTA·H₂O					
O4A-H4A···O16A	0.840	1.837	2.630	156.80	*x, y+1, z*
C14A-H14A···O3A	1.000	2.387	3.153	132.82	*-x, y-1/2, -z*
O17A-H17A···O27A	0.840	1.781	2.586	160.03	
O27A-H27C···O4A	0.853	2.307	3.119	159.22	*x, y-1, z*
O27A-H27C···O7A	0.853	2.480	2.982	118.40	*x, y-1, z*
O4B-H4B···O16B	0.840	1.873	2.665	156.75	*x, y+1, z*
C14B-H14B···O3B	1.000	2.410	3.184	133.72	*-x+2, y-1/2, -z+1*
O17B-H17B···O27B	0.840	1.765	2.575	161.36	
O27B-H27D···O4B	0.854	2.296	3.119	162.21	*x, y-1, z*
O27B-H27D···O7B	0.854	2.501	2.990	117.30	*x, y-1, z*
L-DBTA·DMSO (ILEZEF)*					
O(2)-H(7)···S(1)	0.84	2.73	3.5089(1)	156	*1/2-x,-1/2+y,-z*
O(2)-H(7)···O(1)	0.84	1.70	2.5218(1)	168	*1/2-x,-1/2+y,-z*
C(1)-H(2)···O(5)	0.98	2.45	3.3518(1)	153	
C(1)-H(3)···O(3)	0.98	2.53	3.2936(1)	135	*x,1+y,z*

** Hydrogen bond values were calculated with Platon.[3]*

[3] A. L. Spek, PLATON, A Multipurpose Crystallographic Tool, Utrecht University, Utrecht, The Netherlands, 2008.

3.1.1 (*rac*)-DBTA hydrate and DMSO solvate

The (*rac*)-DBTA·H_2O structure was solved in a tetragonal crystal system and in the achiral space group $I4_1/a$ (No. 88) with half a DBTA and a full water molecule in the asymmetric unit. (Fig 3.1a) The origin was selected at $\bar{1}$ on the glide plane *b*, at 0, ¼, ⅛ from $\bar{4}$ and the molecule is in Wyckoff position *e*. (Fig 3.1b) The crystal contains both enantiomers of the DBTA in 1:1 ratio and the *L*-DBTA (or (-)-*R,R*-DBTA) was selected to represent the asymmetric unit (ASU). Both carboxylic acid functional groups form hydrogen bonds to water molecules via O4-H4···O14, thus the crystallisation ratio is 1:2 DBTA to H_2O.

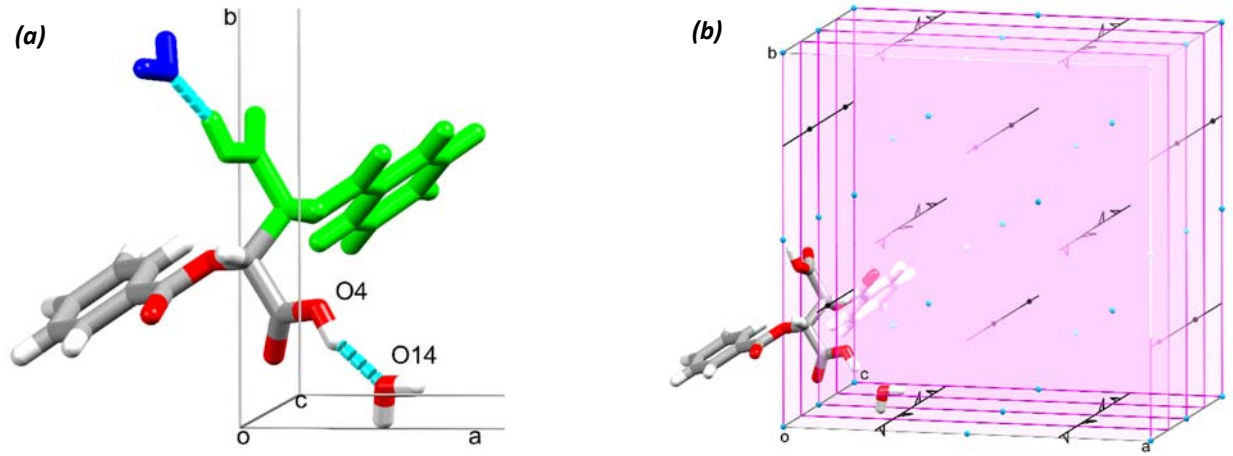

Figure 3.1. The molecular unit of (rac)-DBTA·H_2O with labelled atoms involved in the hydrogen bond (a, atoms coloured by element form the asymmetric unit) and the symmetry elements of the unit cell with the DBTA in Wyckoff position e (b)

The DBTA molecule may be described as V-shaped because of the homologous chirality of the two asymmetrical carbons (*L* ≡ (-)-*R,R* or *D* ≡ (+)-*S,S*) forces the benzoate groups to be positioned on the same side of the molecule. The benzoate group is planar (O7-C6-C8-C13 is -1.17°) and he torsion angle describing the tilt around the central alkane bond of the molecule (O5-C1-C1'-O5') is -53.28°. The plane angle between the two phenyl rings is 28.37° for the presented *L*-DBTA. (Fig 3.2ab) (The values are the same but opposite in direction for the *D*-DBTA molecules in the crystal structure by of virtue of symmetry.) Neighbouring molecules of opposite chirality are bonded together via water bridges and form heterochiral linear branches in [100] and [010] crystallographic directions. The supramolecular synthon formed between the neighbouring DBTA and water molecules may be described with the $R_4^4(18)$ descriptor. (Fig 3.3a) To form this synthon, the water acts as both hydrogen bond acceptor (O4-H4…O14) and donor (O14-H14B…O7*, *-x, -y, 1-z). These hydrogen bonded tapes interact in a manner that molecules of opposite chirality generated by a 4-fold rotoinversion axis (Fig 3.3b) interlock and hold together via C10-H10···O3* hydrogen bonds (* y-¼, ¼-x, ¼-z).

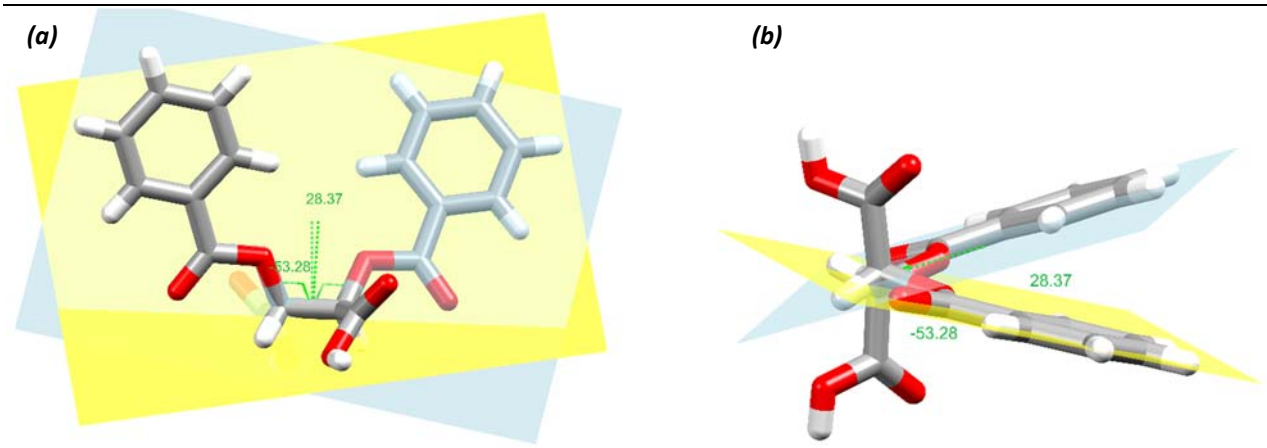

Figure 3.2 Torsion angle and the plane selection for the conformation description of the DBTA molecule.

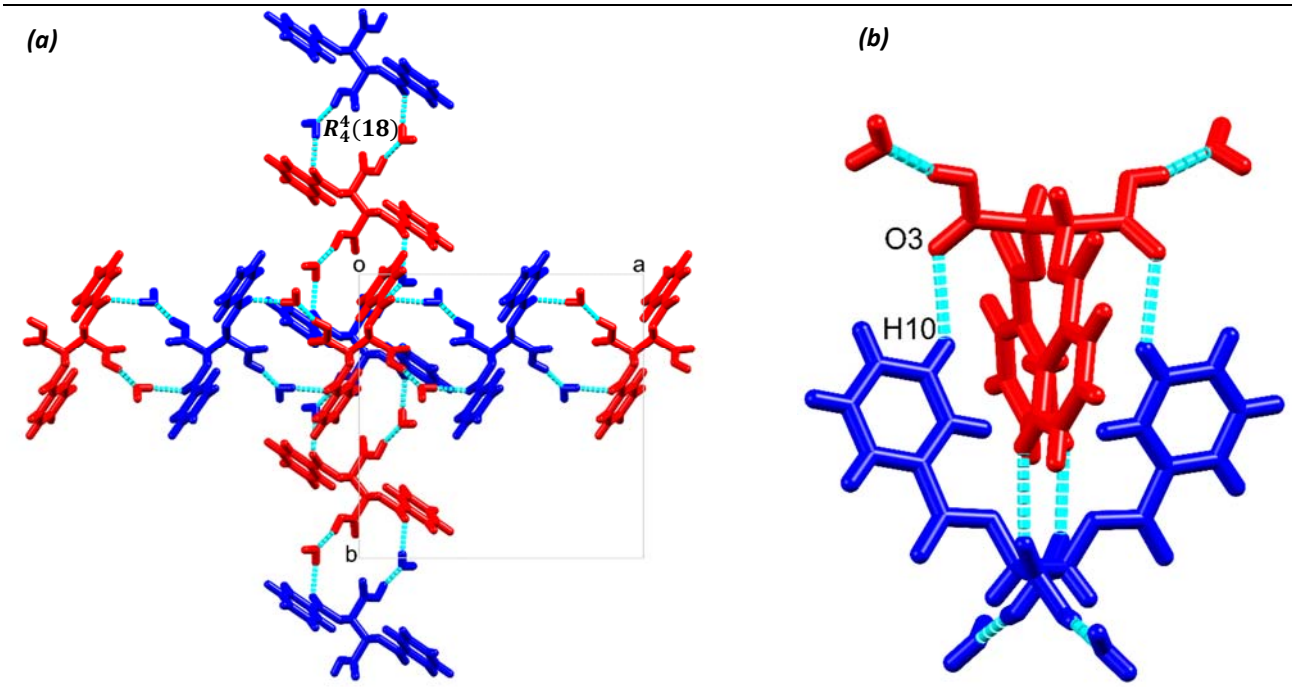

Figure 3.3 (a) Hydrogen bonded DBTA and water molecules forming heterochiral tapes. (b) The interlocking unit of (rac)- DBTA·H_2O (D-DBTA blue, L-DBTA red).

The (*rac*)-DBTA·DMSO solvate was solved in the same space group as the hydrate, $I4_1/a$ (No. 88), with half a DBTA and a full DMSO molecule in the asymmetric unit. (Fig 3.4a) Similarly, the origin was selected at $\bar{1}$ on the glide plane *b*, at 0, ¼, ⅛ from $\bar{4}$, but the DBTA molecule is in Wyckoff position *f*. The torsion angle describing the tilt around the central alkane bond of the DBTA molecule (O5-C1-C1'-O5') and the plane angle between the two phenyl rings is very similar to what was found in the hydrate structure (-54.72° and 22.24° for the *L*-DBTA). The benzoate group is not perfectly planar because of a slight rotation around the single bond (O7-C6-C8-C9 is -7.87°). The main difference between the hydrate and the DMSO solvate is the way how the

neighbouring molecules of opposite chirality interconnect. Both carboxylic acid functional groups form hydrogen bonds to the DMSO molecules via O4-H4···O14 to build the 1:2 DBTA:DMSO crystal, but the rotation of the carboxylic acid groups enable the formation of two additional hydrogen bonds between the aromatic ring of the neighbouring DBTA (C12-H12···O4 and C11-H11···O14). (Fig 3.4b) In this structure the main supramolecular unit is the heterochiral molecular assembly because there is not further hydrogen bond formation with neighbouring molecules. The packing of the seemingly individual units is shown on Fig 3.5.

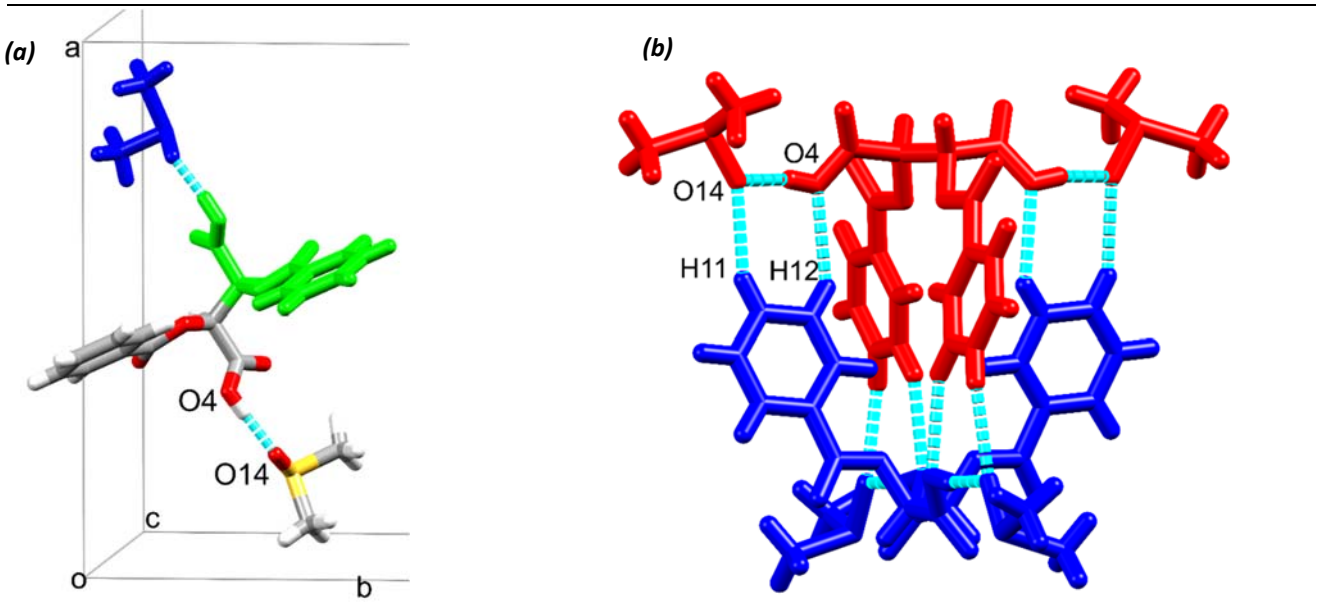

Figure 3.4 (a) Asymmetric unit (atoms coloured by elements) of (rac)-DBTA·DMSO with labelled atoms involved in the hydrogen bond. (b) The interlocking unit of (rac)- DBTA·DMSO (D-DBTA blue, L-DBTA red).

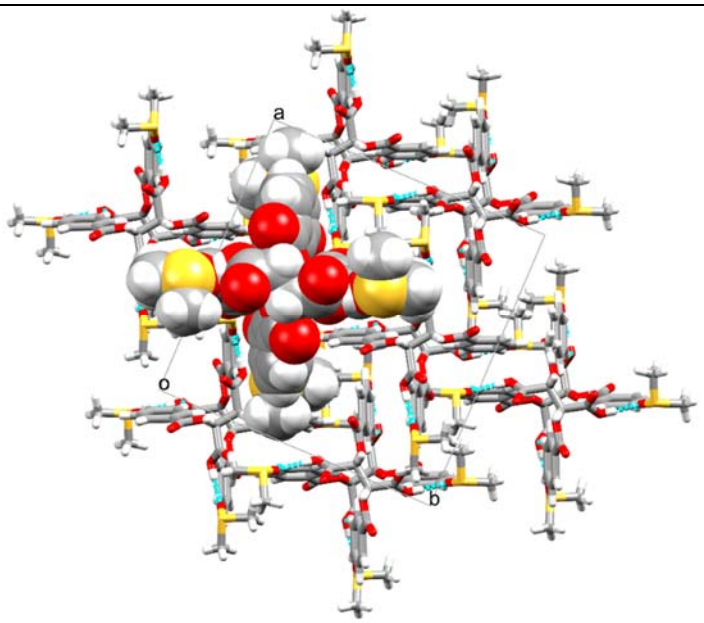

Figure 3.5 The packing of the hydrogen bonded supramolecular units of (rac)- DBTA·DMSO.

3.1.2. L-DBTA hydrate and DMSO (ILEZEF) solvate

The *L*-DBTA·H_2O structure was solved in a monoclinic crystal system and in the space group $P2_1$ (No. 4) with two molecules of *L*-DBTA and two waters in the asymmetric unit. One of the carboxylic acid group of each DBTA is hydrogen bonding to the water via O17-H17···O27 (Fig 3.6) The conformation of the two DBTA molecules is very similar (RMSD= 0.0572 Å and Max. D= 0.1156 Å) and their molecular fitting is shown in Fig 3.7. The torsion angles describing the tilt around the central alkane bond of the DBTA molecules (O5A-C1A-C14A-O18A; O5B-C1B-C14B-O18B) are virtually the same (-71.94° and -72.33°, respectively) but significantly larger when compared to the *(rac)*-DBTA·H_2O and *(rac)*-DBTA·DMSO structures. The plane angles between the phenyl rings for the two molecules are also very similar (56.69° and 55.33°, respectively) but differ considerably from the previously discussed structures. Another difference is the more obvious lack of planarity of the four benzoate groups. The values of the torsion angles are significantly larger when compared to the previous structures and vary from -10.80° to 20.36°.

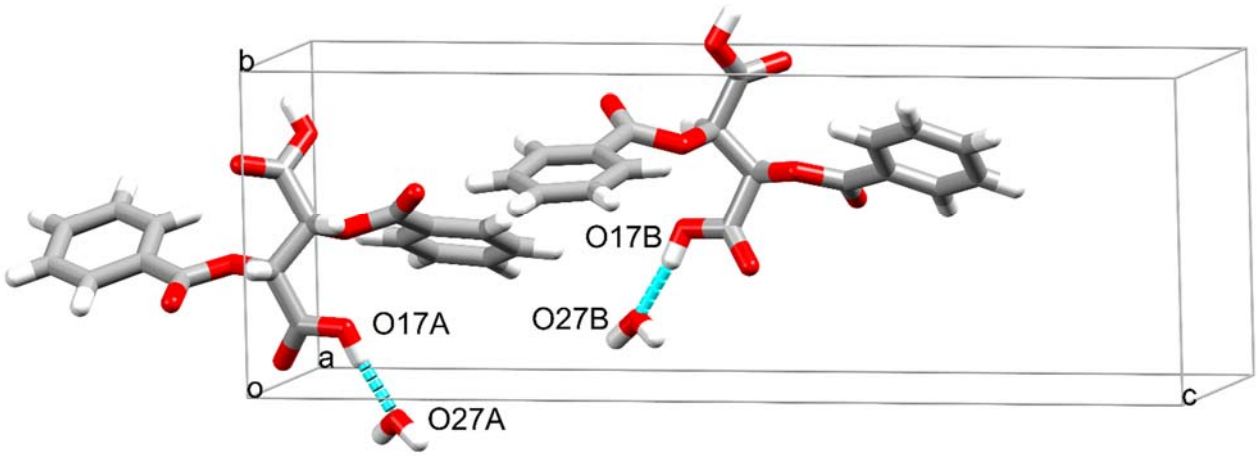

Figure 3.6 The asymmetric unit of L-DBTA·H_2O with the relevant hydrogen bonding. Only heavy atoms involved in hydrogen bonding are labelled for clarity.

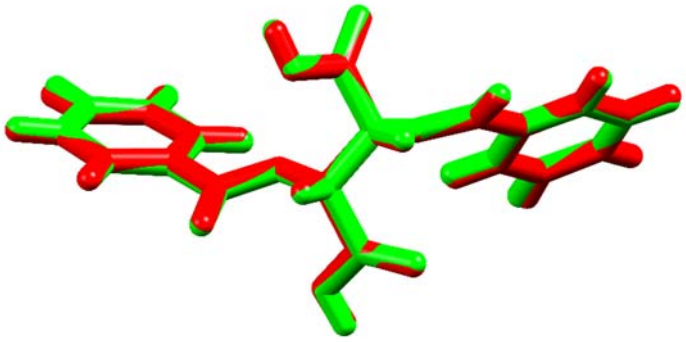

Figure 3.7 Molecular fitting of molecule A and B of L-DBTA·H_2O. (molecule A- green, molecule B- red)

Further inspection of the different intermolecular interactions of the *L*-DBTAs was carried out with the aid of *CrystalExplorer* and once the relevant Hirshfeld surfaces were calculated and the 2D fingerprint plots were generated (Fig 3.8). It is concluded that the shape of the fingerprint plots are almost identical and there is no significant difference between the % distributions of the selected interactions (see bar chart, Fig 3.8).

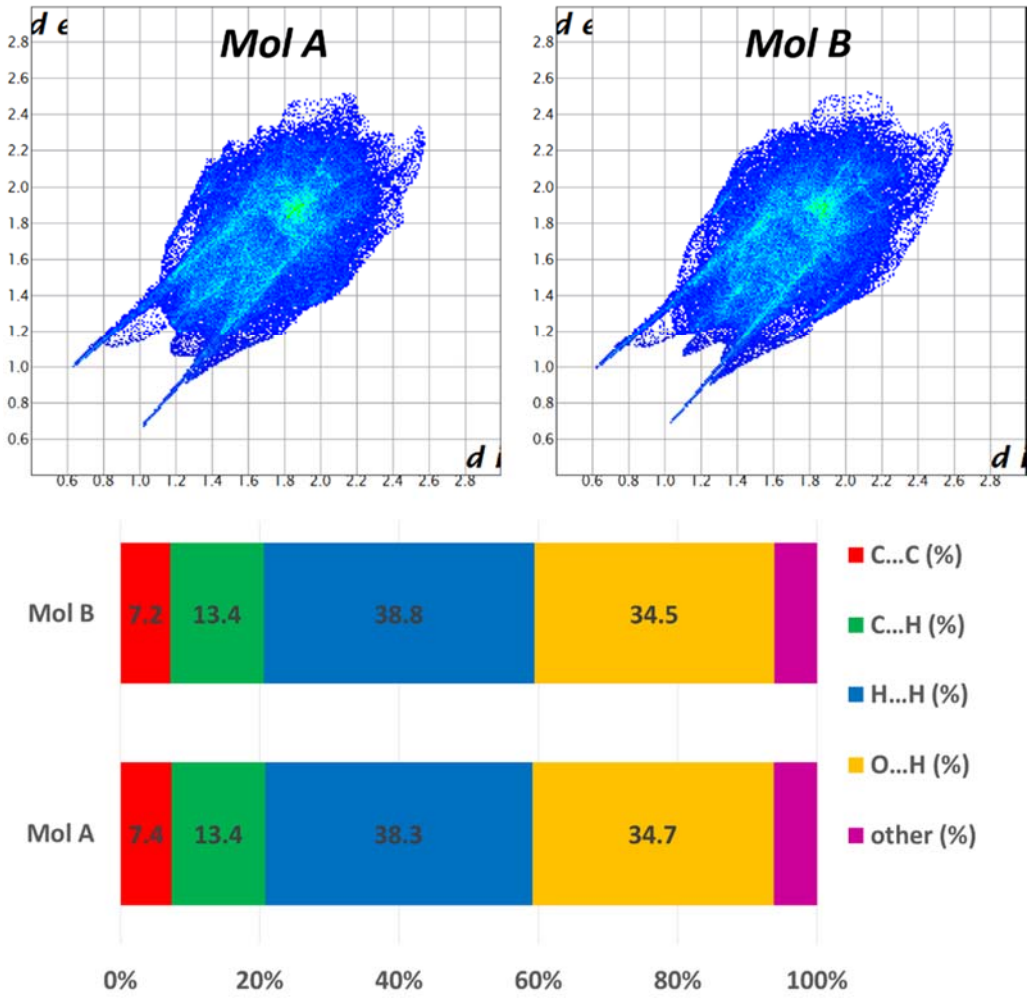

Figure 3.8 Fingerprint plots and the summary of the % contributions of the different interactions for molecule A and B in L-DBTA·H_2O.

The atoms involved in the formation of the main hydrogen bonds are presented in Fig 3.9. The carboxylic acid moieties link the DBTAs into chains in (010) direction and the water is incorporated into this motif to form $R_3^3(8)$ synthon. The parallel molecular chains are linked via C24A-H24A···O7B weak hydrogen bonds to form layers. The sheets pack in a manner that symmetry equivalent molecules form channels in the (010) direction. The channels are virtually empty and the included water molecules are positioned at the outskirts of the channel-forming DBTAs. (Fig 3.10)

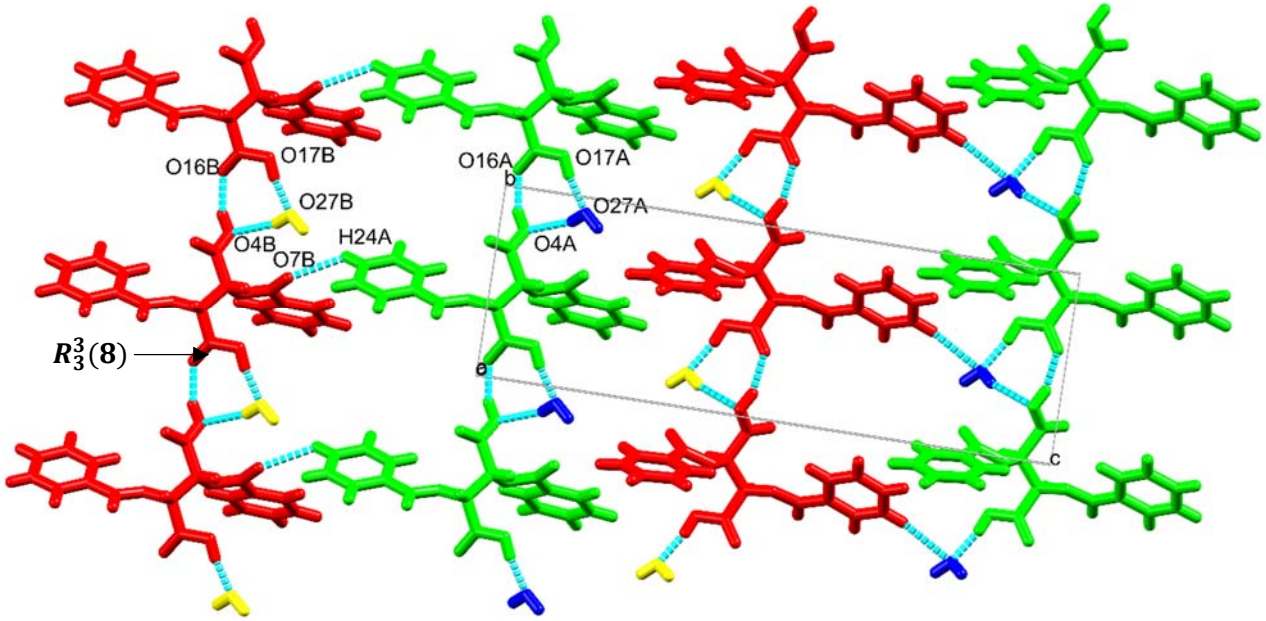

Figure 3.9 Crystal packing and main hydrogen bonding in L-DBTA·H_2O down (100). (Molecules are coloured by symmetry equivalence.)

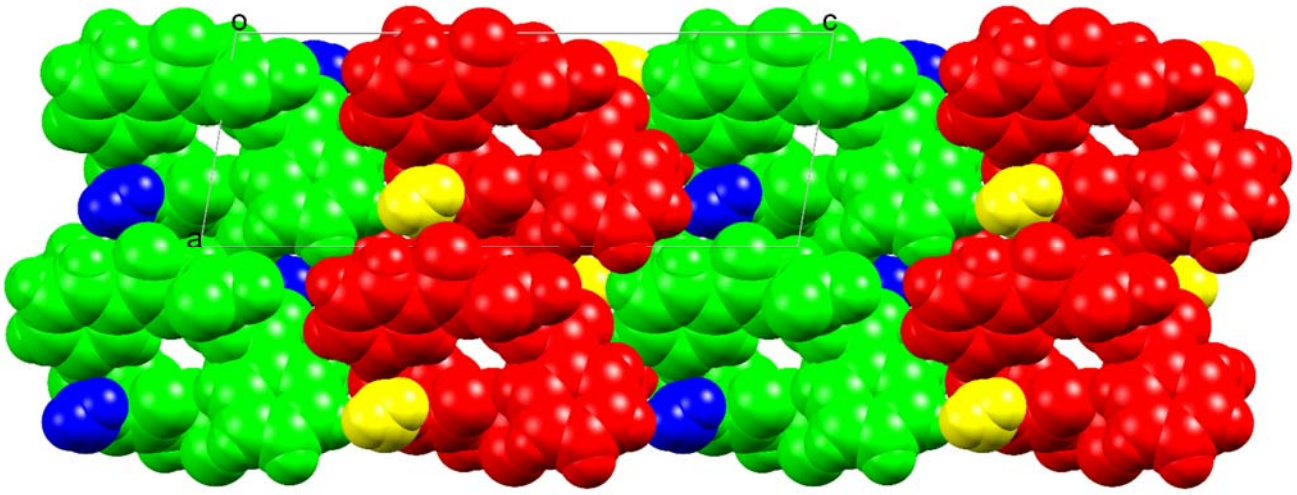

Figure 3.10 Crystal packing and hydrogen bonding in L-DBTA·H_2O down (010). (Molecules are coloured by symmetry equivalence.) Note the empty space inside the channels formed by DBTAs.

The analysis of the two symmetry independent channels reveals subtle differences in their main interactions. Molecules A (green, Fig 3.11) are hold together via aromatic interactions (centroid distances are ca. 4.3 Å and 3.9 Å). Molecules B (red, Fig 3.11) have very similar centroid distances, but also two additional hydrogen bonds formed between aromatic hydrogens and the carbonyl moiety of the interacting DBTA (C12-H12···O3B and C13-H13···O16B). It is interesting to note that the channels are very similar and thus it may be concluded that the hydrogen bonds are not essential to their formations. This suggest a level of flexibility in the formation of the interactions and although the size of the channels does not allow a water molecule to fit into them, it would be worthwhile to test the sorption/desorption properties of these crystals in the future.

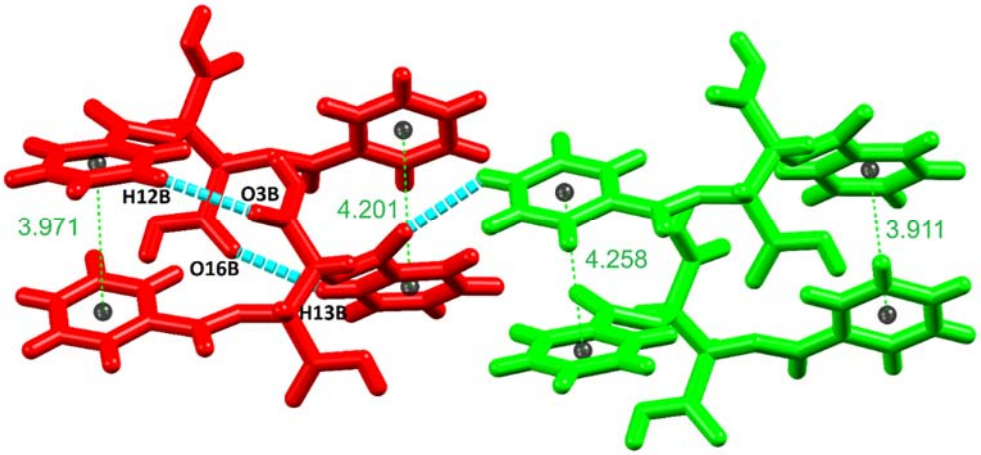

Figure 3.11 Intermolecular interactions in L-DBTA·H_2O between the neighbouring DBTA molecules during channel formation.

The crystal structure of *L-DBTA·DMSO* has been published already (CSD code: ILEZEF). New crystals were grown by dissolving L-DBTA in DMSO. The crystals were formed after a week and their phase was identified via matching their powder X-ray diffraction patterns with the ILEZEF structure. When the two powder patterns are compared (Fig 3.12 new bulk vs. ILEZEF single crystal) the peak positions are very similar but some intensity differences can be found. An obvious example of these more intense peaks is pointed out with a red arrow on Fig 3.12 at 31° in 2Θ. This is the result of preferred orientation of the crystallites parallel to (002). Because the level of similarity between the two patterns was satisfactory the single crystal data were not collected and the data of ILEZEF will be used in this section to discuss the structural features of the *L-DBTA·DMSO* solvate. The newly obtained crystals were used only to acquire additional thermoanalytical data for completeness.

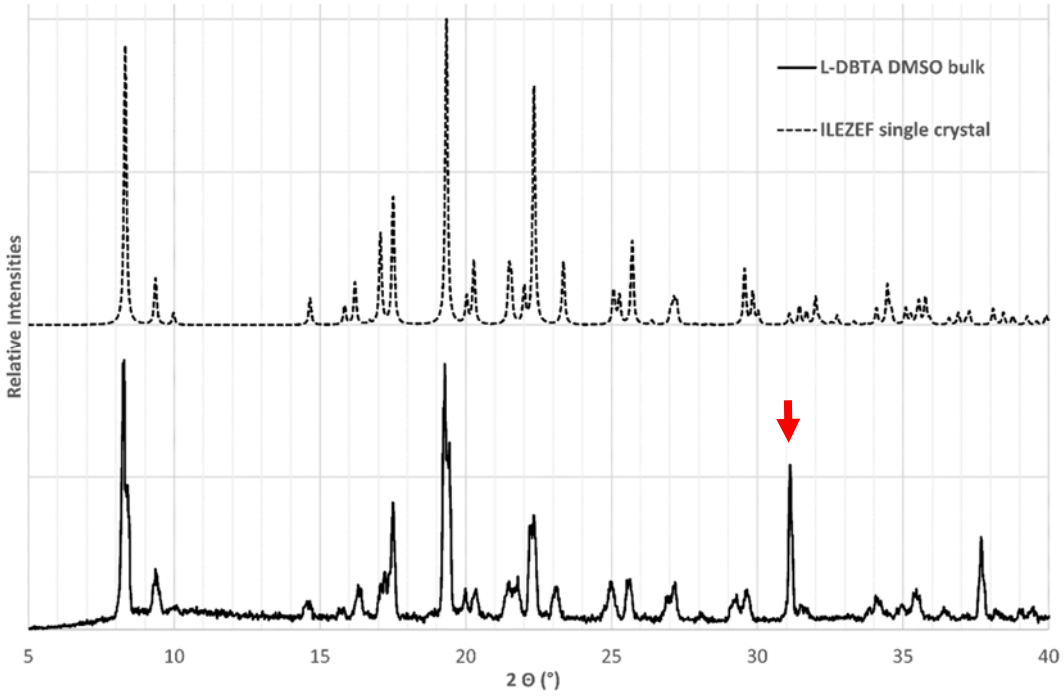

Figure 3.12 Powder X-ray diffraction patterns used for identification of newly prepared crystals of L-DBTA·DMSO to the known structure (ILEZEF). Minimal preferred orientation of the crystallites parallel to (002) is noted (red arrow).

The crystals of *L-DBTA·DMSO* (ILEZEF) crystallizes in the monoclinic *C*2 (No. 5) space group with half a molecule L-DBTA and one DMSO in the asymmetric unit and the full molecule is generated by a 2-fold axis. The DBTA is located in Wyckoff position *a,* and hydrogen bonds to two DMSO molecules via O2-H2···O1. (Fig 3.13a) The torsion angles describing the tilt around the central alkane bond of the DBTA molecule (O4-C4-C4*-O4*) is similar to the hydrate structure (-74.73°), the benzoate group is more planar (-8.18°) and the plane angle between the phenyl rings are larger (79.86°) when compared to the hydrate equivalent. The 'wider opening' of the DBTA molecules give an opportunity to positioned themselves in a head-to-tail manner along the 2-fold axis down *b* and form polar columns of hydrogen bonded molecules (Fig 3.13b). These hydrogen bonds are formed between neighbouring DBTAs (C13-H13···O2*) and between DBTA and neighbouring DMSO molecules (C12-H12···O1*). The polar columns are also connected via C-H···O=C hydrogen bonds between neighbouring DBTA molecules. (Fig 3.14a) The DMSO molecules are positioned in channels created between the polar columns of the DBTAs down (010) direction. (Fig 3.14b)

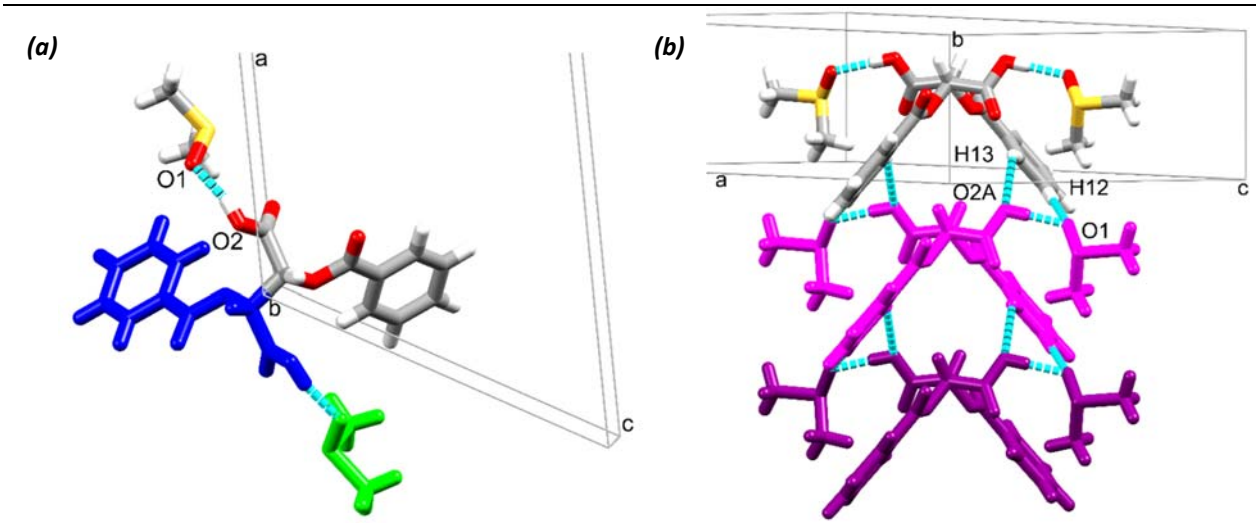

Figure 3.13 The main molecular assembly of L-DBTA·DMSO (a, only heavy atoms involved in hydrogen bonding are labelled for clarity and atoms coloured by element form the asymmetric unit). (b) The structure of the polar columns formed by the assemblies.

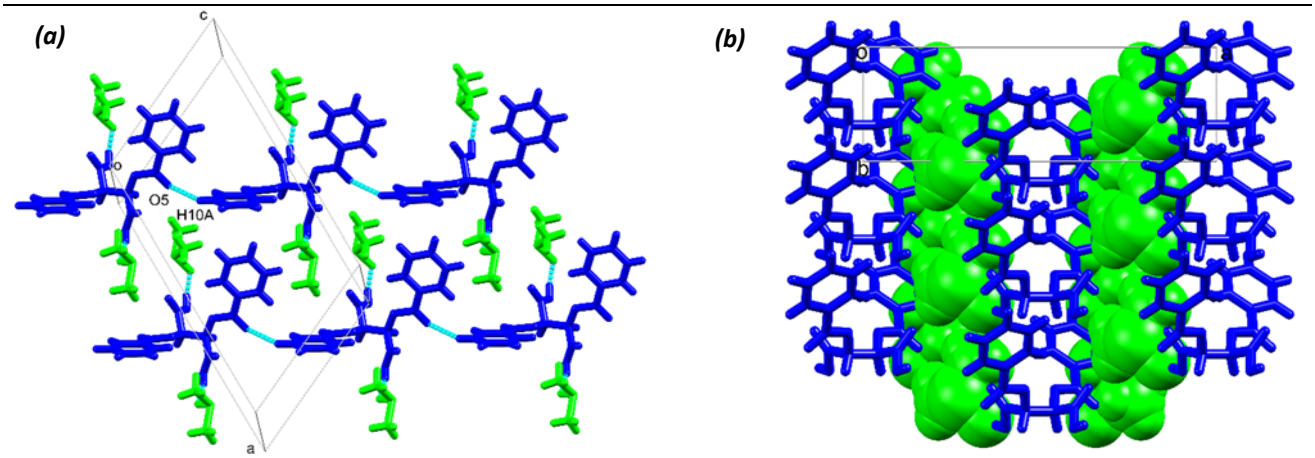

Figure 3.14 (a) Interactions between neighbouring DBTA molecules. (b) DMSO molecules (green space fill model) are positioned in channels down (010).

3.2 DTTA solvates

In the following chapters, the crystal structures of the hydrates and DMSO solvates of O,O'-di-p-toluoyl-tartaric acid (DTTA) will be discussed. The racemic mixtures of DTTA were formed by mixing the *L* or *(-)-R,R* and the *D* or *(+)-S,S* enantiomers in an equal amount and dissolved them in water or DMSO. Table 3.3 contains crystallographic data for the structures and Table 3.4 summarizes their most important hydrogen bonds.

Table 3.3 Crystallographic data for DTTA crystals

Compounds	***(rac)*-DTTA·H_2O**	***(rac)*-DTTA·DMSO**	***L*-DTTA·H_2O**	***L*-DTTA·DMSO**
Molecular formula	$C_{40}H_{38}O_{17}$	$C_{24}H_{30}O_{10}S_2$	$C_{20}H_{20}O_9$	$C_{24}H_{30}O_{10}S_2$
Formula Weight ($g.mol^{-1}$)	790.70	542.60	404.36	542.60
Crystal system	monoclinic	tetragonal	orthorhombic	Monoclinic
Space group (No.)	$P2_1/n$ (14)	$I\bar{4}$ (82)	$P2_12_12_1$ (19)	$C2$ (5)
a (Å)	12.043(2)	14.209(2)	7.8813(16)	19.924(4)
b (Å)	12.086(2)	14.209(2)	11.945(2)	5.7649(12)
c (Å)	27.456(6)	13.314(3)	21.599(4)	25.614(5)
α (°)	90	90	90	90
β (°)	96.40(3)	90	90	112.56(3)
γ (°)	90	90	90	90
V ($Å^3$)	3971.2(14)	2688.1(9)	2033.3(7)	2717.0(11)
Z	4	4	4	4
ρ_{calc} ($g.cm^{-3}$)	1.323	1.341	1.321	1.326
μ (MoKα) (mm^{-1})	0.104	0.251	0.105	0.248
F(000)	1656	1144	848	1144
Crystal Size (mm)	0.12×0.28×0.41	0.25×0.26×0.28	0.11×0.12×0.40	0.14×0.22×0.60
Temperature (K)	173(2)	173(2)	173(2)	173(2)
Radiation (Å)	MoKα,0.71073	MoKα,0.71073	MoKα,0.71073	MoKα,0.71073
Theta min-max (°)	1.49; 28.46	2.02;27.92	2.54;28.34	1.72;28.02
Dataset (±h; ±k; ±l)	-16:16;-16:-16;-36:36	-15:18;-18:16;-17:17	-9:10;-15:15;-28:28	-26:26;-7:7;-33:33
Final R indices [I>2σ(I)]	0.0465; 0.1157	0.0459;0.1123	0.0368,0.0844	0.0336;0.0817
R indices [all data]	0.0643,0.1263	0.0535;0.1182	0.0462;0.0896	0.0374;0.0839
Tot., uniq. data, R (int)	9985,7663;0.0329	3229,2863;0.0335	5063,4376;0.0394	6589,6099;0.0302
N_{ref}, N_{par}	9985;543	3229;167	5063;268	6589;333
S	1.029	1.059	1.027	1.044
Max. and av. Shift/error	0.000/0.000	0.000/0.000	0.000/0.001	0.000/0.000
Min. and max. resd. dens.($Å^3$)	-0.235;0.311	-0.338;0.897	-0.198;0.204	-0.217;0.321

Table 3.4 Hydrogen bond details for hydrates and DMSO solvates of DTTA.

D-H···A	d(D-H) (Å)	d(H···A) (Å)	d(D···A) (Å)	D-H···A (°)	Symmetry Operators
(rac)-DTTA·H₂O					
O4-H4A···O17B	0.840	1.814	2.650	173.41	*x+1/2, -y+3/2, z+1/2*
O18A-H18A···O3B	0.840	1.776	2.615	175.79	
O4B-H4B···O17A	0.840	1.794	2.633	178.69	
O18B-H18B···O31b	0.840	1.771	2.591	164.96	*-x+1, -y+2, -z*
O31b-H31Ab···O7B	0.859	1.973	2.827	173.02	
O31b-H31Bb···O7A	0.882	2.072	2.949	172.77	*-x+3/2, y+1/2,-z+1/2*
(rac)-DTTA·DMSO					
C1H1···O4	1.000	2.630	3.599	163.35	*y, -x+1, -z*
O4-H4···O15	0.840	1.749	2.571	165.86	
O4-H4···S16	0.840	2.581	3.379	158.97	
C17-H17C···O15	0.980	2.607	3.413	139.60	*-y+1/2, x-1/2, -z+1/2*
C18-H18A···O7	0.980	2.588	3.537	163.11	*-y+1, x, -z*
L-DTTA·H₂O					
O4-H4···O17	0.840	1.785	2.619	171.54	*x+1, y, z*
O18-H18···O29	0.840	1.793	2.587	156.98	
O29-H29B···O7	0.856	2.206	3.030	161.51	*x-1, y, z*
O29-H29A···O7	0.824	2.031	2.828	162.46	*x-1/2, -y-1/2, -z*
L-DTTA·DMSO					
O4A-H4A···O15A	0.840	1.710	2.547	173.50	
O4A-H4A···S16A	0.840	2.930	3.742	163.28	
C17A-H17B···O3A	0.980	2.425	3.306	149.36	
C18A-H18A···O3A	0.980	2.637	3.473	143.31	
C18A-H18C···O3A	0.980	2.403	3.255	145.05	*-x+1/2, y-1/2, -z*
C18A-H18B···O7A	0.980	2.484	3.309	141.65	*-x+1/2, y+1/2, -z*
O4B-H4B···O15B	0.840	1.687	2.521	171.68	
O4B-H4B···S16B	0.840	2.753	3.546	158.04	
C18B-H18D···O3B	0.980	2.560	3.283	130.58	*-x+1/2, y-1/2, -z+1*
C18B-18E···O7B	0.980	2.456	3.392	159.57	*-x+1/2, y+1/2, z+1*

3.2.1 (rac)-DTTA hydrate and DMSO solvate

The *(rac)*-DTTA·H_2O structure is completely different from the DBTA counterpart. The *(rac)*-DTTA·H_2O structure was solved in a monoclinic crystal system and in the achiral space group $P2_1/n$ (No. 14) with two DTTAs and a full water molecule in the asymmetric unit. (Fig 3.15) The crystal contains both enantiomers of the DTTA in 1:1 ratio and the asymmetric unit was selected in a way that both enantiomers are included. The torsion angles describing the tilt around the central alkane bond of the DTTA molecules (O5A-C1A-C15A-O19A and O5B-C1B-C15B-O19B) are -64.14° and 63.20, respectively. The benzoate groups are almost planar: -8.53° and 2.71° for molecule A (*L*-enantiomer), and -6.25° and -6.32° for molecule B (*D*-enantiomer). The plane angle between the phenyl rings are similar to the equivalent DBTA structure (34.32° and 21.19° for *L*- and *D*-DTTA, respectively) as a result of a more closed conformation. The overlay of the two enantiomers shows minor differences in their overall molecular geometry (RMSD= 0.2123 Å and Max. D= 0.4653 Å) when inversion of permitted.

The fingerprint plots are presented on Fig 3.16 and their visual comparison illustrates a very similar crystallographic environment for the two molecules. However, when the values of the % contribution of the different interactions are compared, there are some noticeable differences. The % contribution from the C···H interactions is ca. 2 % more for molecule A while the O···H interactions are more prominent in molecule B (39.2% vs. 36.3%).

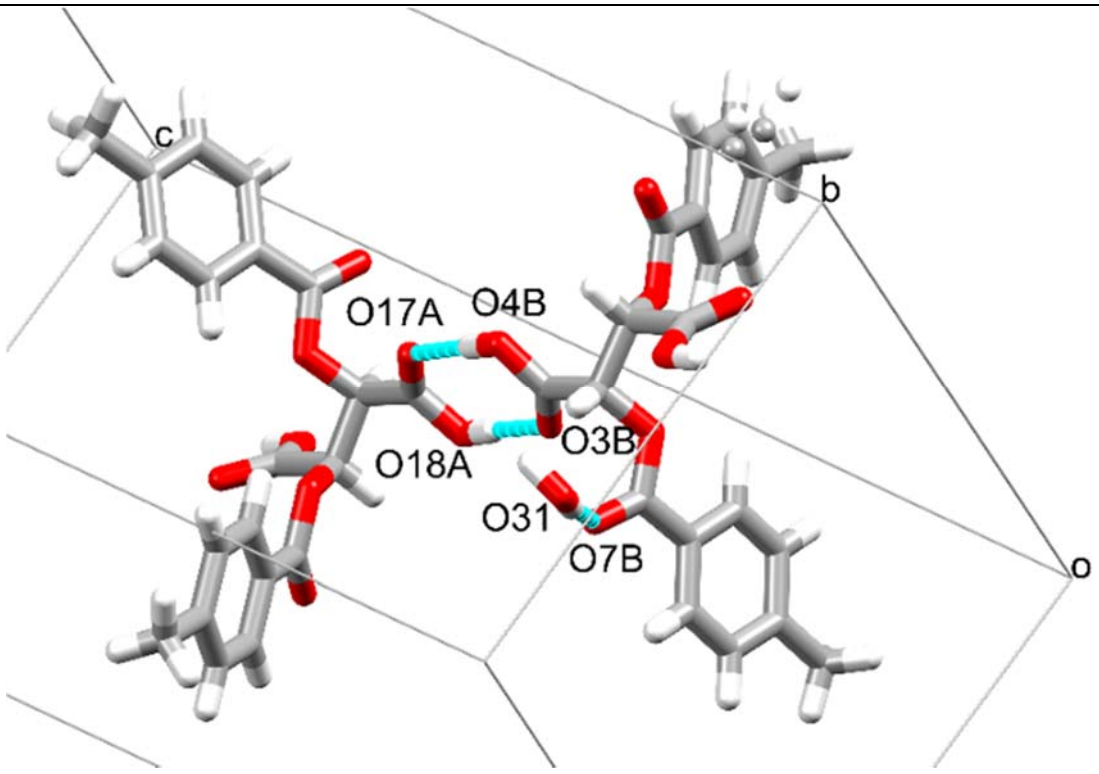

Figure 3.15 The asymmetric unit of (rac)-DTTA·H_2O with the two enantiomers forming a carboxylic acid dimer.

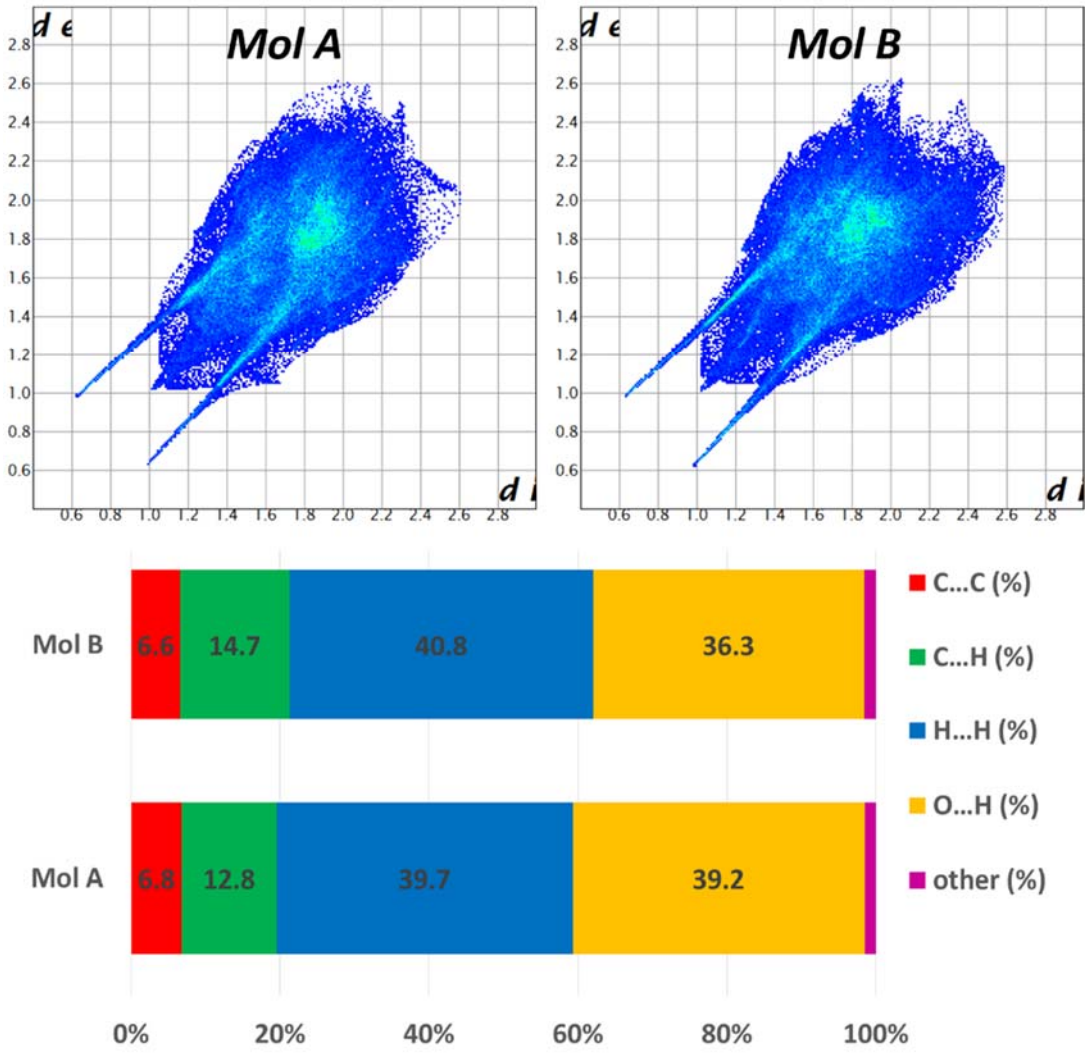

Figure 3.16 Fingerprint plots and the summary of the % contributions of the different interactions for Mol A and Mol B in (rac)-DTTA·H_2O.

This is the only structure where the well-known $R_2^2(8)$ carboxylic acid dimer formed between two tartaric acid derivatives (molecule A and B) via O18A-H18A···O3B and O4B-H4B···O17A. (Fig 3.17) The other carboxylic acid groups form $R_3^3(13)$ synthons with the involvement of a water molecule and a carbonyl group. The *D* enantiomer (Fig 3.17, blue) shows disorder in the position of one of its aromatic rings with 67 % site occupancy for the main atoms (blue). The atoms related to the minor disorder are shown with yellow on Fig 3.17. The heterochiral units arrange to form chains of molecules (Fig 3.18, purple molecules) and the neighbouring chains interact via water bridges and aromatic interactions with the centroid distance of 3.67 Å.

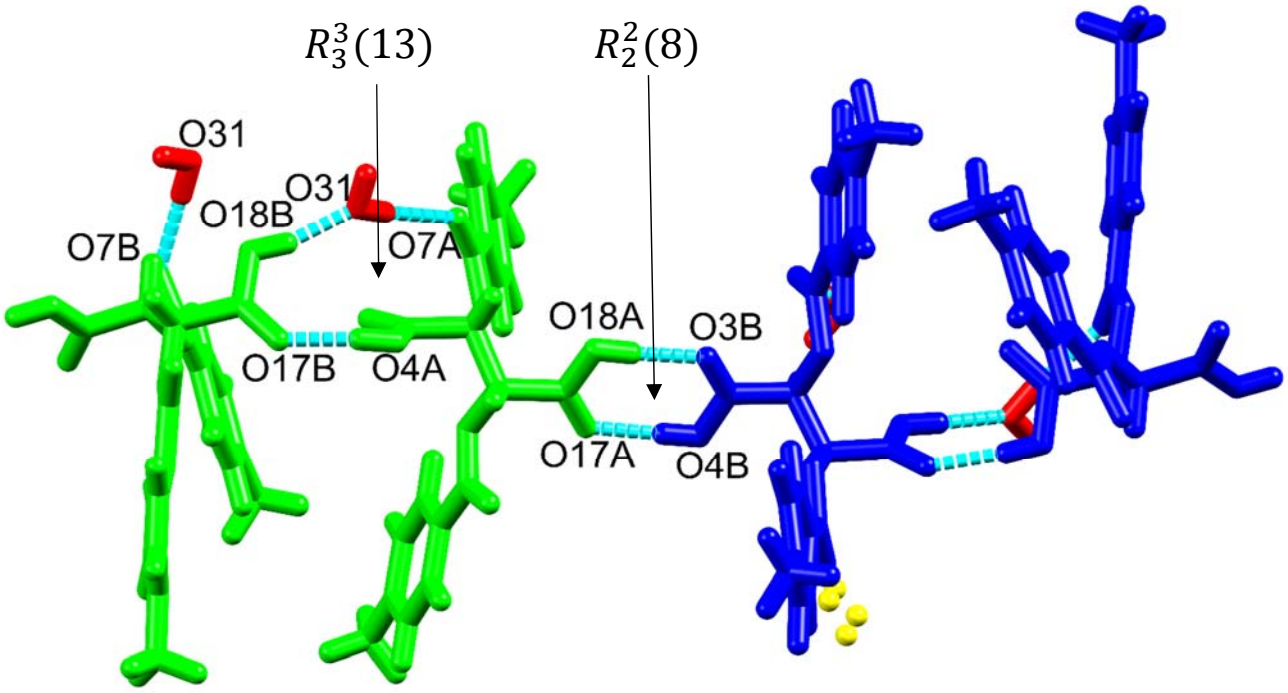

Figure 3.17 Hydrogen bonding and relevant synthons between L and D-DTTAs in (rac)-DTTA·H_2O (coloured with green and blue, respectively). Molecule B shows disorder in the position of the aromatic ring (yellow atoms).

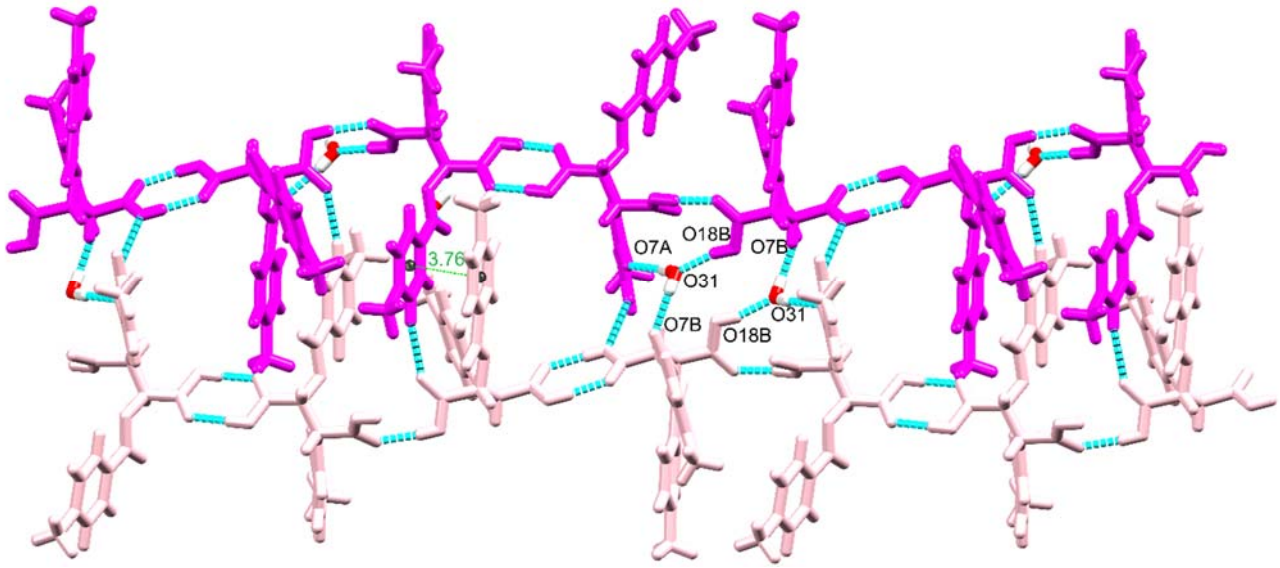

Figure 3.18 Packing arrangement of (rac)-DTTA·H_2O with the hydrogen bonded chains of molecules (purple) and the interactions formed with the neighbouring chain (light purple).

The structure of the DMSO solvate of *(rac)*-DTTA is very similar to the DBTA equivalent. The (*rac*)-DTTA·DMSO solvate was solved in the tetragonal space group $I\bar{4}$ (No. 82), with half a *D*-DBTA and a full DMSO molecule in the asymmetric unit (Fig 3.19a) and the DBTA molecule is in Wyckoff position *e*. The other enantiomer is generated by a 2-fold rotoinversion axis. The torsion angle describing the tilt around the central alkane bond of the DTTA molecule (O5-C1-C1'-O5') is 65.36° (measured on the *D*-enantiomer), and the plane angle between the two phenyl rings is 31.45°. The benzoate group is more tilted when compare to previously discussed structures (O7-C6-C8-C9 is -15.53°). Similarly to the *(rac)*-DBTA·DMSO structure, both carboxylic acid functional groups form hydrogen bonds to the DMSO molecules via O4-H4···O15 to build the 1:2 DTTA:DMSO crystal, and the rotation of the carboxylic acid groups enable the formation of two additional hydrogen bonds between the aromatic ring of the neighbouring DTTA (C12-H12···O3). (Fig 3.19b) Because of the additional methyl groups on the aromatic rings, there is no hydrogen bond formation possible between the DMSO and the aromatic hydrogens, what can be seen in the molecular units formed in the *(rac)*-DBTA·DMSO structure. Similarly to that, the main supramolecular unit is the heterochiral molecular assembly and the packing of the units is shown on Fig 3.20. Contrary to the *(rac)*-DBTA·DMSO structure, these heterochiral units interact via weak C10-H10···O7 hydrogen bonds.

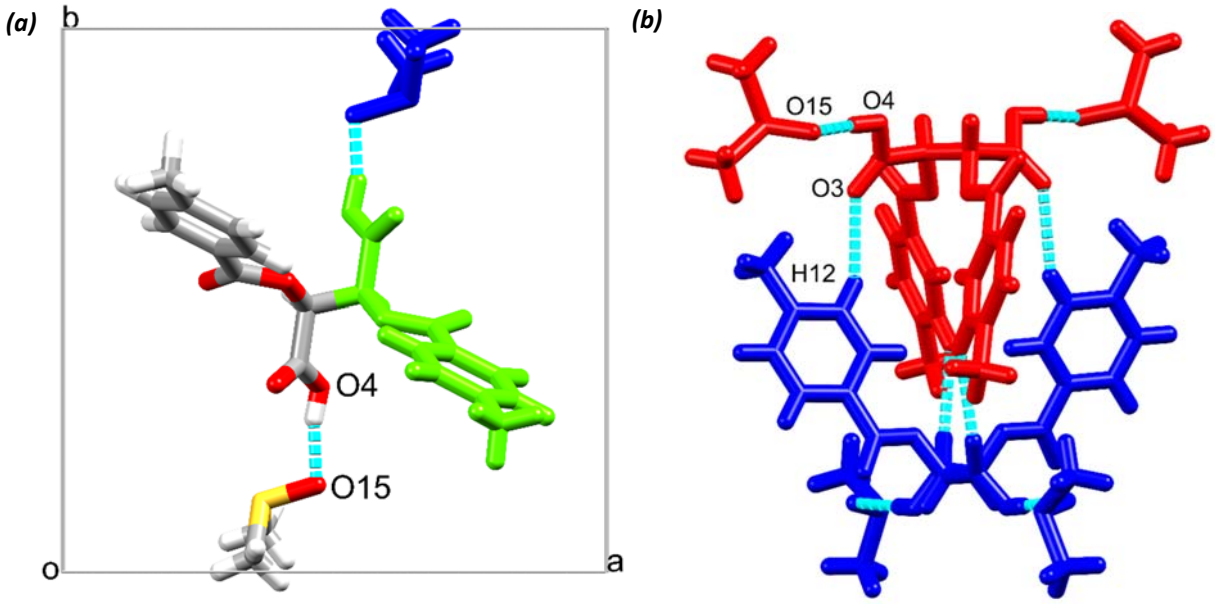

Figure 3.19 (a) Asymmetric unit (atoms coloured by elements) of (rac)-DTTA·DMSO with labelled atoms involved in the hydrogen bond. (b) The interlocking unit of (rac)- DTTA·DMSO (D-DTTA blue, L-DTTA red).

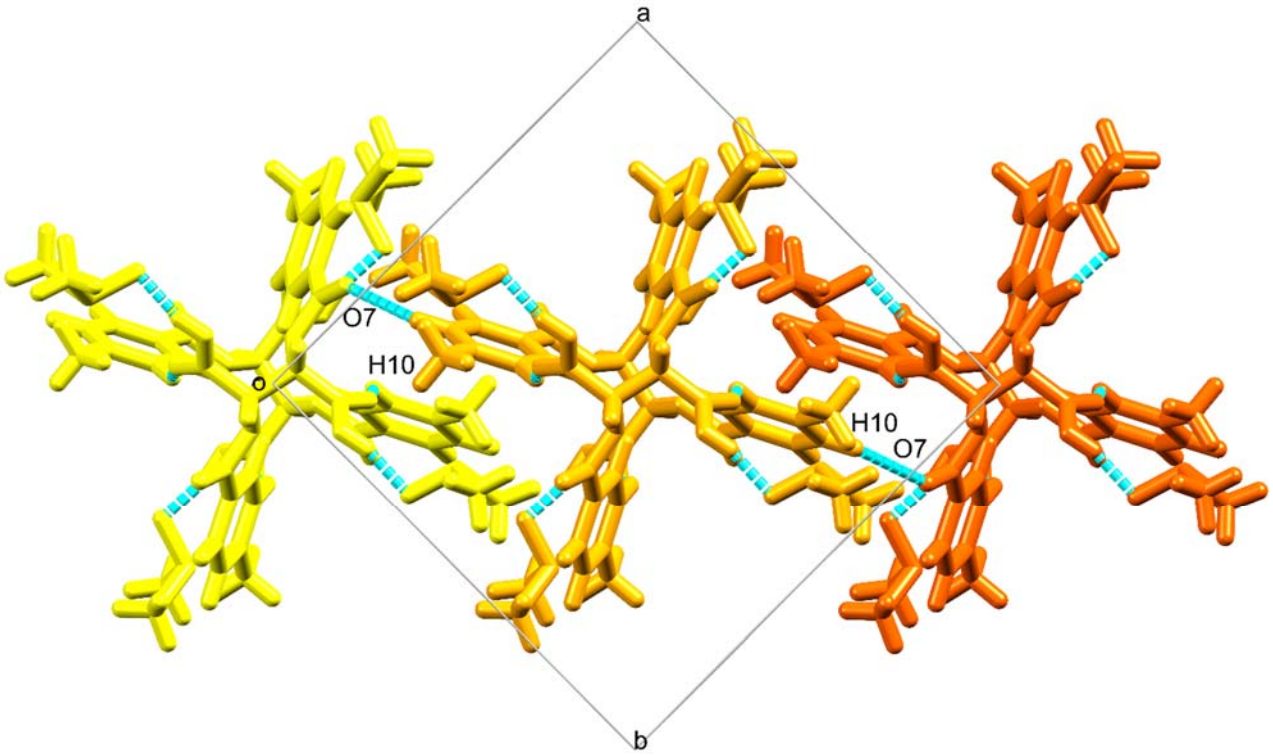

Figure 3.20 Packing view down 001 of the neighbouring heterochiral units via weak interactions between the aromatic hydrogens and the carbonyl groups in (rac)-DTTA DMSO.

3.2.2 L-DTTA hydrate and DMSO solvate

The *L*-DTTA·H_2O structure was solved in an orthorhombic crystal system and in the space group $P2_12_12_1$ (No. 19). Its packing and hydrogen bonding are very similar to the *L*-DBTA·H_2O structure but has one molecule of *L*-DTTA and one water in the asymmetric unit only. Similarly to the *L*-DBTA·H_2O, one of the carboxylic acid group of the DTTA is hydrogen bonding to the water via O18-H18···O29 (Fig 3.21). The torsion angles describing the tilt around the central alkane bond of the DTTA molecule (O5-C1-C15-O19) is very similar to the values found in the previously described DTTA structures (-67.73°). However, the plane angle between the phenyl rings is significantly larger in this structure (43.49°). It is interesting to note that one of the benzoate groups is basically coplanar with the phenyl ring (O21-C20-C22-C27 is 3.86°), while the other is similar to the values of the previous DTTA structures (O7-C6-C8-C9 is 16.83°).

The atoms involved in the formation of the main hydrogen bonds are presented in Fig 3.22. The carboxylic acid moieties link the DTTAs into chains in (100) direction via O4-H4···O17 hydrogen bonds and the water is incorporated into this motif to form $R_3^3(13)$ synthon.

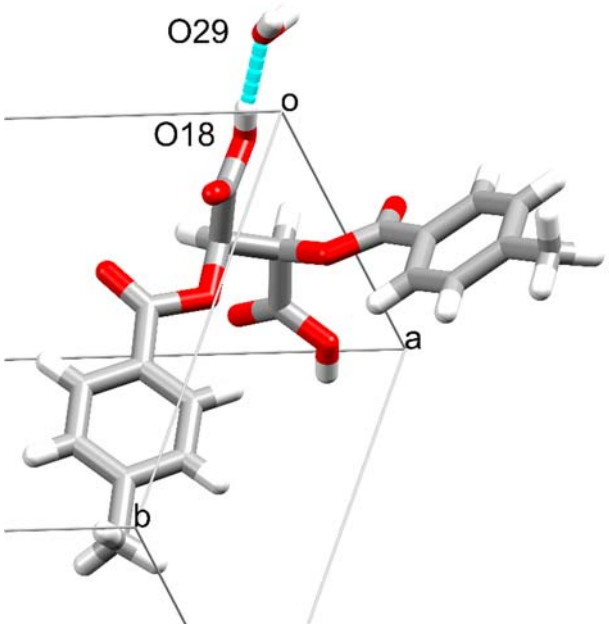

Figure 3.21 The asymmetric unit of L-DTTA H_2O showing the hydrogen bonding between the DTTA and the water molecules.

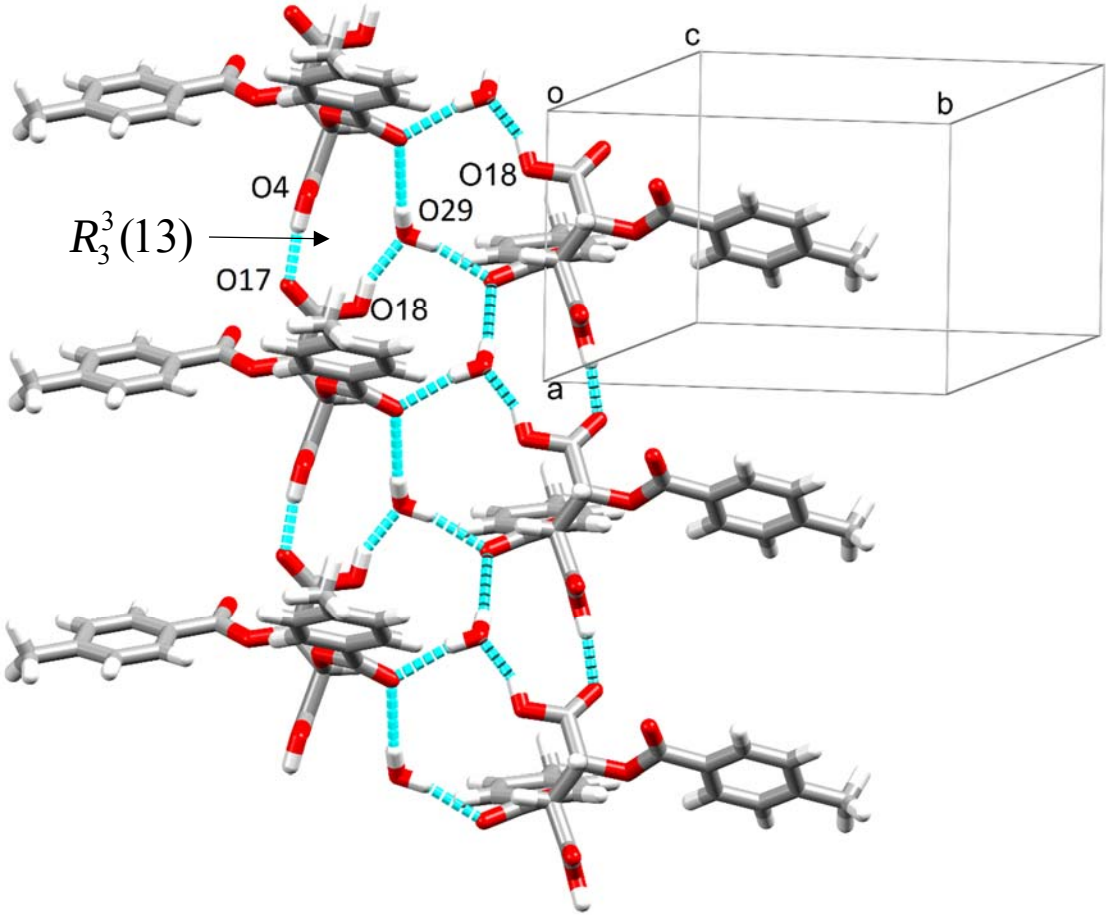

Figure 3.22 Main hydrogen bonding in L-DTTA·H_2O down (100).

The neighbouring hydrogen bonded *L*-DTTA molecules are interlock into each other via aromatic interactions between their phenyl rings (Fig 3.23) with centroid distances of 3.9 Å. This interlocking happens in a manner that results in the formation of channels in the (100) direction. Similarly to the *L*-DBTA·H_2O structure, the channels are empty and the included water molecules are positioned at the outskirts of the channel forming DTTAs. (Fig 3.24)

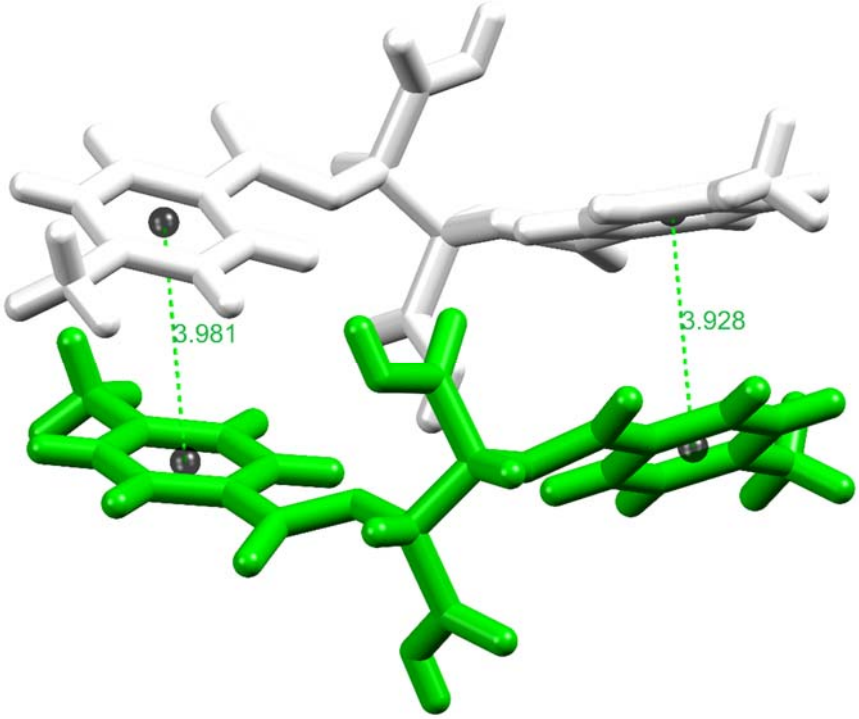

Figure 3.23 Aromatic interactions between the L-DTTA molecules of parallel chains.

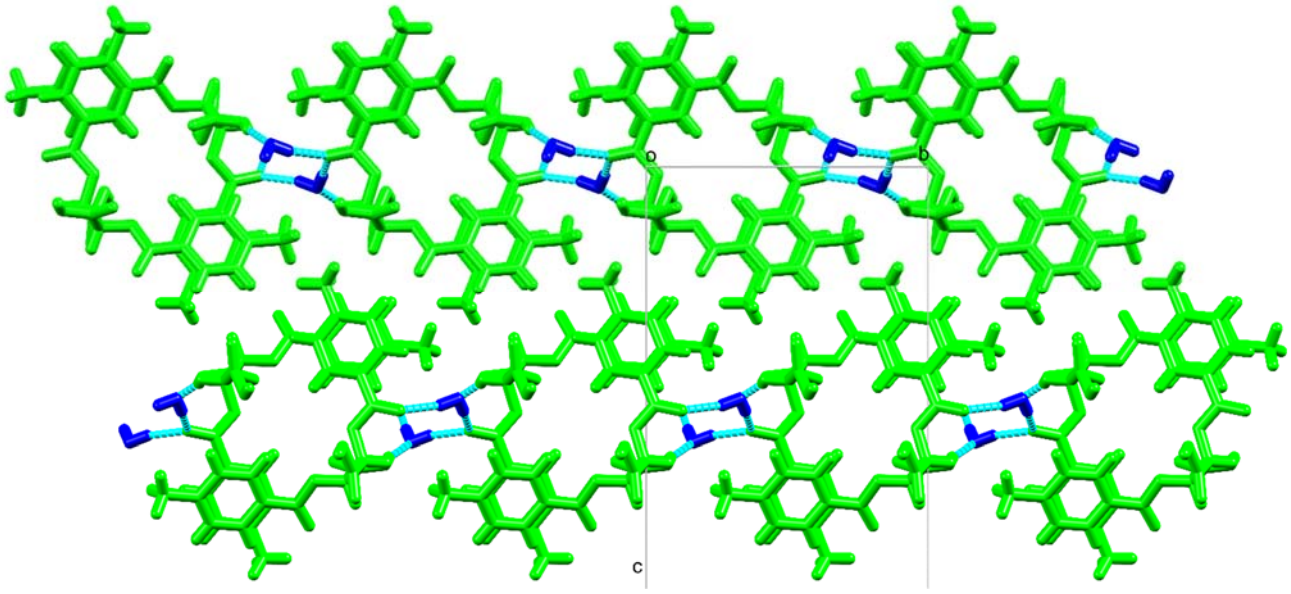

Figure 3.24 Crystal packing and hydrogen bonding in L-DTTA·H_2O view down (100). Note the empty space inside the channels formed by the L-DTTA molecules.

The crystals of *L*-DTTA·DMSO crystallizes in the monoclinic *C*2 (No. 5) space group with two half molecules of *L*-DTTA and two DMSOs in the asymmetric unit and the full molecules are generated by a 2-fold axis. One of the DTTA (molecule A) is located in Wyckoff position 2*a,* while molecule B is on Wyckoff position 2b. Both *L*-DTTA hydrogen bonds to two DMSO molecules via O4-H4···O15. (Fig 3.25) The conformation of the two symmetry independent DTTA molecules is very similar (RMSD= 0.2411 Å and Max. D= 0.4382 Å) and their molecular fitting is shown in Fig. 3.26. The torsion angles describing the tilt around the central alkane bond of the DTTA molecules (O5-C1-C1*-O5*) is similar to the *L*-DBTA·DMSO structure (-81.72° and -75.74° for molecules A and B, respectively). The benzoate groups are almost coplanar with the phenyl rings (-5.33° and -2.15° for molecule A and B, respectively) and the plane angles between the phenyl rings are almost identical to the value found in the *L*-DBTA·DMSO structure (79.28° and 77.94° for molecule A and B, respectively).

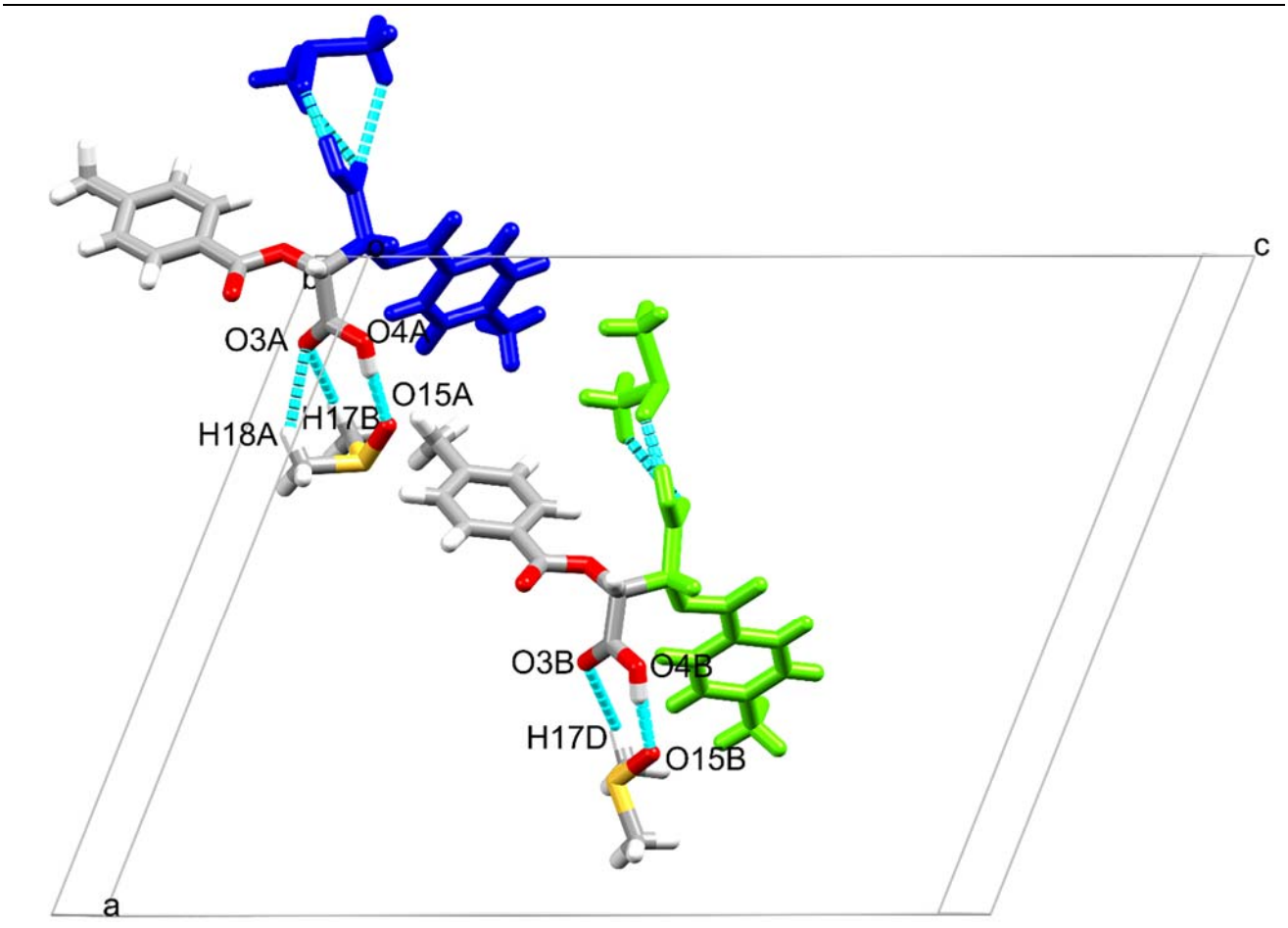

Figure 3.25 The molecular unit of L-DTTA·DMSO with labelled atoms involved in the hydrogen bond (atoms coloured by element form the asymmetric unit).

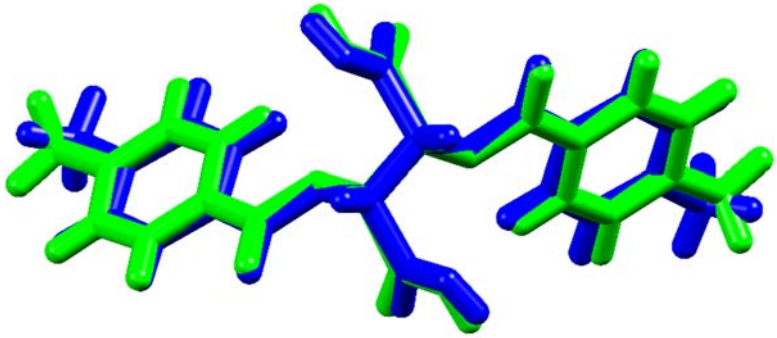

Figure 3.26 Molecular fitting of molecule A and B of L-DTTA·DMSO. (molecule A- blue, molecule B- green).

Contrary to the conformational similarities, the assessment of the fingerprint plots of the two symmetry independent molecules reveal that the interactions of these molecules with the surrounding molecules are different. (Fig 3.27) Although the shape of the plots are still very similar, but there is notable differences in the C·· H and the H···H % contributions. Namely, the % C·· H is larger for molecule B, while the H···H % contributions is more around molecule A. The more evident % C·· H contribution is the result of the close proximity of the methyl hydrogens of the DMSO to the aromatic rings of molecule B. The larger % of H···H contributions for molecule A is the result of the interaction formed with neighbouring DTTA molecules.

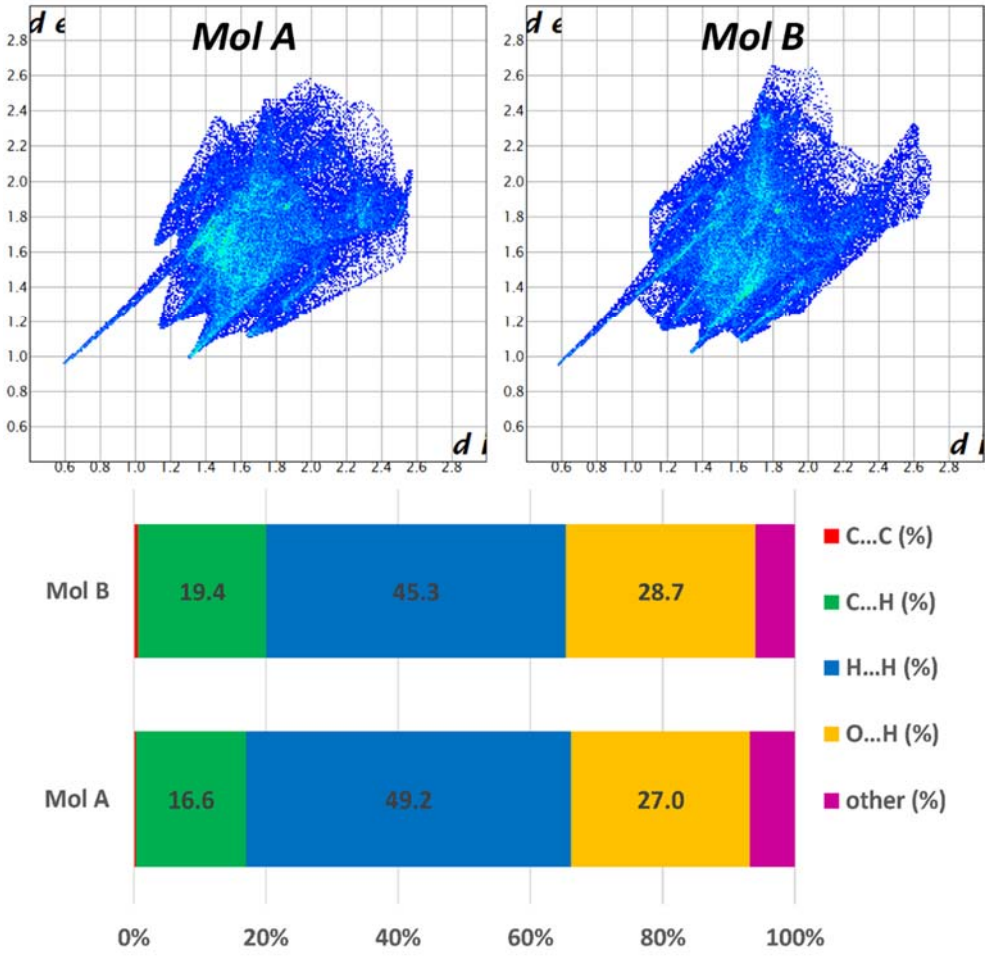

Figure 3.27 Fingerprint plots and the summary of the % contributions of the different interactions for molecule A and B in L-DTTA·DMSO.

The packing of the *L*-DTTA·DMSO crystal structure is very similar to the *L*-DBTA counterpart. The more opened *L*-DTTA molecules are positioned in a head-to-tail manner along the 2-fold axis down *b*, similarly what was described in the *L*-DBTA·DMSO structure, and form polar columns of hydrogen bonded molecules (Fig 3.28).

The main difference is that this structure has two symmetry independent *L*-DTTA molecules and these are forming two slightly different columns. In the column formed from molecule As, there is no strong interactions are noted between the molecular units (Fig 3.28a). Contrary to this, in the other column, a few additional weaker hydrogen bond is formed between the neighbouring *L*-DTTA molecules (C13B-H13B···O4*), among the *L*-DTTAs and the DMSOs (C12-H12···O15*) and between two neighbouring DMSOs (C17B-H17E···O15B). The DMSO molecules are positioned in channels created between the polar columns of the DTTAs down (010) direction. (Fig 3.29) The dissimilarities of the arrangements of the molecules in the two columns are best presented in this figure, when the packing is viewed down the *b* axis, because of the noticeable striking difference between the positions of the hydrogen bonded DMSOs.

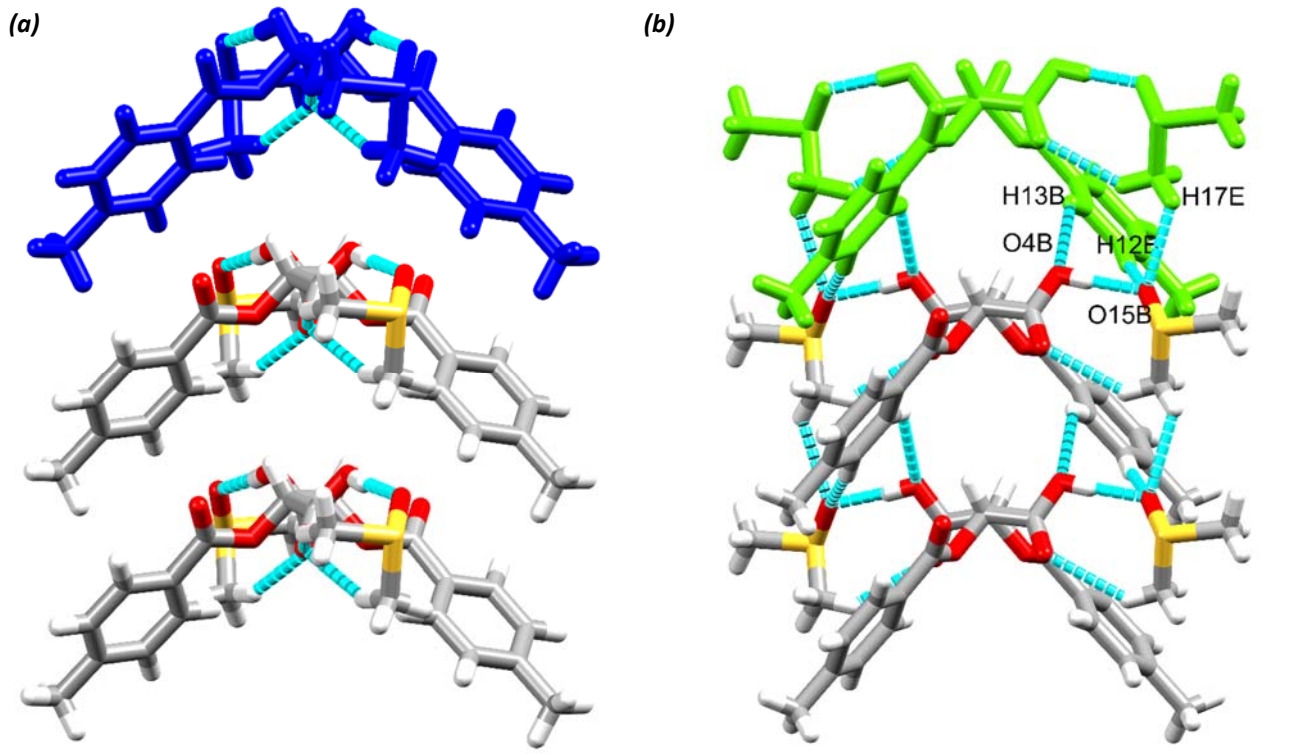

Figure 3.28 The structures of the polar columns formed in L-DTTA DMSO (a-column formed by molecule As, b- formed by molecule Bs) Note the lack of close contacts between molecules in column built from molecule As.

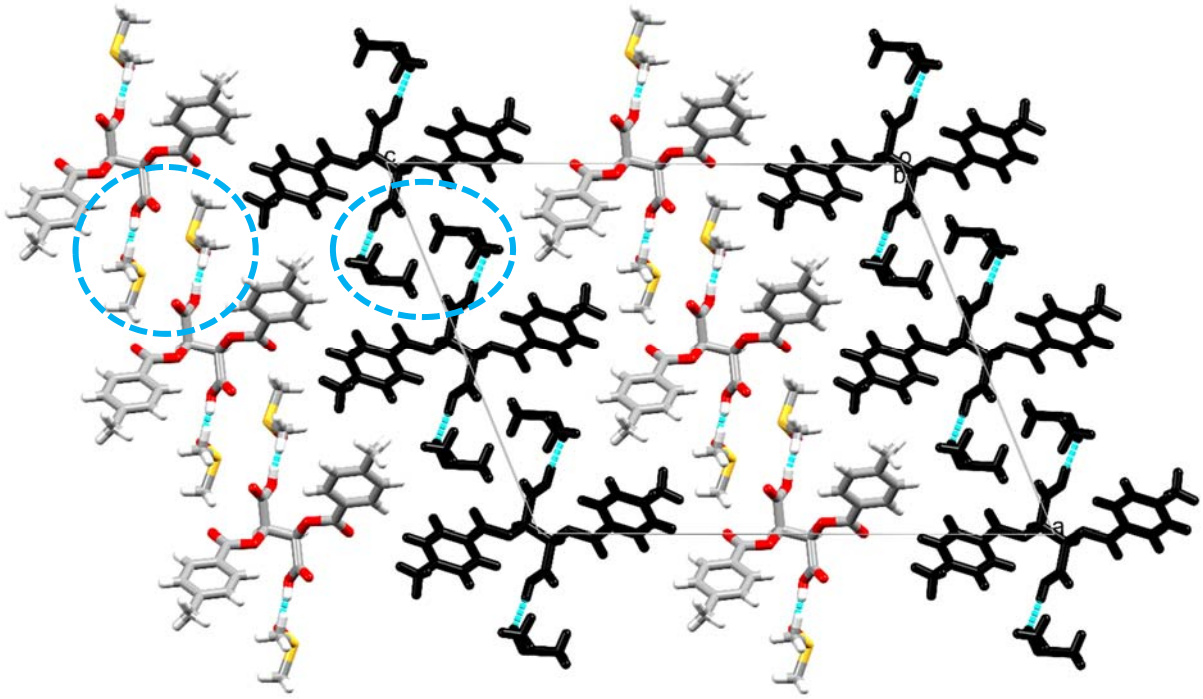

Figure 3.29 Packing differences of the DMSO molecules between hydrogen bonded columns formed from molecule As (black) and molecule Bs (coloured by elements) view down (010). Note the blue circled section to emphasize the different positions of the DMSO molecules.

3.3 Bulk property analysis of solvates of TA derivatives (DSC, TG and PXRD)

The racemic mixtures of DBTA and DTTA were made by mixing the *L*- and the *D*-enantiomers in a 1:1 ratio. Thus the purity of both the *L*- and *D*-DBTA/DTTA were analysed before crystallisations were carried out. The compound were purchased and the supplier did not state the existence of any possible solvent residue in the samples. The melting point of the *L*- and the *D*-enantiomer pairs are expected to be the same, and, in our case, also for the 1:1 physical mixture of the two enantiomers. The thermal behavior of the crystals are represented by the onset and the peak temperature of the melting and the concomitant enthalpy change. (Appendix Fig. A1-A10) The DSC results (summarized in Table 3.5) showed that some of the starting materials contained water, possibly as surface solvent, or a small amount of solvent of crystallisation. The amount was not stoichiometric, thus the compounds were dried under vacuum for a short time to get rid of the water, and were used without further purification. The visual analysis of the DSC curves revealed that the hydrate crystals go through a desolvation step below 100°C and the remaining solid melts at a temperature close to the melting temperature of the pure starting material. In contrast, the lack of the endotherm related to the melting of the DBTA/ DTTA host after the decomposition of the DMSO solvates suggests congruent melting, i.e. the desolvation of these inclusion compounds leads directly to a liquid region with solid-liquid coexistence at a single temperature, the actual melting point.

The analysis of the thermogravimetric results (Appendix Fig. A11-A18, summarized in Table 3.6) showed that the hydrates are prone to dehydrate even during a short storage. The typical crystallisation stoichiometry is 1:2 (host-guest) hence the two carboxylic acid is likely to hydrogen bond to two guests. Interesting to note the appearance of the occasional 1:1 or 2:1 host-guest stoichiometry in *L*-DTTA·H_2O and *(rac)*-DTTA·H_2O. These crystals seem to be less likely to dehydrate and this property may be reasoned with the more hydrogen bond formation around the water molecules. In case of the DMSO solvates the desolvation overlaps with the melting when observed with TG and the solvent content cannot be calculated reliably. Based on the DSC results, the starting materials (mainly the *L*- and the *D*-DTTA) are hygroscopic and thus the received samples have some possibly surface water bounded. This minimal water content of the starting materials cannot be seen on the TGs.

Table 3.5 Summary of DSC results

Compounds/crystals	**Desolvation (T_{on} / T_{peak} / °C)**	**Melting (T_{on} / T_{peak} / °C)**
Starting materials (literature results)		
L-DBTA	-	152 / 155
D-DBTA	-	154 / 156
L-DTTA	-	169 / 171
D-DTTA	-	169 / 171
Starting materials (onsite laboratory measurements)		
L-DBTA·xH_2O	89.76 / 92.07	154.8 / 157.6
D-DBTA·xH_2O	90.15 / 92.04	156.5 / 158.5
L/D-DBTA (1:1)	89.76 / 98.11	166.6 / 172.3
L-DTTA·xH_2O	114.81 / 118.10	-
D-DTTA·xH_2O	115.18 / 118.87	-
L/D-DTTA (1:1)	114.92 / 117.73	163.4 / 169.5
Crystals		
(rac)-DBTA·H_2O	76.80 / 95.83	171.3/ 175.8
(rac)-DBTA·DMSO	106.08 / 112.97	-
L-DBTA·H_2O	83.97 / 95.06	210.0 /218.0
L-DBTA·DMSO	107.10 / 110.41	-
(rac)-DTTA·H_2O	95.18 / 111.35	194.0 / 199.8
(rac)-DTTA·DMSO	95.29 / 127.62	-
L-DTTA·H_2O	59.24 / 84.47	152.0 / 162.7
L-DTTA·DMSO	93.08 / 95.71	-

Table 3.6 Summary of TG results

Crystals	Host:Guest	Mass loss % (Calc)	Mass loss % (Exp)	Δ %	remarks
(rac)-DBTA·H_2O	1:2	9.56	7.98	-1.58	Crystals dehydrated
(rac)-DBTA·DMSO	1:2	35.8	-	-	-
L-DBTA·H_2O	1:1	4.78	3.87	-0.91	Crystals dehydrated
L-DBTA·DMSO	1:2	35.8	-	-	-
(rac)-DTTA·H_2O	2:1	2.27	2.27	0	
(rac)-DTTA·DMSO	1:2	28.79	-	-	-
L-DTTA·H_2O	1:1	4.45	1.93	-2.52	Crystals dehydrated
L-DTTA·DMSO	1:2	28.79	-	-	-

The homogeneity of the bulk material was also tested with PXRD and was compared to the single crystal structures (Appendix Fig. A19-A26). Good agreement between the single crystal structure and the bulk material was found in 5 compounds: *(rac)*-DBTA·H_2O, *L*-DBTA·DMSO, *(rac)*-DTTA·DMSO, *L*-DTTA·H_2O and *L*-DTTA·DMSO. Only partial agreement can be seen between the single crystal and the bulk structure in case of *L*-DBTA·H_2O; and no similarities are noted for *(rac)*-DBTA·DMSO and *(rac)*-DTTA·H_2O. The differences for the latter two hydrates can be explained with the dehydration of the crystals and the concomitant structural changes, while the explanation of the difference observed for the DMSO solvate needs further experiments.

4. Chiral discrimination experiments

The chiral discrimination experiments of racemic mixture of DBTA and DTTA were carried out with the 4 traditional cinchona alkaloids: *(-)*-quinine (QUIN), *(+)*-quinidine (QUID), *(+)*-cinchonine (CINC) and *(-)*-cinchonidine (CIND). The crystallisations were set in a 2:1 (base:diacid) molar ratio to ensure that the dicarboxylic acid can maximize the hydrogen bond formation, i.e. the solutions contain enough base to hydrogen bond to both carboxylic acid moieties. The general method was, at first, exposing the racemic mixture of acids to the cinchona alkaloid and harvesting the first possibly suitable crystals for single crystal X-ray diffraction. When the preference of the alkaloid towards a given enantiomer was established from the crystal structure, a new crystallisation were set with the same alkaloid and with the uncaptured enantiomer only. The structures of the harvested crystals from these, so called 'forced' crystallisations, were compared to the outcome of the first experiments. Results were obtained from all combination but only the experiments with cinchonidine will be discussed in this thesis. (Table 4.1) Table 4.2 contains crystallographic data for the structures and Table 4.3 summarizes their most prominent hydrogen bonds. The homogeneity of the bulk materials were analysed by DSC and PXRD, and their similarity with the single crystal structures were analysed and the results are shown in the Appendix (Fig. A27-A38)

Table 4.1 Outcome of the discrimination experiments with CIND and their meting points.

	***(rac)*-DBTA**	***D*-DBTA**	***(rac)*-DTTA**	***D*-DTTA**
CIND	[CIND$^+$][*L*-DBTA$^-$]	2[CIND$^+$][*D*-DBTA^{2-}]	[CIND$^+$][*L*-DTTA$^-$]	2[CIND$^+$][*D*-DTTA^{2-}]·2DMSO·0.7H_2O
MP (°C)	205.07 / 214.18	219.49 / 224.63	216.30 / 218.65	152.42 / 156.74

4.1 Discrimination of DBTA enantiomers

When racemic mixture of *L*- and *D*-DBTA was crystallized with CIND from ethanol-water (1:1), the single crystal X-ray analysis of the harvested crystals revealed that the CIND formed a salt with the *L*-enantiomer of the acid only, [CIND$^+$][*L*-DBTA$^-$]. The structure was solved in the orthorhombic $P2_12_12_1$ (No. 19) space group with a full L-DBTA and one CIND in the asymmetric unit. One of the carboxylic acid group of the DBTA is deprotonated and the hydrogen is transferred to the quinuclidine moiety of the CIND to form a molecular salt. (Fig. 1) The carboxylic acid and the phenyl, i.e. the benzoate groups are almost planar (O41-C40-C42-C47 is -6.00° and O49-C48-C50-C51 is 7.03°); the torsion angle describing the tilt around the central alkane bond of the molecule (O36-C31-C32-O37) is –70.81°, and the plane angle between the two phenyl rings is 56.26°. These values suggest that the conformation of the *L*-DBTA is similar to what was found in *L*-DBTA·H_2O.

Table 4.2 Crystallography data for salts of CIND.

Compounds	**[CIND$^+$][*L*-DBTA$^-$]**	**2[CIND$^+$][*D*-DBTA^{2-}]**	**[CIND$^+$][*L*-DTTA$^-$]**	**2[CIND$^+$][*D*-DTTA^{2-}] ·2DMSO·0.7H$_2$O**
Molecular formula	$C_{37}H_{36}N_2O_9$	$C_{56}H_{58}N_4O_{10}$	$C_{39}H_{40}N_2O_9$	$C_{62}H_{75.40}N_4O_{12.70}S_2$
Formula Weight (g.mol^{-1})	652.68	947.06	680.73	1143.98
Crystal system	orthorhombic	monoclinic	orthorhombic	Monoclinic
Space group (No.)	$P2_12_12_1$ (19)	$P2_1$ (4)	$P2_12_12_1$ (19)	$P2_1$ (4)
a (Å)	12.0627(3)	10.3762(3)	11.794(2)	9.9025(9)
b (Å)	12.5145(3)	25.2895(18)	12.994(3)	24.403(2)
c (Å)	21.4636(5)	10.4028(8)	22.858(5)	12.3472(11)
α (°)	90	90	90	90
β (°)	90	115.624(1)	90	92.680(2)
γ (°)	90	90	90	90
V (Å^3)	3240.12(13)	2461.3(3)	3502.9(12)	2980.4(5)
Z	4	2	4	2
ρ_{calc} (g.cm^{-3})	1.338	1.278	1.291	1.275
μ (MoKα) (mm^{-1})	0.096	0.088	0.092	0.115
F (000)	1376	1004	1440	1218
Crystal Size (mm)	0.30×0.30×0.37	0.362×0.398×0.612	0.040×0.170×0.360	0.293×0.376×0.489
Temperature (K)	173(2)	173(2)	173(2)	173(2)
Radiation (Å)	MoKα, 0.71073	MoKα, 0.71073	MoKα, 0.71073	MoKα, 0.71073
Theta min-max (°)	1.937; 26.370	2.171; 28.355	1.782; 28.308	2.059; 28.408
Dataset (±h; ±k; ±l)	-15:12; -11:15; -13:26	-13:13; -31:33; -13:12	-15:15; -16:17; -24:30	-8:13; -32:31; -16:31
Final R indices [I>2σ(I)]	0.0317; 0.0317	0.0371; 0.0884	0.0937; 0.1836	0.0528: 0.1372
R indices [all data]	0.0365; 0.0793	0.0419; 0.0917	0.1128; 0.1916	0.0528; 0.1440
Tot., uniq. data, R (int)	6469; 5888; 0.0182	10976; 10046; 0.0159	8697; 6980; 0.0353	14278; 12654; 0.0243
N_{ref}, N_{par}	6469; 435	10976; 635	8697; 473	14278; 771
S	1.030	1.018	1.109	1.044
Max. and av. Shift/error	0.000/0.000	0.000/0.000	0.000/0.000	2.265/0.019
Min. and max. resd. dens.(Å^3)	-0.153; 0.194	-0.204; 0.197	-0.322 ;0.357	-0.617 ;0.858

Table 4.3 Hydrogen bond details for salts of CIND.

D-H···A	d(D-H) (Å)	d(H···A) (Å)	d(D···A) (Å)	D-H···A (°)	Symmetry Operators
[CIND$^+$][*L*-DBTA$^-$]					
C9-H9···O34	1.000	2.639	3.377	130.66	
N11-H11···O34	0.977	1.668	2.642	173.46	
C13-H13···O49	1.000	2.624	3.387	133.11	*x-1, y, z*
C17-H17B···O24	0.990	2.299	2.992	126.20	
C17-H17B···O49	0.990	2.529	3.135	119.36	*-x,y-1/2,-z+1/2*
O24-H24···O35	0.840	1.954	2.726	152.24	*-x,y-1/2, -z+1/2*
C32-H32···O24	1.000	2.197	3.059	143.57	*-x,y-1/2, -z+1/2*
O38-H38···N1	0.966	1.631	2.577	164.98	*-x+1/2,-y+1,z-1/2*
2[CIND$^+$][*D*-DBTA^{2-}]					
N11A-H11A···O34	0.884	1.855	2.739	177.35	
N11A-H11A···O35	0.884	2.486	3.060	123.08	
C12A-H12A···O35	0.990	2.576	3.185	119.73	
C15A-H15B···N1B	0.990	2.574	3.457	148.56	*-x+1, y+1/2, -z*
C17A-H17B···O24A	0.990	2.466	3.082	119.95	
O24A-H24A···O39	0.840	1.850	2.667	163.97	*x+1, y, z*
C9B-H9B···O38	1.000	2.618	3.403	135.34	
N11B-H11B···O38	0.974	1.718	2.691	176.40	
N11B-H11B···O39	0.974	2.500	3.126	121.91	
C13B-H13B···O34	1.000	2.627	3.556	154.47	*x-1, y, z*
C17B-H17C···O24B	0.990	2.391	3.022	120.90	
O24B-H24B···O35	0.840	1.815	2.648	171.23	*x, y , z+1*
[CIND$^+$][*L*-DTTA$^-$]					
N11-H11···O34	0.811	175.05	2.624	175.05	
C13-H13a···O49	1.000	167.18	3.546	167.18	*x+1, y ,z*
C17-H17B···O24B	0.990	125.82	3.025	125.82	
C17-H17B···O49	0.990	132.01	3.157	132.01	*-x+1 , y-1/2 , -z+1/2*
O24B-H24···O35	0.840	150.48	2.729	150.48	*-x+1 , y-1/2, -z+1/2*
C32-H32··· O24B	1.000	151.58	3.275	151.58	*-x +1 ,y+1/2 ,-z +1/2*
O38-H38··· N1	0.840	155.36	2.626	155.36	*-x+1/2 , -y+1 ,z+1/2*
2[CIND$^+$][*D*-DTTA^{2-}]·2DMSO·0.7H$_2$O					
N11A-H11A···O34	0.880	1.791	2.658	167.71	
N11A-H11A···O35	0.880	2.598	3.201	126.53	
C12A-H12A···O35	0.990	2.512	3.206	126.85	
C16A-H16A···O24A	0.990	2.470	3.018	114.50	
C16A-H16B···O64b	0.990	2.523	3.472	160.58	*-x, y-1/2,-z*
C16A-H16B···O68a	0.990	2.502	3.463	163.59	*-x , y-1/2 , -z*

C17A-H17A···O58c	0.990	2.420	3.397	168.83	
O24A-H24A···O37	0.840	2.551	3.132	127.27	*x-1, y, z*
O24A-H24A···O39	0.840	1.805	2.603	157.95	*x-1, y , z*
C9B-H9B···O38	1.000	2.472	3.290	138.59	
N11B-H11B···O38	0.802	1.926	2.706	163.97	
N11B-H11B···O39	0.802	2.477	3.082	133.28	
C17B-H17C···O24B	0.990	2.548	3.225	125.49	
C17B-H17C···O64b	0.990	2.654	3.541	149.23	
C17B-H17C···O68a	0.990	2.611	3.483	147.05	
O24B-H24B···O64b	0.840	1.949	2.783	172.00	
O24B-H24B···O68a	0.840	1.858	2.689	169.78	
O58c-H58Bc···O35	0.851	2.217	2.750	120.65	
O58c-H59Ac···O60	0.850	1.863	2.706	171.37	
O58c-H59Ac···S61	0.850	2.898	3.635	146.10	
C63-H63B···O64b	0.980	2.645	3.285	123.11	*-x+1 , y -1/2 , -z*
C63-H63C···O35	0.980	2.570	3.522	163.89	
C66a-H66Aa···O38	0.980	2.637	3.570	159.04	
C66a-H66Ba···O60	0.980	2.441	3.310	147.63	*-x , y+1/2 , -z*
C67b-H67Cb···N1B	0.980	2.564	3.537	172.29	*x, y , z-1*

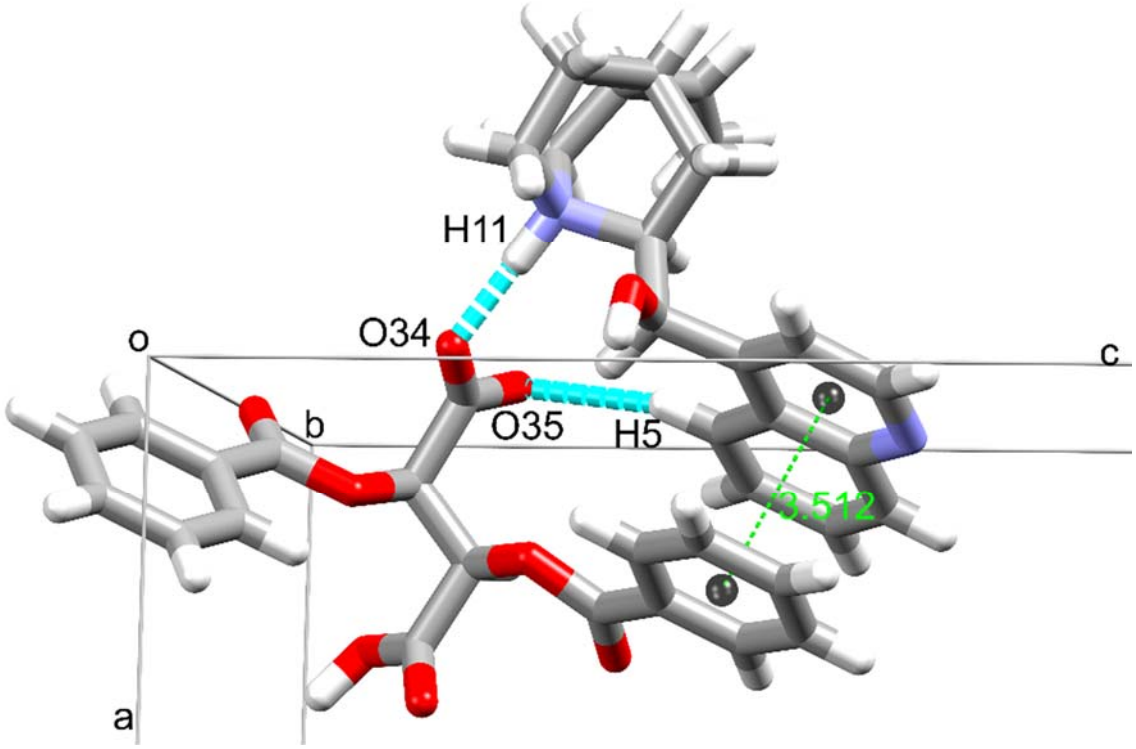

Figure 4.1 Asymmetric unit of [CIND⁺][L-DBTA⁻] with hydrogen bonding between the molecules. Note the aromatic interaction between the phenyl of the acid and the quinoline rings.

The two molecules are held together by a charge assisted hydrogen bond (N11-H11···O34), a weak CH···O contact (C5-H5···O35) and a π···π interaction between the phenyl ring of the acid and the quinoline ring of the base. The rings are almost parallel (∠ 2.74°) and their centroid distance (3.512 Å) lies in the ideal range for aromatic interactions. As an addition to the aromatic interaction formed between the ion pair (shown Fig 4.1), the phenyl ring of the neighbouring DBTA also overlaps with the quinoline ring and forms a three component aromatic system (Fig 4.2). The distance between the quinoline ring and the neighbouring phenyl ring is very similar to the one found amongst the acid and the base forming the ion pair (3.688 Å), but the angle between the two ring is slightly larger (∠ 12.50°). Also, the ion pairs are bonded together via extensive hydrogen bonding running in the two-fold screw axis. The most prominent hydrogen bond forms between the quinoline nitrogen and the carboxylic acid functionality (O38-H38···N1, Fig 4.3).

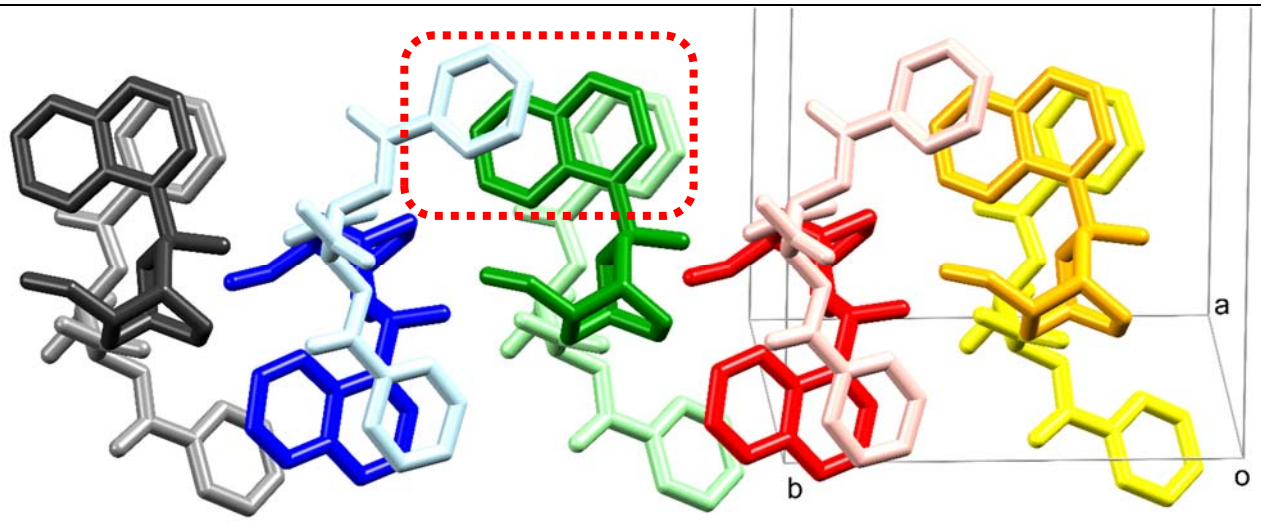

Figure 4.2 Aromatic interactions in [CIND$^+$][L-DBTA$^-$]. Ion pairs are coloured with the same colour (acid with lighter, base with darker shade). The three component aromatic system (circled with red) is formed between neighbouring ion pairs.

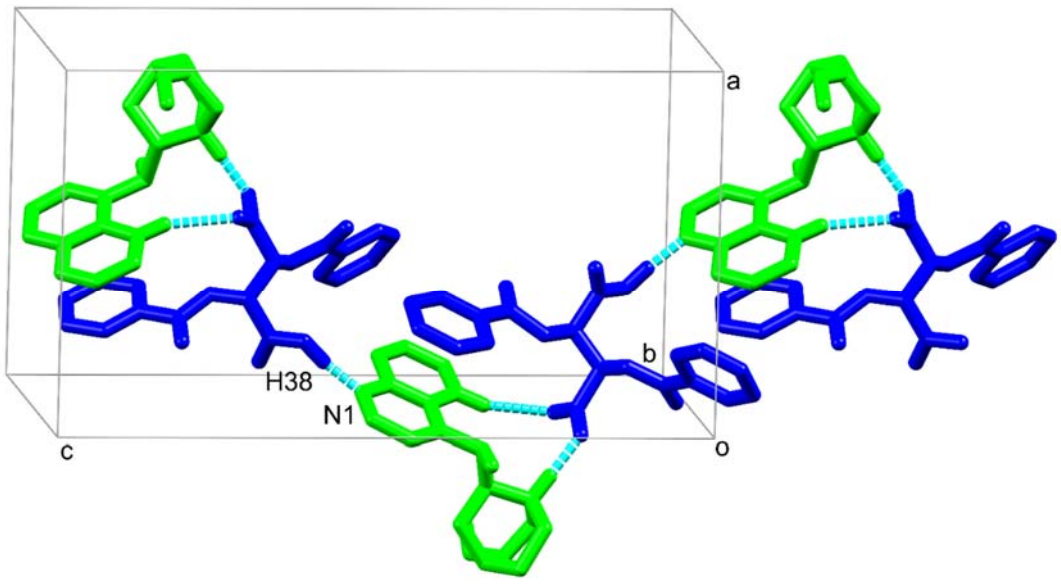

Figure 4.3 Hydrogen bonds between neighbouring ion pairs in [CIND$^+$][L-DBTA$^-$]. (Ion pairs are coloured by symmetry equivalence.)

To understand the preference of CIND for the *L*-enantiomer of DBTA, crystals of CIND and the *D*-enantiomer were crystallized. The crystallisation ratio was kept the same, 1:2 acid vs. base, and the harvested crystals resulted in a salt may be described as 2[CIND^{+}][*D*-DBTA^{2-}]. The structure was solved in the monoclinic $P2_1$ (No. 4) space group with two CINDs and one *D*-DBTA in the asymmetric unit. (Fig 4.4) The acid is di-deprotonated and both CINDs carry positive charges. (The deprotonation of the carboxylic acid groups were confirmed by not only finding the hydrogen atoms in the electron density map in close proximity to the quinuclidine nitrogens, but also by analysing the C-O bond length, which were found to be in the 1.24-1.26 Å range, typical for a carboxylate moiety.) The torsion angle describing the tilt around the central alkane bond of the molecule (O36-C31-C32-O37) is 68.13°, the plane angle between the two phenyl rings is 39.08°, and the benzoate moieties are tilted (O36-C40-C42-C47 is -16.49° and O37-C48-C50-C55 is -15.07°). These values differ from the values observed for DBTA when crystallized in its solvates, and suggest that the *D*-DBTA molecule taken up a more strained, probably less favoured conformation in this 'forced' crystal structure.

The DBTA hydrogen bonds to two CINDs on a very similar manner via the carboxylates to the quinuclidine moiety (N11A-H11A···O34 and N11B-H11···O38) and to the aromatic system of the CINDs (C5A-H5A···O34 and C5B-H5B···O38). The DBTA also forms week interactions with the quinoline ring via its carbonyl moiety (C6A-H6A···O49, C6B-H6B···O41). The conformation of the two symmetry independent CINDs are almost identical (RMSD is 0.1025 Å, Max. D. is 0.2455 Å). These molecular units interact with each other by forming hydrogen bonds via the hydroxyl groups of the CIND to the carboxylate moieties of the neighbouring units (O24A-H24A···O39 and O24B-H24B···O35, Fig 4.5).

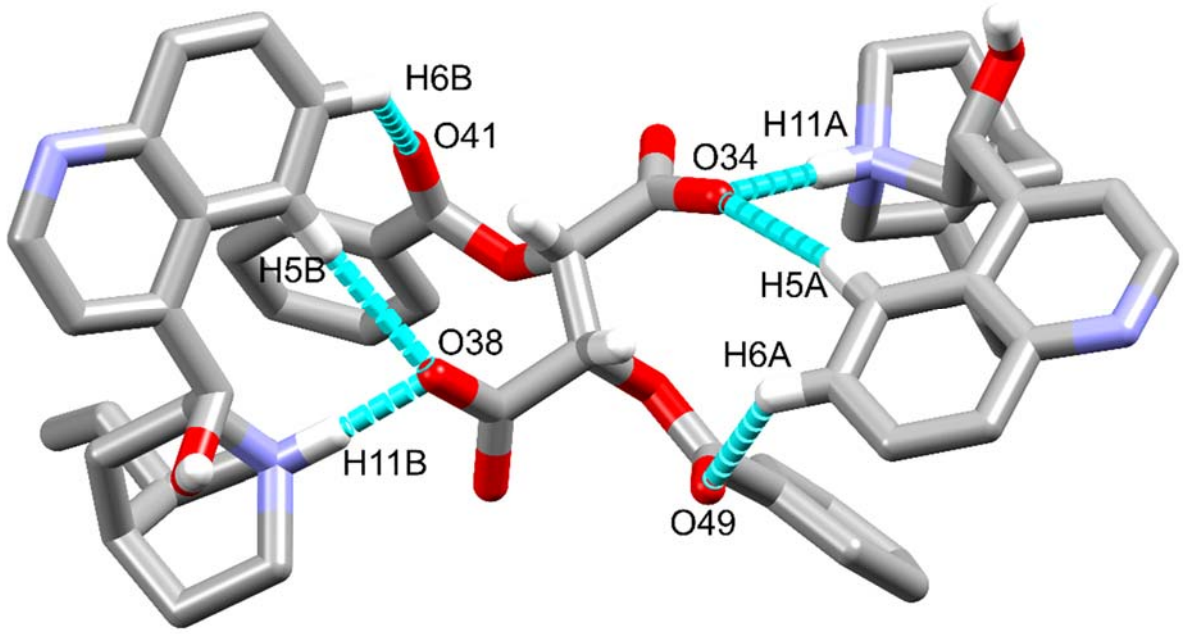

Figure 4.4 Asymmetric unit of 2[CIND^{+}][D-DBTA^{2-}] with hydrogen bonding between the molecules (only hydrogen atoms involved in hydrogen bonding are shown for clarity).

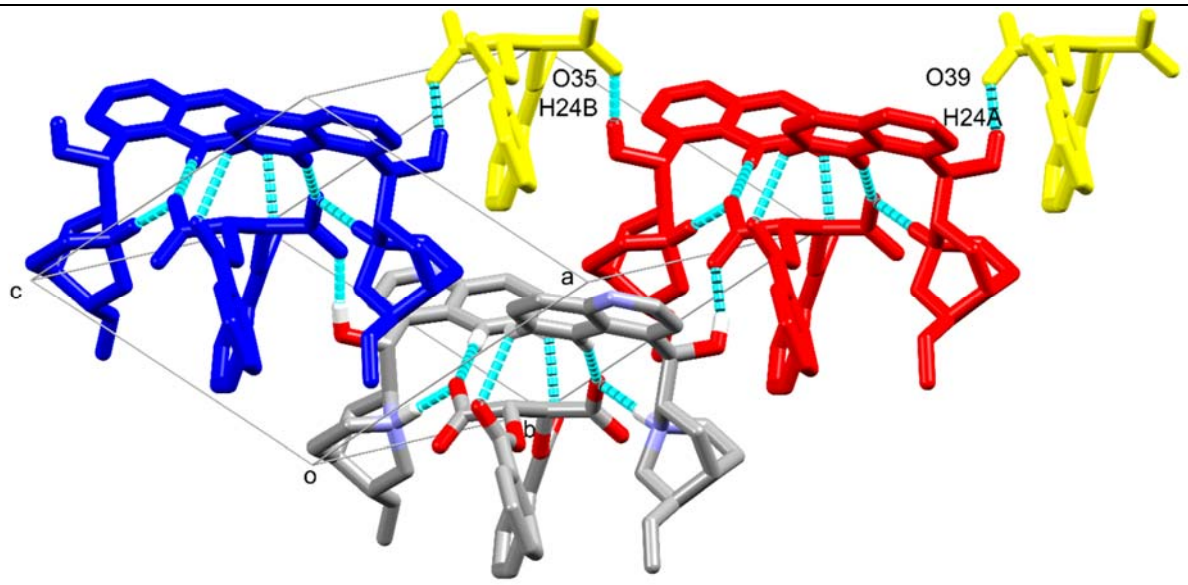

Figure 4.5 Hydrogen bonding between the molecular units in 2[CIND$^+$][D-DBTA^{2-}] (ASU fragments are coloured with the same colour).

4.2 Discrimination of DTTA enantiomers

When racemic mixture of *L*- and *D*-DTTA was crystallized with CIND from ethanol-water (1:1) mixture, the outcome was very similar to the equivalent experiment with DBTA, i.e. the CIND formed a salt with the *L*-enantiomer, [CIND$^+$][*L*-DTTA$^-$]. The structure was solved in the orthorhombic $P2_12_12_1$ (No. 19) space group with a full *L*-DTTA and one CIND in the asymmetric unit. One of the carboxylic acid group of the DTTA is deprotonated and the hydrogen is transferred to the quinuclidine moiety of the CIND (Fig 4.6). One of the benzoate groups is almost planar (O41-C40-C42-C43 is -1.15°), while the other one is more tilted (O49-C48-C50-C51 is 12.23°); the torsion angle describing the tilt around the central alkane bond of the molecule (O36-C31-C32-O37) is –74.09°, and the plane angle between the two phenyl rings is 47.92°. The vinyl moiety of the CIND is disordered in two positions, with a 57% occupancy of the main disorder site. This suggests that the fit between the CIND and the *L*-DTTA is not as perfect as in the equivalent DBTA structure.

The two molecules are held together by a charge assisted hydrogen bond (N11-H11···O34), a weak CH···O contact (C5-H5···O35) and a π···π interaction between the phenyl ring of the acid and the quinoline ring of the base (∠ 1.83°, c_g= 3.519 Å). Similarly to [CIND$^+$][*L*-DBTA$^-$], a three component aromatic stack is formed as a phenyl ring of the neighbouring DTTA also overlaps with the quinoline ring (Fig 4.7). The distance between the quinoline ring and the neighbouring phenyl ring is 3.806 Å and their angle is slightly larger (∠ 16.11°). The ion pairs are hydrogen bonded in the two-fold screw axis with the most noticeable hydrogen bond forms between the quinoline nitrogen and the carboxylic acid functionality (O38-H38···N1, Fig 4.8), similarly to the DBTA equivalent structure.

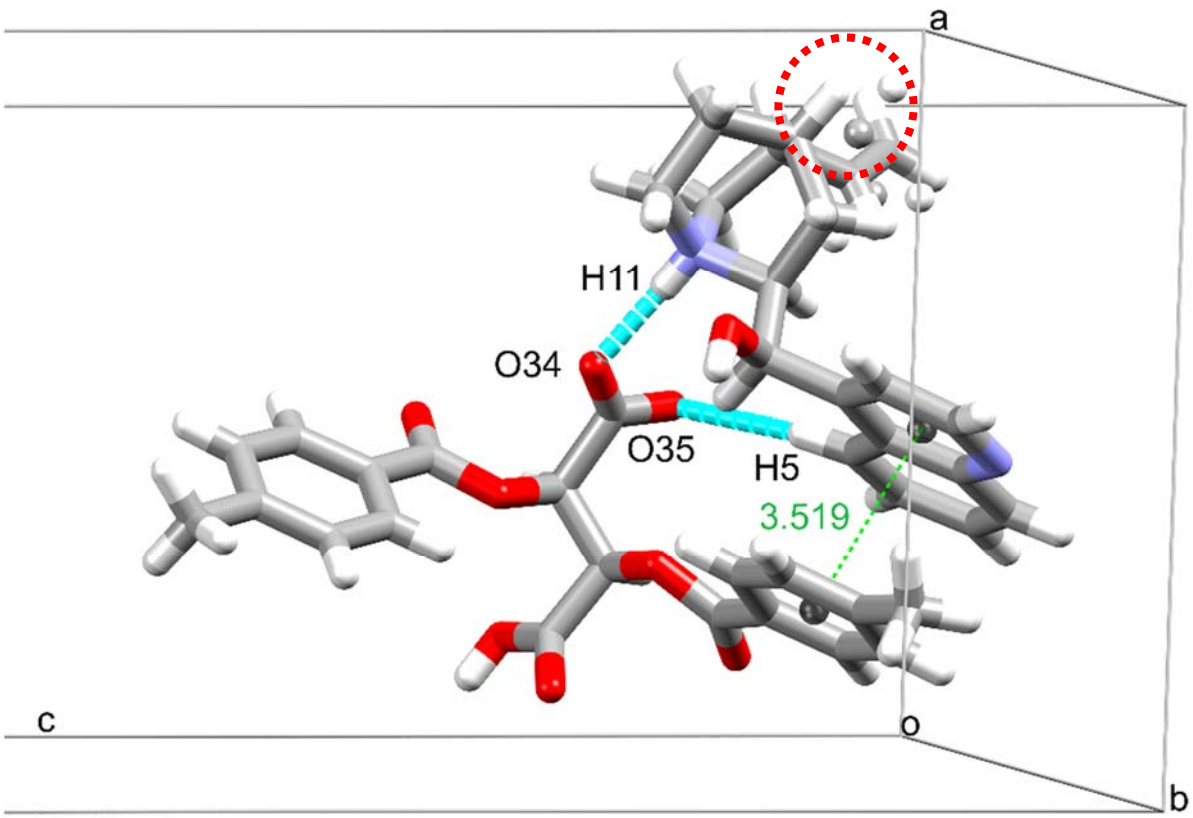

Figure 4.6 Asymmetric unit of [CIND$^+$][L-DTTA$^-$] with hydrogen bonding between the molecules. Note the aromatic interaction between the phenyl of the acid and the quinoline rings. The disordered vinyl moiety is circled with red dotted line.

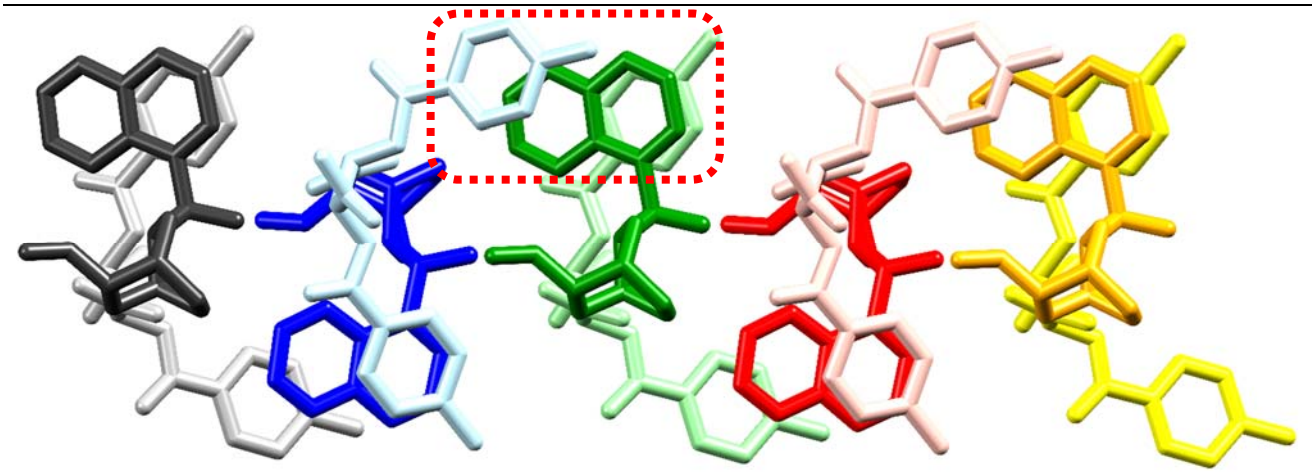

Figure 4.7 Aromatic interactions in [CIND$^+$][L-DTTA$^-$]. Ion pairs are coloured with the same colour (acid with lighter, base with darker shade). The three component aromatic system (circled with red) is formed between neighbouring ion pairs.

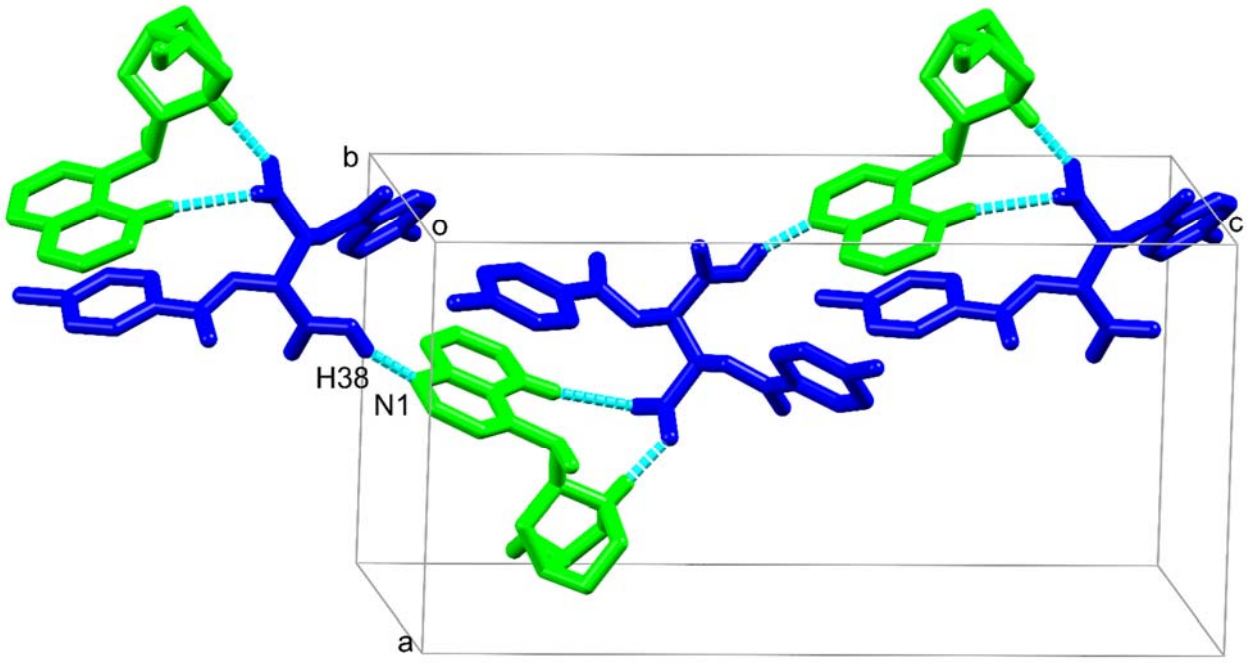

Figure 4.8 Hydrogen bonds between neighbouring ion pairs in [CIND$^+$][L-DTTA$^-$]. (Ion pairs are coloured by symmetry equivalence.)

When the dimensions of the two crystal structures obtained from the crystallisation of CIND with the racemic acids are compared, they show high level of unit cell similarity. Although the origins of the cells are allocated in different positions, the structures are isostructural (packing view down (010), Fig 4.9). The configuration of the CIND and the substituted tartaric acid molecules are also very similar; the root mean square error of the molecular fitting is 0.0323 and 0.0184, respectively. The larger deviation for the CINDs is attributed mainly to the disorder in the vinyl group in [CIND$^+$][*L*-DTTA$^-$] (Fig 4.10).

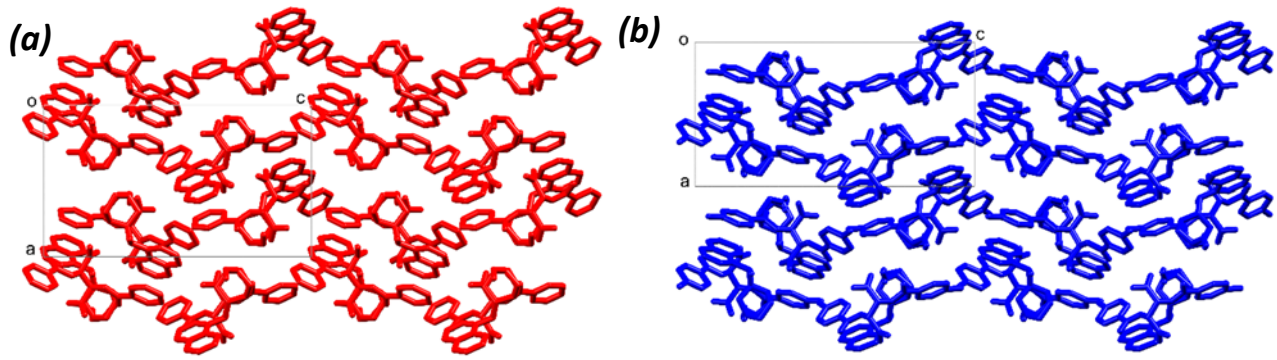

Figure 4.9 Packing diagrams of isostructural [CIND$^+$][L-DBTA$^-$] (a, red) and [CIND$^+$][L-DTTA$^-$] (b, blue) view down (010).

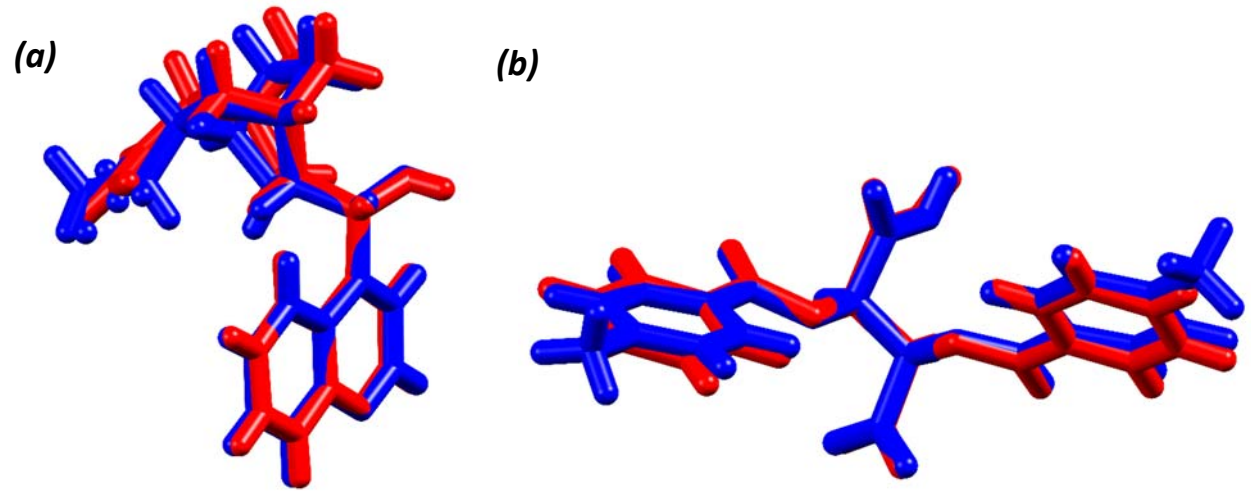

Figure 4.10 Molecular fitting of CINDs and DBTA/DTTA from structures [CIND$^+$][L-DBTA$^-$] (red) and [CIND$^+$][L-DTTA$^-$] (blue).

To be able to evaluate the formation of the preferred salt, [CIND$^+$][*L*-DTTA$^-$], crystallisations were set between CIND and *D*-DTTA. It was challenging to obtain quality crystals for single crystal X-ray diffraction analysis and thus the solvent of crystallisation was varied while the crystallisation ratio of the acid vs. base was kept the same (1:2). The harvested crystals resulted in a salt-solvate, 2[CIND$^+$][*D*-DTTA^{2-}]·2DMSO·0.7H_2O. The structure was solved in the monoclinic $P2_1$ (No. 4) space group with two CINDs, one *D*-DTTA, two DMSOs and one water molecule in the asymmetric unit. (Fig 4.11) Likewise to the DBTA counterpart, the acid is di-deprotonated. The torsion angle describing the tilt around the central alkane bond of the molecule (O36-C31-C32-O37) is 73.33°, the plane angle between the two phenyl rings is 50.82°, and the benzoate moieties are tilted (O41-C40-C42-C43 is -10.09° and O49-C48-C50-C55 is –13.47°). These values are similar to the [CIND$^+$][*L*-DTTA$^-$], with the exception of the tilt in one of the benzoate groups.

The *D*-DTTA hydrogen bonds to two CINDs on a very similarly as in 2[CIND$^+$][*D*-DBTA^{2-}] via the carboxylates to the quinuclidine moiety (N11A-H11A···O34 and N11B-H11···O38) and to the aromatic system of the CINDs (C5A-H5A···O34 and C5B-H5B···O38). The DTTA also forms a week interaction with one of the quinoline rings via its carbonyl moiety (C6B-H6B···O41) and also the ordered DMSO molecule forms hydrogen bonds with the carboxylate of the *D*-DTTA via a water bridge (O58-H58A···O60 and O58-H58B···O35), where the water's site occupancy is 70%. The other DMSO is disordered in two positions with 80 % occupancy of the main disorder site and forms a hydrogen bond with the hydroxyl of the CIND (O24-H24···O68). The conformation of the two symmetry independent CINDs is more different than was found in 2[CIND$^+$][*D*-DBTA^{2-}]·(RMSD is 0.6889 Å, Max. D. is 2.0294 Å).

The cell parameters of 2[CIND$^+$][*D*-DTTA^{2-}]·2DMSO·0.7H_2O resemble those of 2[CIND$^+$][*D*-DBTA^{2-}]. Both structures were solved in $P2_1$, and the unit cell dimensions for *a* and *b* are very similar, while there is an almost

2 Å difference between the lengths of the *c* axis. Although the cell similarity is high, the structures are not isostructural because the inclusion of the three additional solvent molecules (2 DMSO and 0.7 H_2O) distorts the lattice (Fig 4.12). The comparison of the packing of the CINDs and the DBTA/DTTA units (basically the ASU), when the encapsulated solvent molecules are omitted for clarity, shows how the major building blocks of the crystals, the ASU (circled on Fig 4.12) builds up the crystallographic space and also emphasizes the influence of the solvent molecules on the overall packing of the crystal.

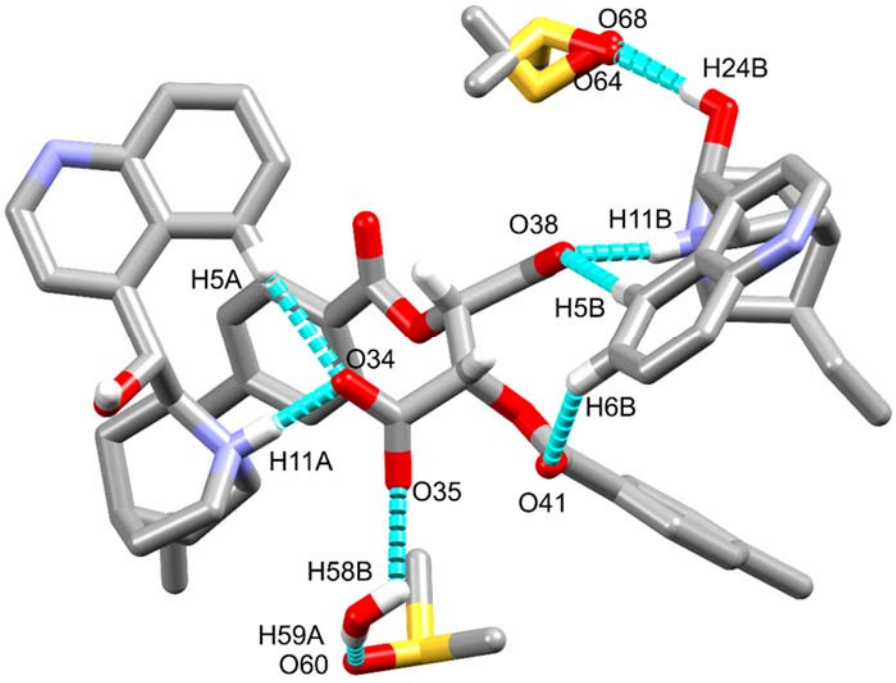

Figure 4.11 The ASU of 2[CIND$^+$][D-DTTA^{2-}]·2DMSO·0.7H_2O showing the most prominent hydrogen bonds and the atoms involved in them are labelled.

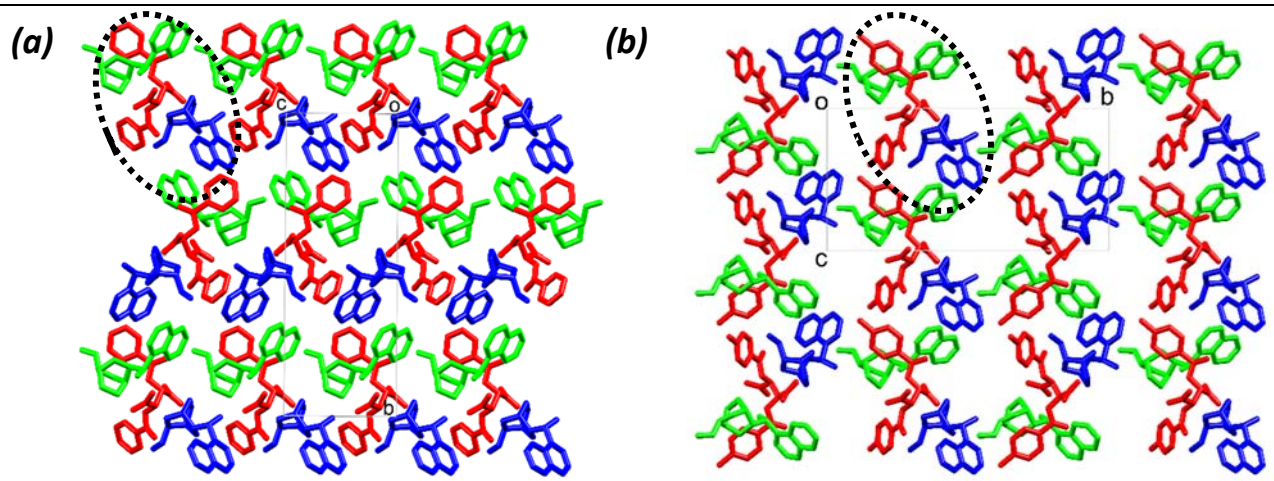

Figure 4.12 Packing similarities of structures 2[CIND$^+$][D-DBTA$^-$] (a, view down (100)) and 2[CIND$^+$][D-DTTA^{2-}]·2DMSO·0.7H_2O (b, view down 100)). The molecules are coloured according to symmetry equivalence. The similar molecular units are circled and the solvent molecules (DMSO, H_2O) are excluded from (b) for clarity.

4.3 Mode of encapsulation of DBTA and DTTA during the discrimination

To comprehend how the acids are encapsulated in the crystal structures, and eventually understand the preference of CIND towards the *L*-enantiomers of DBTA and DTTA, the Hirshfeld surfaces were calculated and transformed to 2D fingerprint plots; and the % contribution of the selected interactions were compared. The calculated Hirshfeld surface for the *L*-DBTA in the structure of [CIND$^+$][*L*-DBTA$^-$] is presented in Fig 4.13 as an example, and the full fingerprint plots and their fractional visual representation of the selected interactions (Table 4.2).

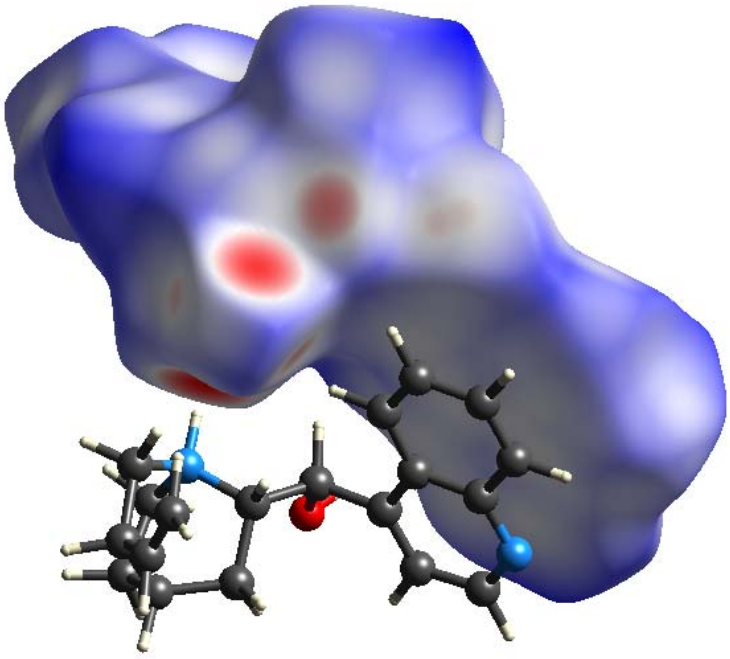

Figure 4.13 Hirshfeld surface for the DBTA ion in [CIND$^+$][L-DBTA$^-$].

As an overall starting point of comparing the four structure, the analysis of their crystal density reveals that the 'favoured' crystals (i.e. the outcome of the crystallisation with the racemic acids, [CIND+][L-DBTA-] and [CIND+][L-DTTA-]) have higher density, than the crystals obtained from the 'forced' crystallisations (2[CIND+][D-DBTA2-] and 2[CIND+][D-DTTA2-]·2DMSO·0.7H2O). The difference is more obvious in the salts of DBTA (1.338 g.cm3 vs. 1.278 g.cm3), while the values are closer for the DTTA salts (1.291 g.cm3 vs. 1.275 g.cm3). The higher density suggests a more efficient packing of the crystal, i.e. supports the outcome of the discrimination experiments.

Table 4.4 Fingerprint plots for the DBTA/DTTA moiety in the analysed crystals with % contributions of main interactions. (Values for the structures with disorders were calculated on the main molecular fragment.)

	Full map	C···C	C···H	H···H	O···H
[CIND$^+$][*L*-DBTA$^-$]	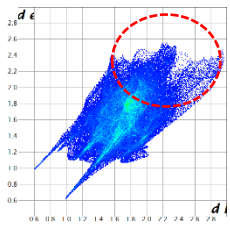	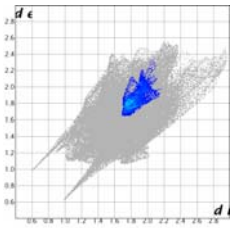 5.9 %	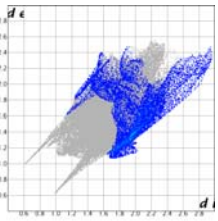 14.3 %	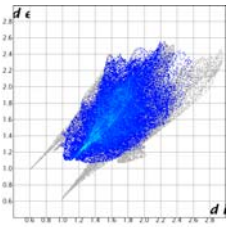 41.9 %	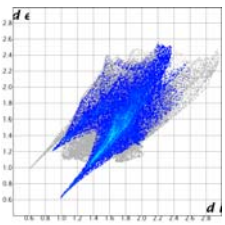 34.6 %
2[CIND$^+$][*D*-DBTA^{2-}]	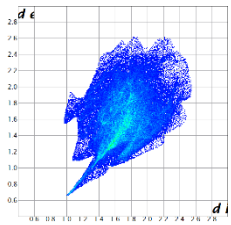	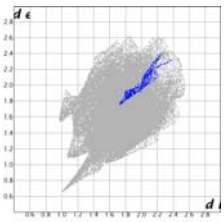 0.7 %	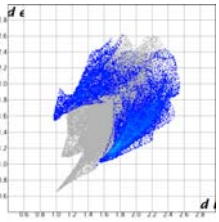 25.1 %	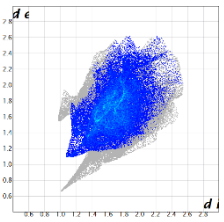 41.0 %	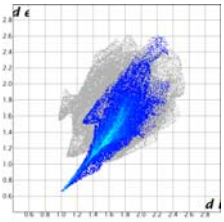 31.9 %
[CIND$^+$][*L*-DTTA$^-$]	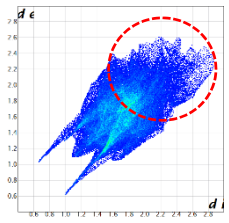	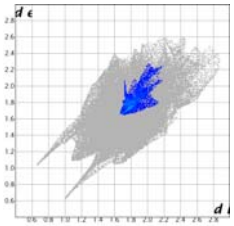 4.7 %	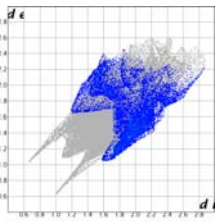 13.3 %	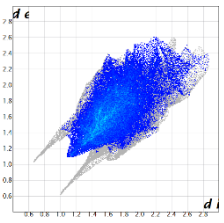 47.1 %	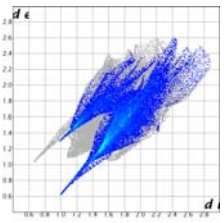 32.4 %
2[CIND$^+$][*D*-DTTA^{2-}]·2DMSO·0.7H$_2$O	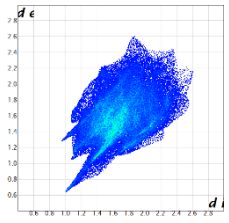	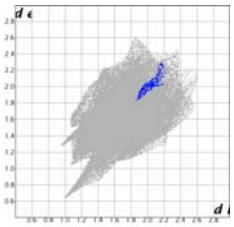 0.4 %	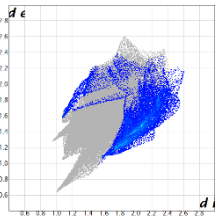 17.0 %	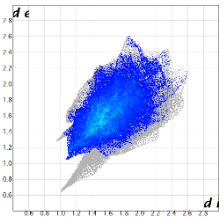 50.1 %	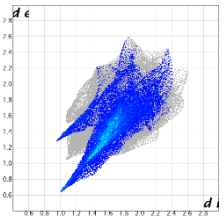 29.9 %

The comparison of the full fingerprint plots reveals a slightly different scenario. Generally, it is understood if a crystal has significant amount of long range contacts, i.e. when the closest possible atoms on the inner side and the outer side of the Hirshfeld surface are farther from each other, that crystal is less efficiently packed. The long range contacts can be seen in the high d_i and d_e region of the fingerprint plots, and this region is circled in figures in Table 4.2. It is interesting to conclude that both 'favoured' structures contain more long range contacts than the structures obtained from the 'forced' crystallisations, and overall the least favoured salts seem to pack more efficiently.

The C···C contacts typically represent the face-to-face π···π interactions in a crystal and generally noted as stabilizing. The C···H contacts are the summary of edge-to-face π···π interactions and also when a C-H moiety is pointing towards the electron cloud of an aromatic ring. The O···H interactions are part of the traditional hydrogen bond formation and understood as attractive. The short H···H contacts in a crystal packing are the indicators of the formation of close contacts between hydrogens and eventually a least favoured packing. In overall, the most favoured packing should represent more C···C and O···H contacts and less H···H contacts, when compared to the crystals of the 'forced' crystallisations. Important to note that these assumptions are rather general and need to be evaluated for each systems with care.

Comparison of [CIND$^+$][*L*-DBTA$^-$] and 2[CIND$^+$][*D*-DBTA^{2-}] shows shorter hydrogen bonds (d_i + d_e = 1.6 Å) with more % contribution (34.6 %), and more C···C contacts (5.9 %) in [CIND$^+$][*L*-DBTA$^-$], whereas the H···H contacts are almost equal in the two structures.

The structure of [CIND$^+$][*L*-DTTA$^-$] and 2[CIND$^+$][*D*-DTTA^{2-}]·2DMSO·0.7H_2O contain disorders and the fingerprint plots and the concomitant % contributions were calculated on the main molecular fragment. Assessment of [CIND$^+$][*L*-DTTA$^-$] and 2[CIND$^+$][*D*-DTTA^{2-}]·2DMSO·0.7H_2O reveal a similar situation to the DBTA equivalents. The shortest O···H interaction is almost the same in the two structures, but the % contribution is more in [CIND$^+$][*L*-DTTA$^-$]. The already described aromatic stacks in [CIND$^+$][*L*-DTTA$^-$] (Fig 4.7) appear on the fingerprint plots as 4.7 % contribution of the C···C contacts. The short range H···H contacts are more prominent on the plot of 2[CIND$^+$][*D*-DTTA^{2-}]·2DMSO·0.7H_2O and the % contribution is larger in this structure.

To conclude, the Hirshfeld surface analysis of the acids in the four crystal structure supported the experimental outcome and highlighted why the *L*-enantiomers are the favoured stereoisomers in the discrimination process.

Summary and Conclusion

The enantiomeric purity of a compound is a key aspect in the analytical, food, pesticide and particularly in the pharmaceutical industries. The isolation and the purification of a single enantiomer product has become an important component of manufacturing pharmaceuticals and fine chemicals. Chiral discrimination between enantiomers is one of the most predominants fields in analytical chemistry. Conversion of a racemate with a chiral resolving agent and separation of the mixure of diastereomeric adducts formed is known as the classical method of resolution, where the newly formed disatereomeric adducts or salts exhibit significant dissimilarity in their physical properties that allow their separation via crystallization.

The current research was aimed at investigating the chiral discrimination process during diastereomeric salt formation, when selected cinchona alkaloids were exposed to racemic mixtures of tartaric acid derivatives. This research is based on the use of *(+)*-cinchonine, *(-)*-cinchonidine, *(-)*-quinidine, *(+)*-quinine, which served as chiral bases in order to resolve racemates of *O,O'*-dibenzoyl-tartaric acid or DBTA, and *O,O'*-di-p-toluoyl-tartaric acid or DTTA. Cinchona alkaloids were selected because of their abilities to form salts with the targeted acids. DBTA and DTTA are commonly used resolving agents to separate racemic bases via diastereomeric salt formation. The two acids were chosen because of their structural similarity to tartaric acid, which were successfully used previously in discrimination experiments with the listed alkaloids. Experimental analytical techniques such as thermal analysis, powder X-ray diffraction, single crystal X-ray diffraction were used to analyze the harvested diastereomeric salts, when the process of molecular recognition were studied. A correlation of molecular parameters derived from the structures and an investigation of the mechanism which drives the resolution process were discussed. The thesis summarizes the findings of 8 crystal structures of DBTA and DTTA with water or DMSO as included solvent, and 4 salts of *(-)*-cinchonidine formed with DBTA and DTTA.

The inclusion compounds of *(–)-O,O'*-dibenzoyl-*(2R,3R)*-tartaric acid (or *L*-DBTA) and *(–)-O,O'*-di-p-toluoyl-*(2R,3R)*-tartaric acid (*L*-DTTA) or their racemic mixtures, *(rac)*-DBTA and *(rac)*-DTTA with achiral common solvents were discussed. The discussed inclusion compounds were obtained serendipitously, as a product of the pre-screening of suitable solvents to dissolve both the acids and the cinchona alkaloids. A wide variety of solvents were tested and in some occasions suitable crystals were harvested. A search in the Cambridge Structural Database concluded that only few crystal structures of solvates of these two tartaric acid derivatives are known or published, and significantly less of these structures do exist when both the racemic and the enantiopure acid

encapsulates the same solvent. To contribute to the pool of available crystal structures when comparing chiral vs. achiral crystal forms of the same compounds, 8 crystal structures of DBTA and DTTA with water or DMSO as included solvent, were analysed and discussed in details. The typical crystallisation stoichiometry was found to be 1:2 (host-guest) hence the two carboxylic acids are likely to hydrogen bond to two guests. The unexpected 1:1 or 2:1 host-guest stoichiometry was observed in *L*-DBTA·H_2O and *(rac)*-DTTA·H_2O. These crystals seem to be less likely to dehydrate and this property may be reasoned with the more hydrogen bond formation around the water molecules. In case of the DMSO solvates the desolvation overlaps with the melting when observed with thermogravimetry and the solvent content cannot be calculated reliably.

The chiral discrimination experiments of racemic mixture of DBTA and DTTA were carried out with the 4 traditional cinchona alkaloids: *(-)*-quinine (QUIN), *(+)*-quinidine (QUID), *(+)*-cinchonine (CINC) and *(-)*-cinchonidine (CIND). The crystallisations were set in a 2:1 (base:diacid) molar ratio to ensure that the dicarboxylic acid can maximize the hydrogen bond formation, i.e. the solutions contain enough base to hydrogen bond to both carboxylic acid moieties. In first step, the racemic mixture of acids was exposed to the cinchona alkaloid and the first appearing crystals were harvested for single crystal X-ray diffraction. Once the preference of the alkaloid towards a given enantiomer was concluded, the unfavoured enantiomer was crystallized with the alkaloid. The structures of the harvested crystals from these, so called 'forced' crystallisations, were compared to the outcome of the first experiments. Results were obtained from all combination but only the experiments with cinchonidine were included in this thesis, namely [$CIND^+$][*L*-$DBTA^-$], 2[$CIND^+$][*D*-$DBTA^{2-}$], [$CIND^+$][*L*-$DTTA^-$] and 2[$CIND^+$][*D*-$DTTA^{2-}$]·2DMSO·0.7H_2O. To comprehend how the acids are encapsulated in the crystal structures, and eventually understand the preference of CIND towards the *L*-enantiomers of DBTA and DTTA, the Hirshfeld surfaces were calculated and transformed to 2D fingerprint plots; and the % contribution of the selected interactions were compared. When [$CIND^+$][*L*-$DBTA^-$] and 2[$CIND^+$][*D*-$DBTA^{2-}$] were compared, it was concluded that the preferred salt, [$CIND^+$][*L*-DBTA] have shorter hydrogen bonds with more % contribution, and more C···C contacts, than in the 'forced' 2[$CIND^+$][*D*-$DBTA^{2-}$] crystal; while the H···H contacts are almost equal in the two structures. The structures of [$CIND^+$][*L*-$DTTA^-$] and 2[$CIND^+$][*D*-$DTTA^{2-}$]·2DMSO·0.7H_2O contain disorders and thus the fingerprint plots and the concomitant % contributions were calculated on the main molecular fragment. Assessment of [$CIND^+$][*L*-$DTTA^-$] and 2[$CIND^+$][*D*-$DTTA^{2-}$]·2DMSO·0.7H_2O reveal a similar situation to the DBTA crystals. The shortest O···H interaction is almost the same in the two structures, but the % contribution is more in [$CIND^+$][*L*-$DTTA^-$]. The short range H···H contacts are more prominent in 2[$CIND^+$][*D*-$DTTA^{2-}$]·2DMSO·0.7H_2O and the % contribution is larger in this structure. It was concluded that the Hirshfeld surface analysis of the acids in the four crystal

explained the experimental outcome and highlighted why the *L*-enantiomers are the favoured stereomers in the discrimination process.

We believe that the findings of this work are a significant contribution to the field of supramolecular chemistry, namely to the understanding of the role of chirality in inclusion compound formation, and the mechanism of chiral discrimination via diastereomeric salt formation. The project is continued with the analysis of the DBTA and DTTA salts of the remaining cinchona alkaloids.

Appendix

1.1 Analytical results of tartaric acid derivatives

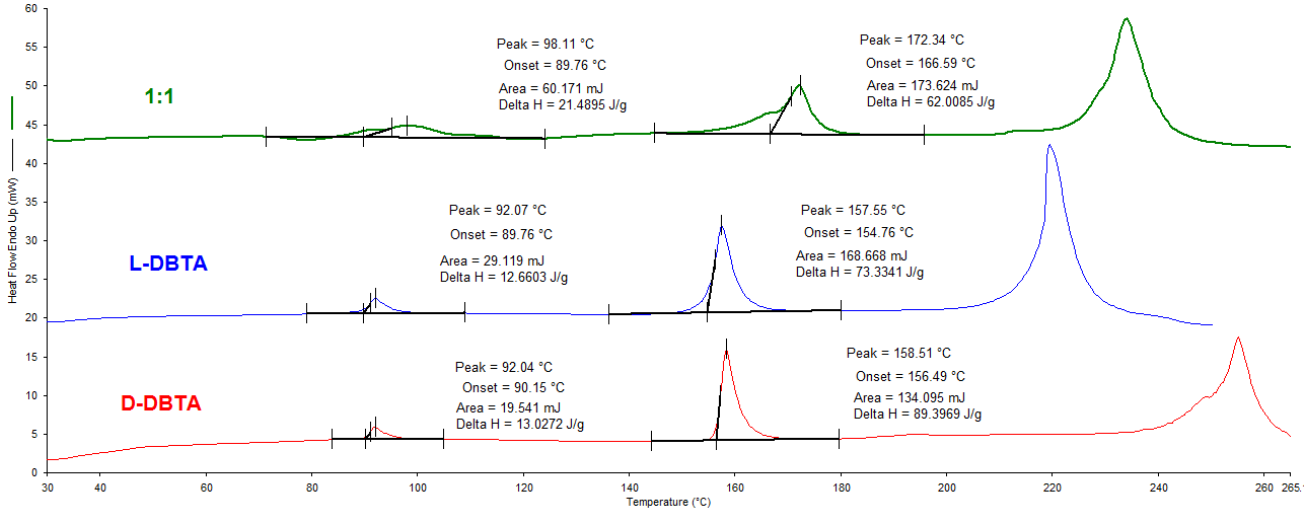

Figure A 1: DSC curve of L-DBTA, D-DBTA starting materials and 1.1 mixture of L and D (rac).

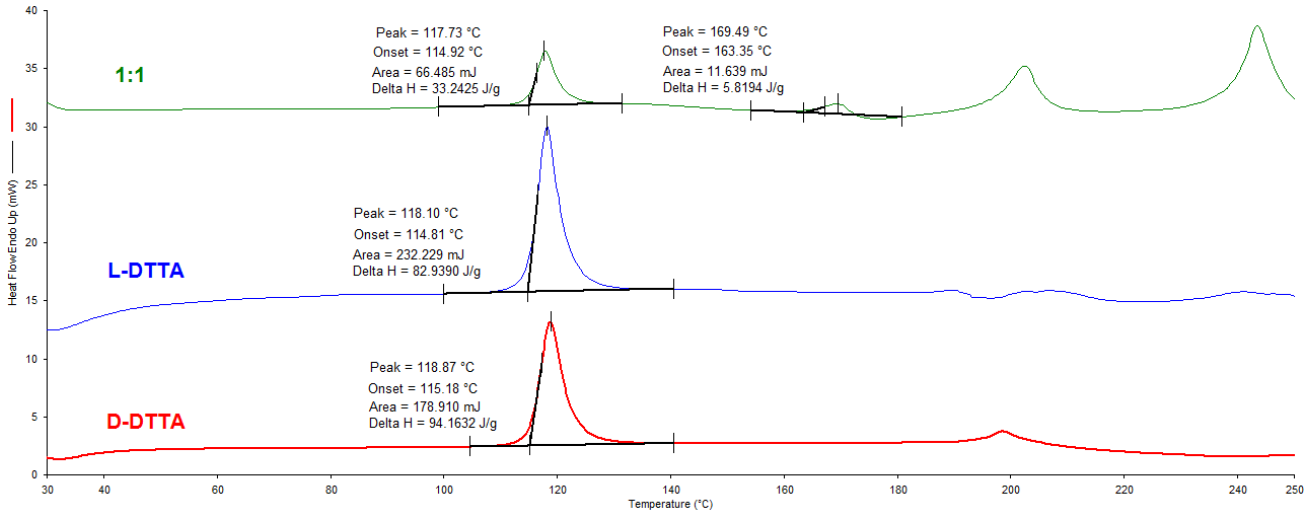

Figure A 2: DSC curve of L-DTTA, D-DTTA starting materials and 1.1 mixture of L and D (rac).

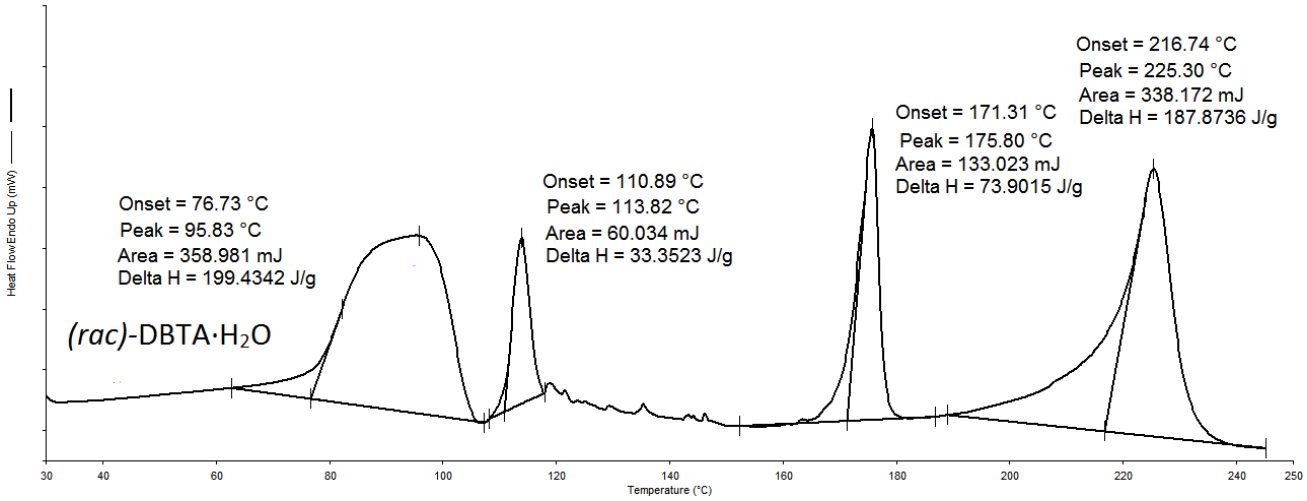

Figure A 3: DSC curve of (rac)-DBTA·$H_2$0.

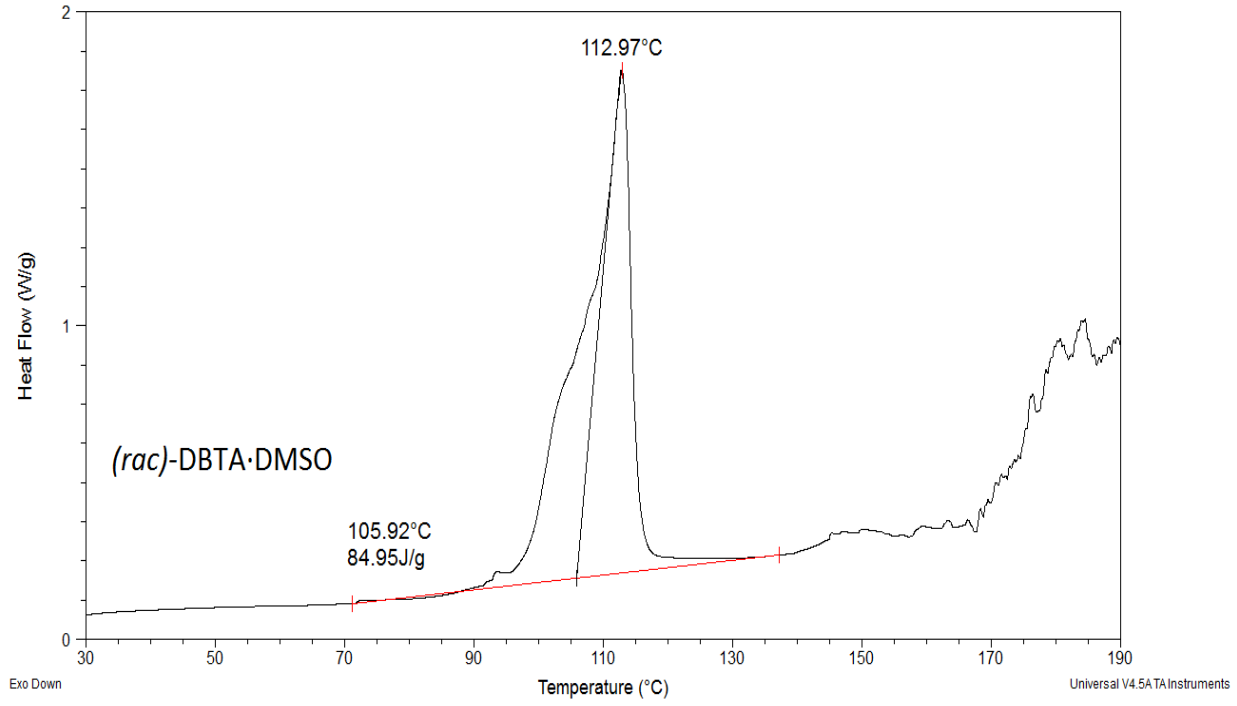

Figure A 4: DSC curve of (rac)-DBTA·DMSO.

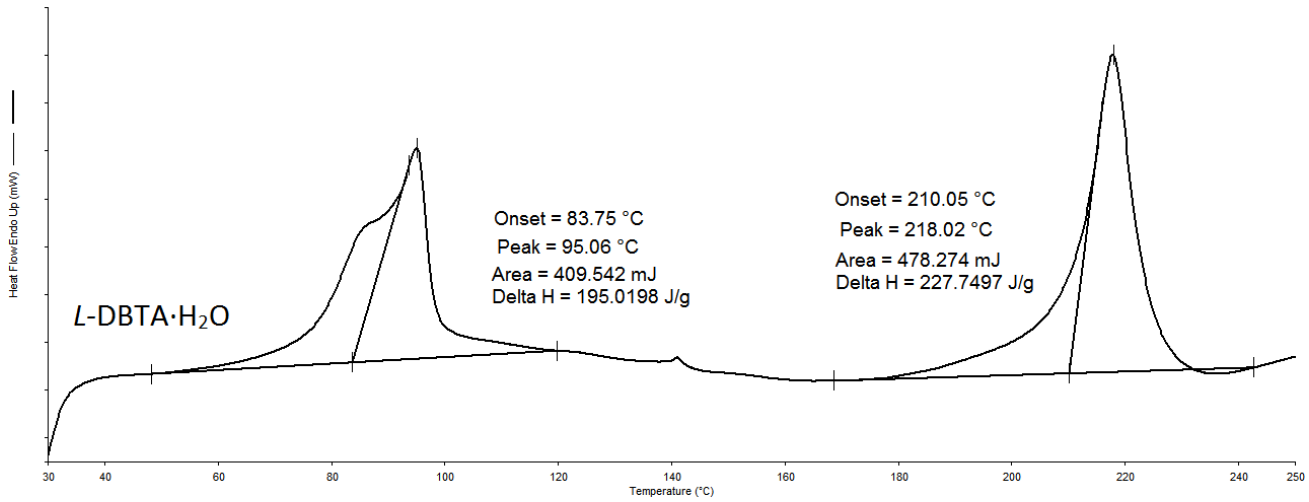

Figure A 5: DSC curve of L-DBTA·H_2O.

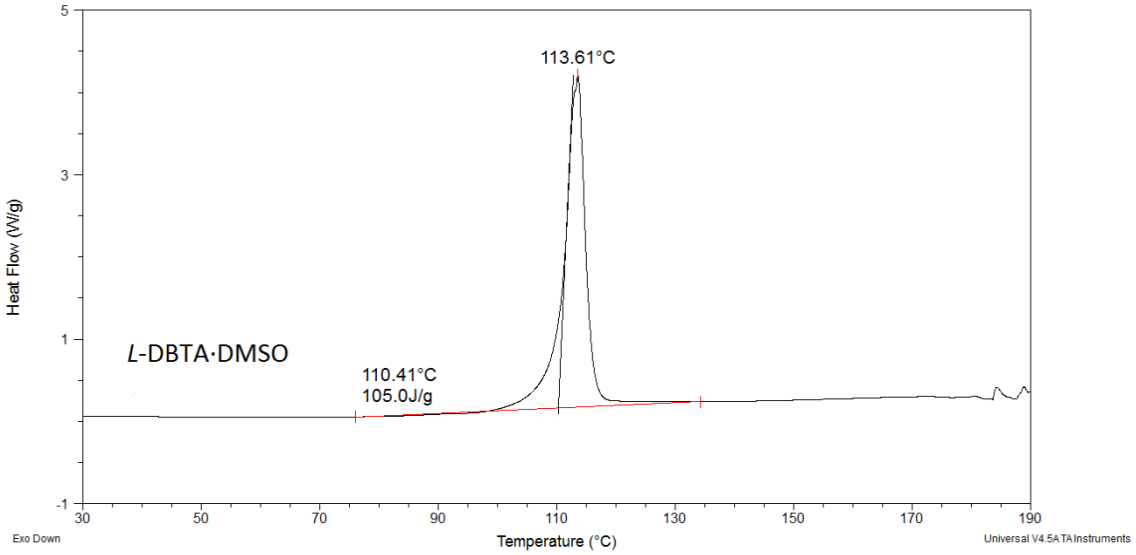

Figure A 6: DSC curve of L-DBTA·DMSO.

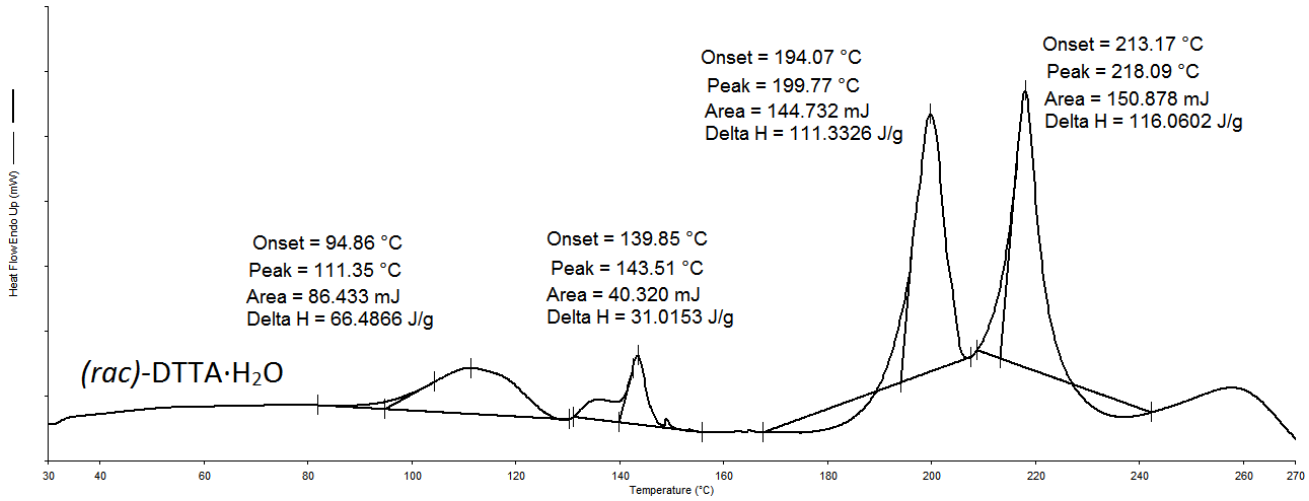

Figure A 7: DSC curve of (rac)-DTTA·H_2O.

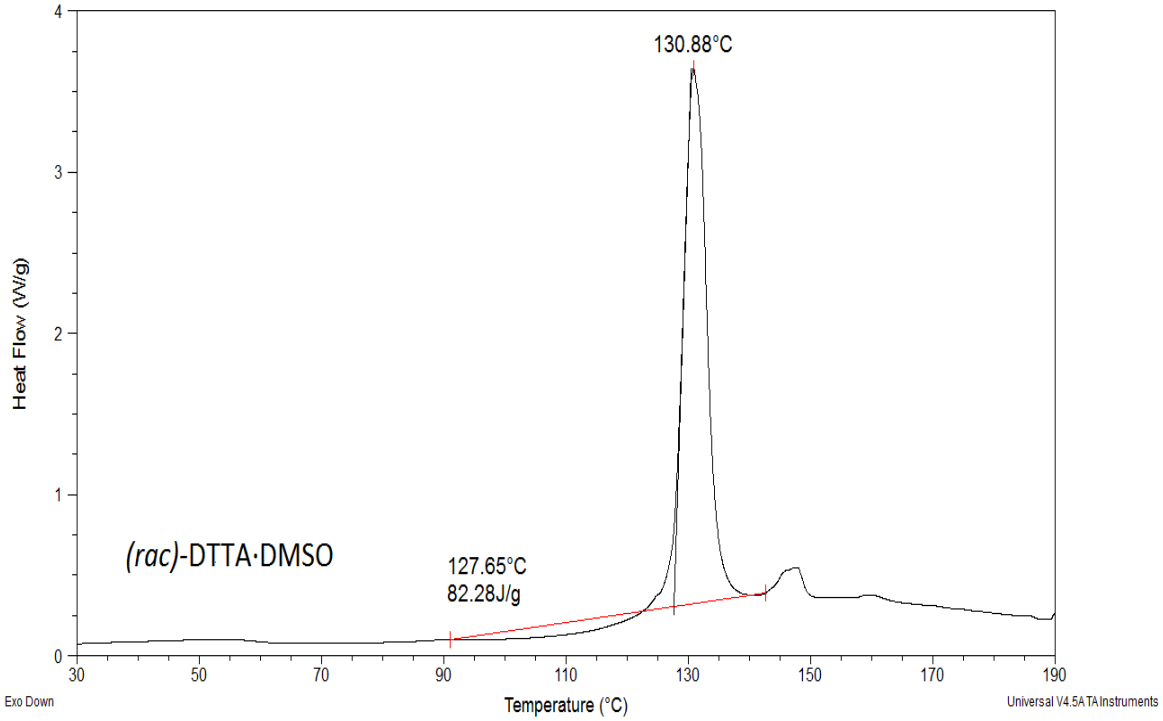

Figure A 8: DSC curve of (rac)-DTTA·DMSO.

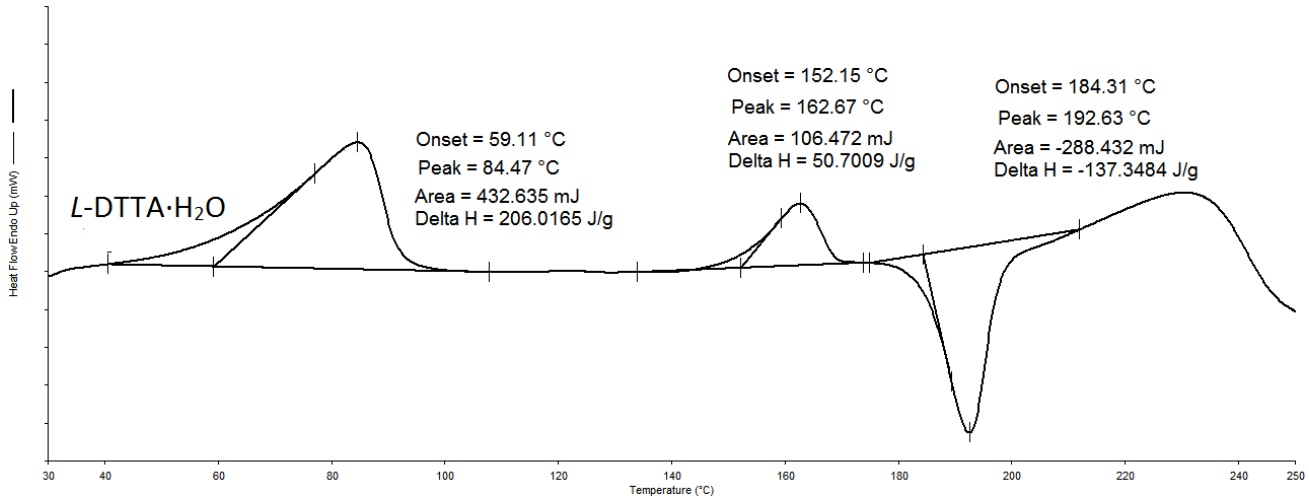

Figure A 9: DSC curve for L-DTTA·$H_2$0.

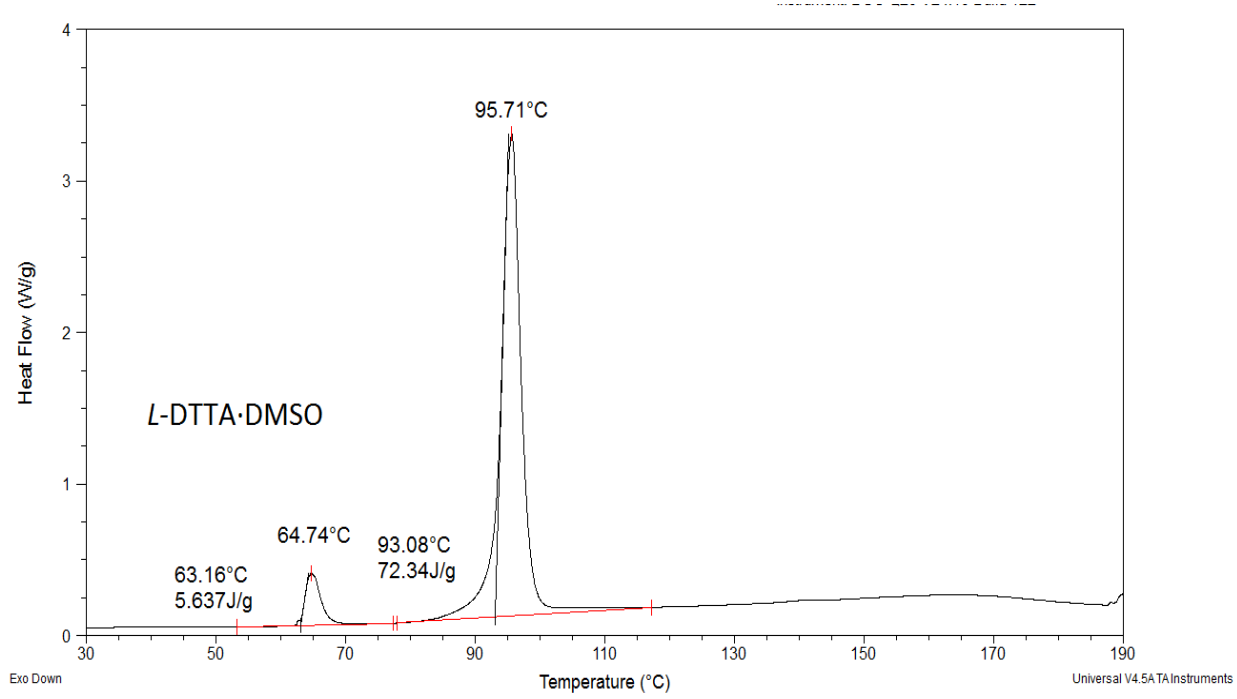

Figure A 10: DSC curve for (L)-DTTA·DMS0.

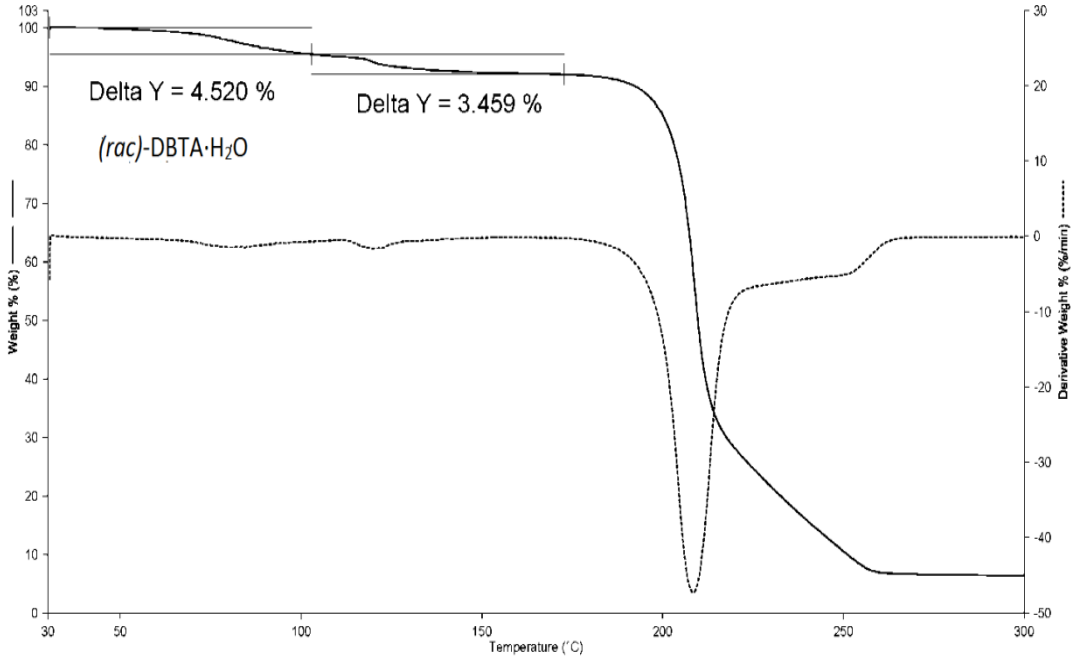

Figure A 11: TG curve for (rac)-DBTA·H_2O

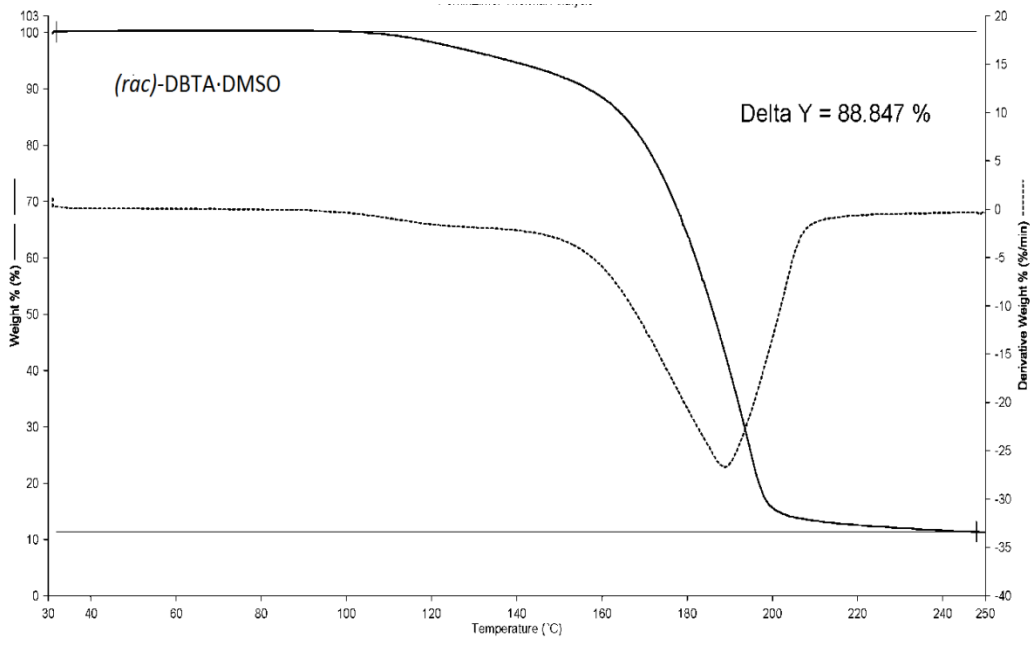

Figure A 12: TG curve of (rac)-DBTA·DMSO.

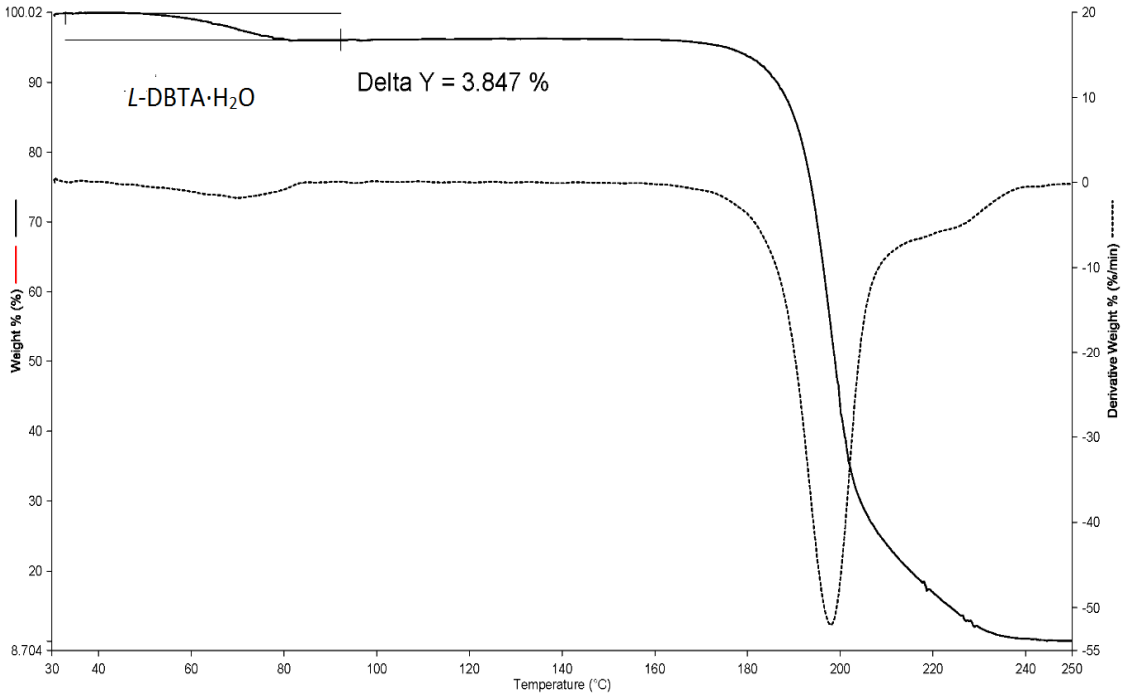

Figure A 13: TG curve of L-DBTA·H_2O.

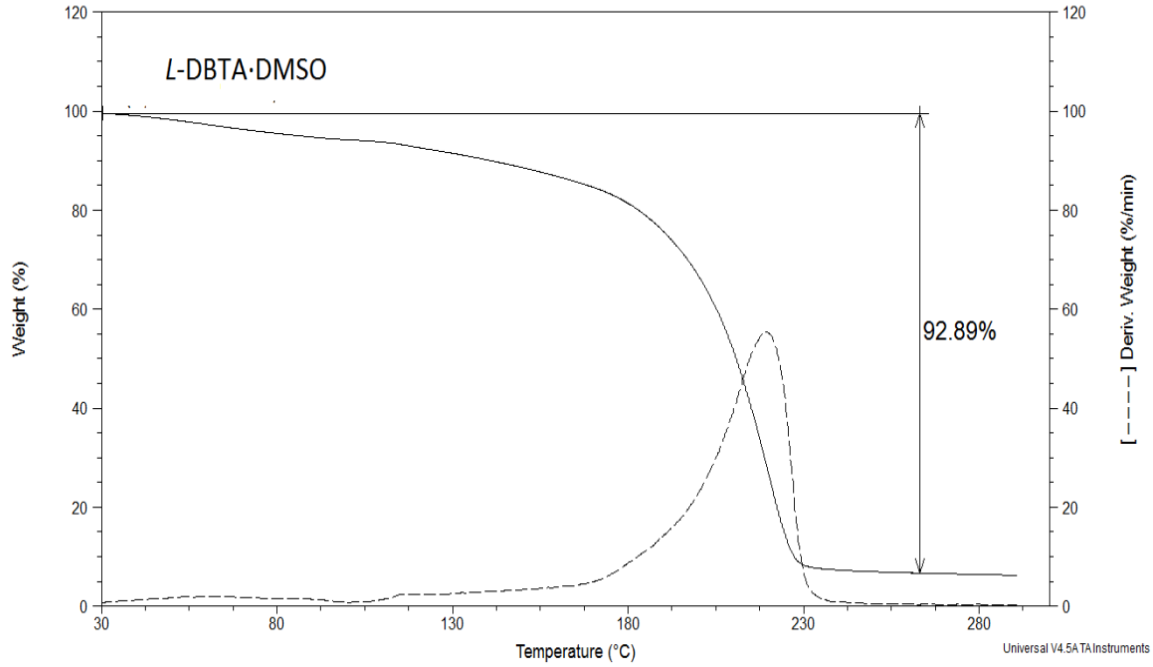

Figure A 14: TG curve of L-DBTA·DMSO.

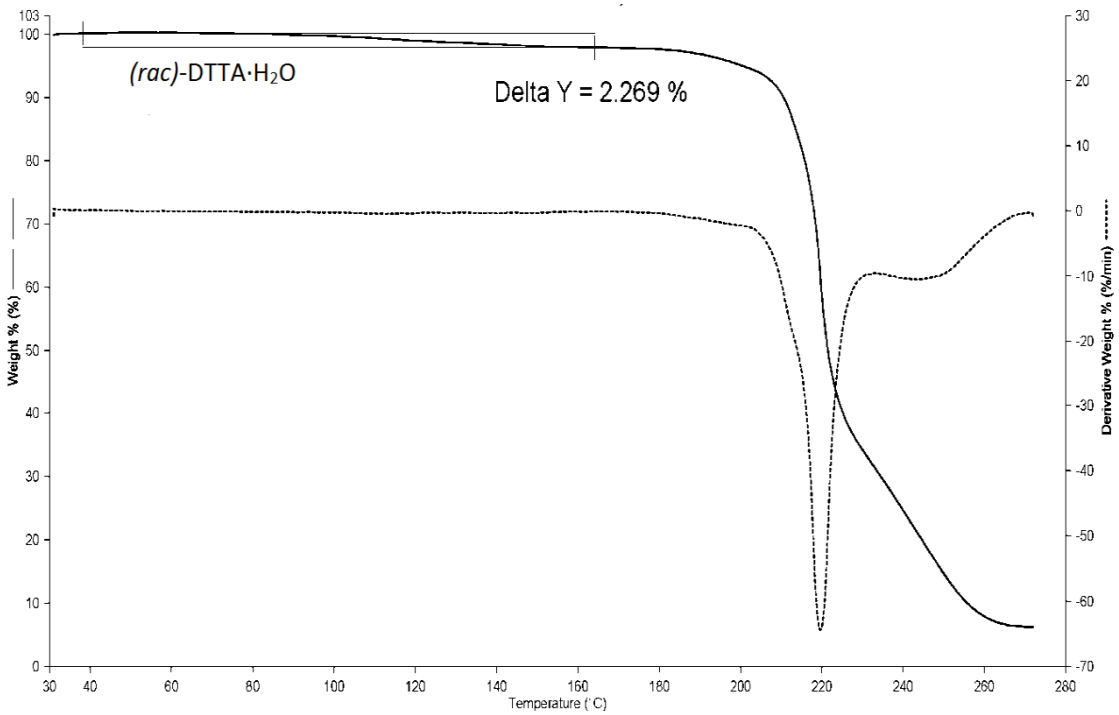

Figure A 15: TG curve of (rac)-DTTA·H_2O.

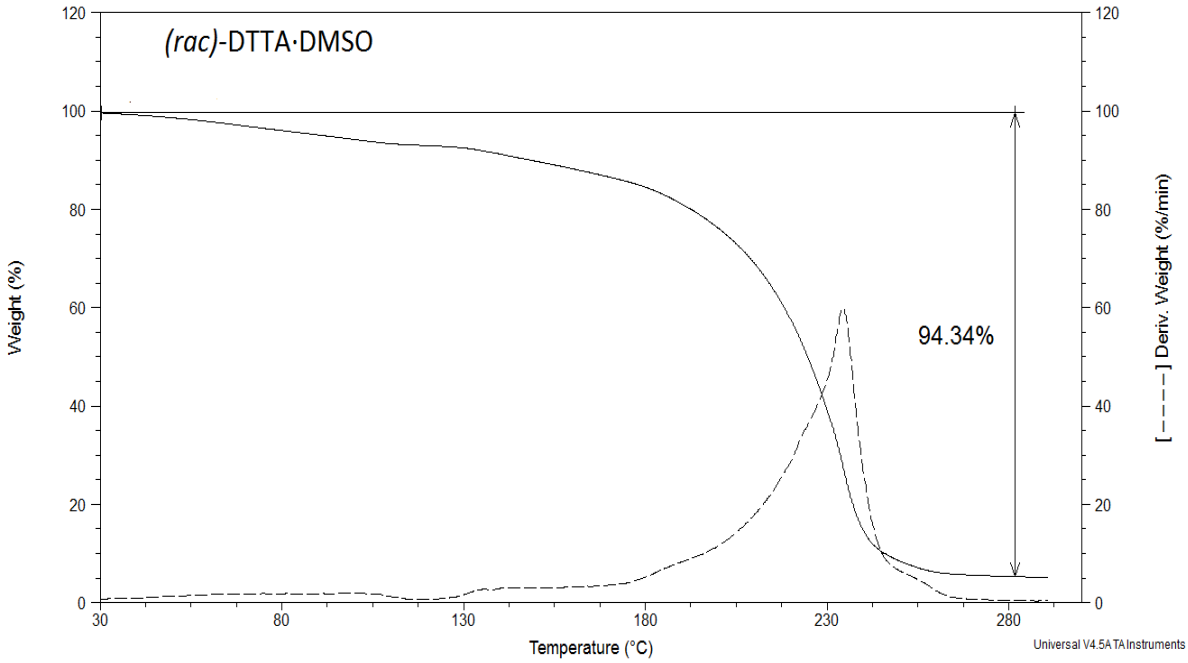

Figure A 16: TG curve of (rac)-DTTA·DMSO.

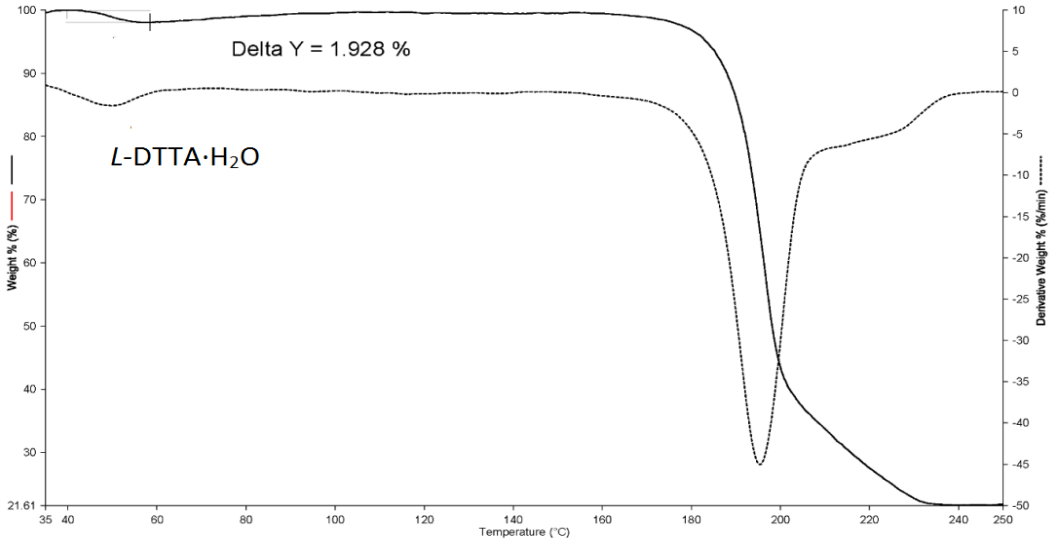

Figure A 17: TG curve of L-DTTA·H_2O.

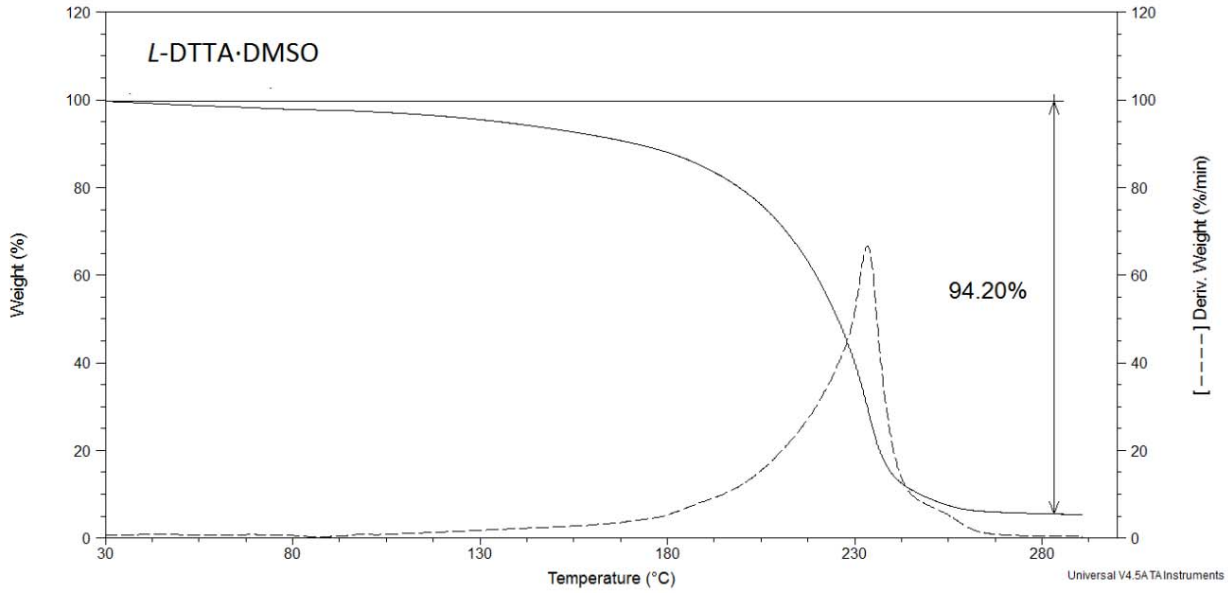

Figure A 18: TG curve of L-DTTA DMSO.

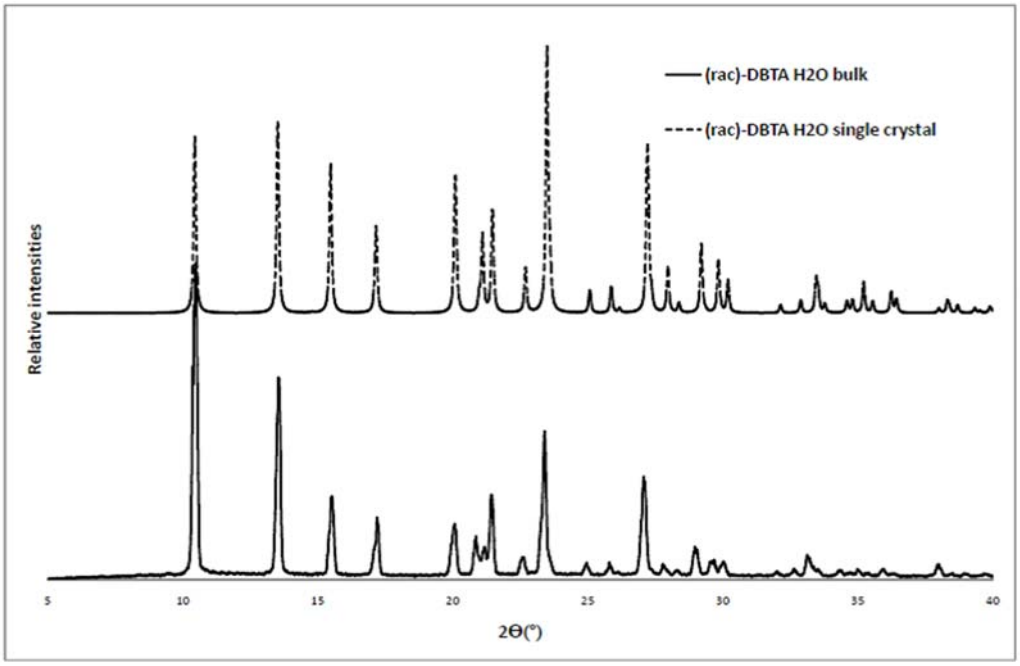

Figure A 19: PXRD patterns for (rac)-DBTA·H_2O (bulk -Continuous line) ; and the generated single crystal structure ((rac)-DBTA·H_2O, dashed line)

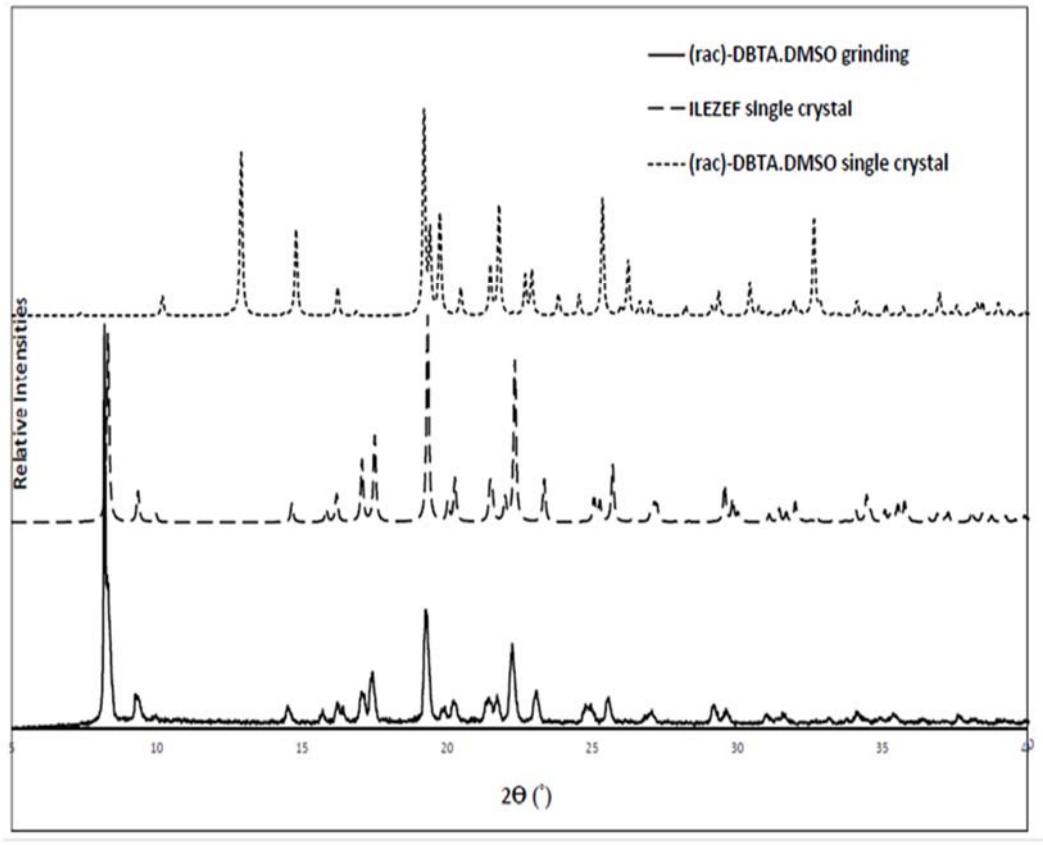

Figure A 20: PXRD patterns for ((rac)-DBTA·DMSO grinding continous line), the generated single crystal structures ILEZEF dashed line and (rac)-DBTA.DMSO, dotted line)

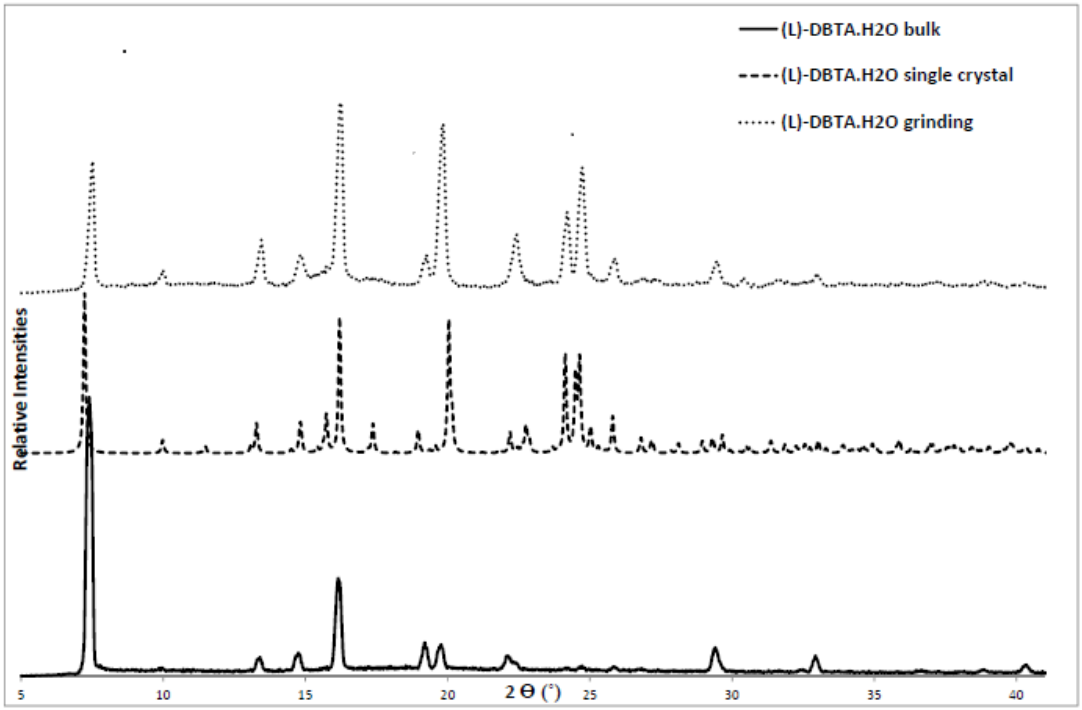

Figure A 21:PXRD patterns for (L-DBTA·H_2O (bulk-continous line)),the generated single crystal structure L-DBTA·H_2O, (dashed line) and (L-DBTA·H_2O grinding dotted line)

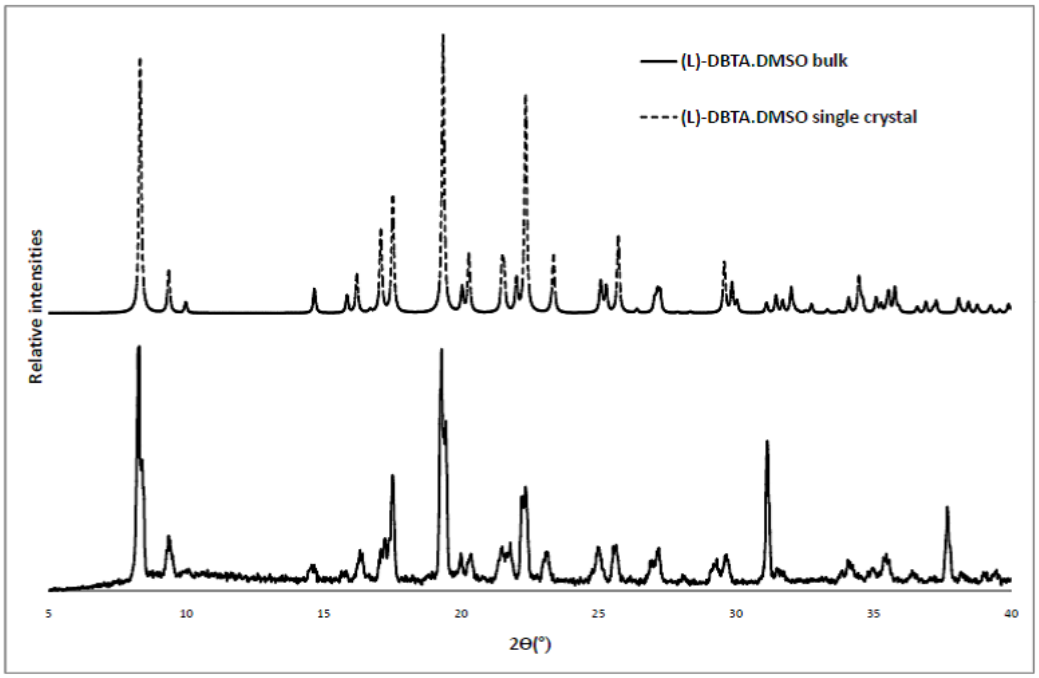

Figure A 22 PXRD patterns for (L-DBTA·DMSO, bulk-Continous line), and the generated single crystal structure L-DBTA·DMSO, (dashed line))

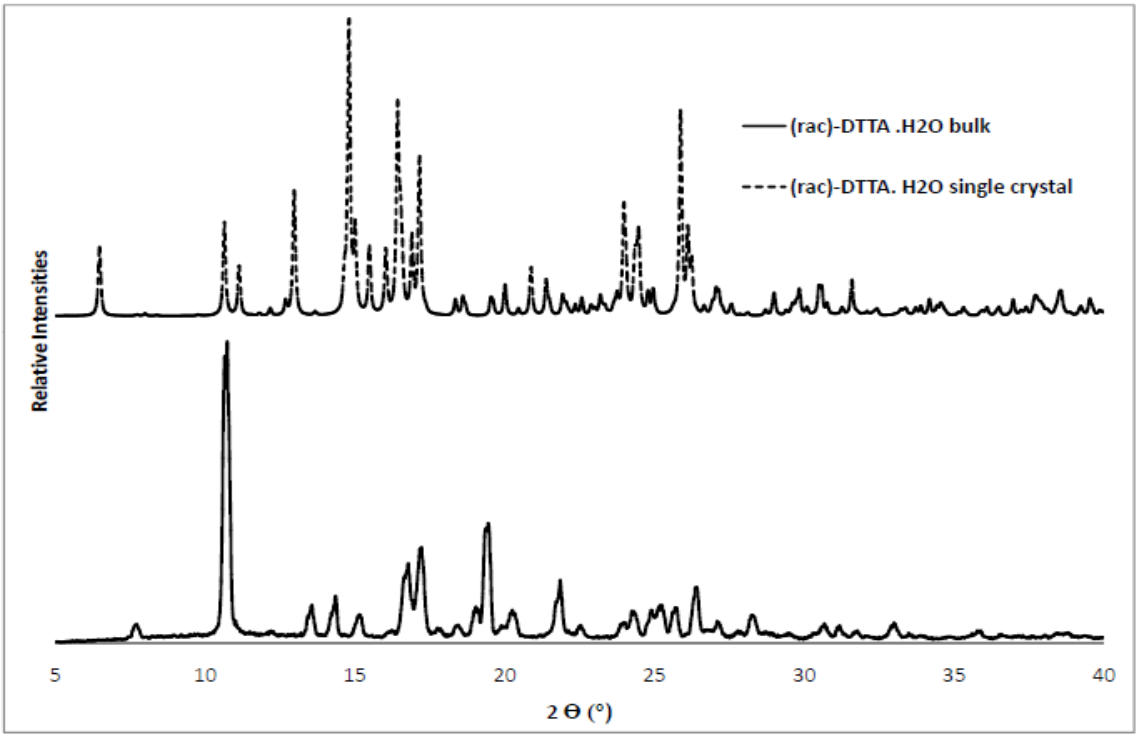

Figure A 23 PXRD patterns for the acid crystalline bulk material ((rac)-DTTA·H_2O, bulk-continuous line), and the single crystal structure (rac)-DTTA·H_2O, (dotted line))

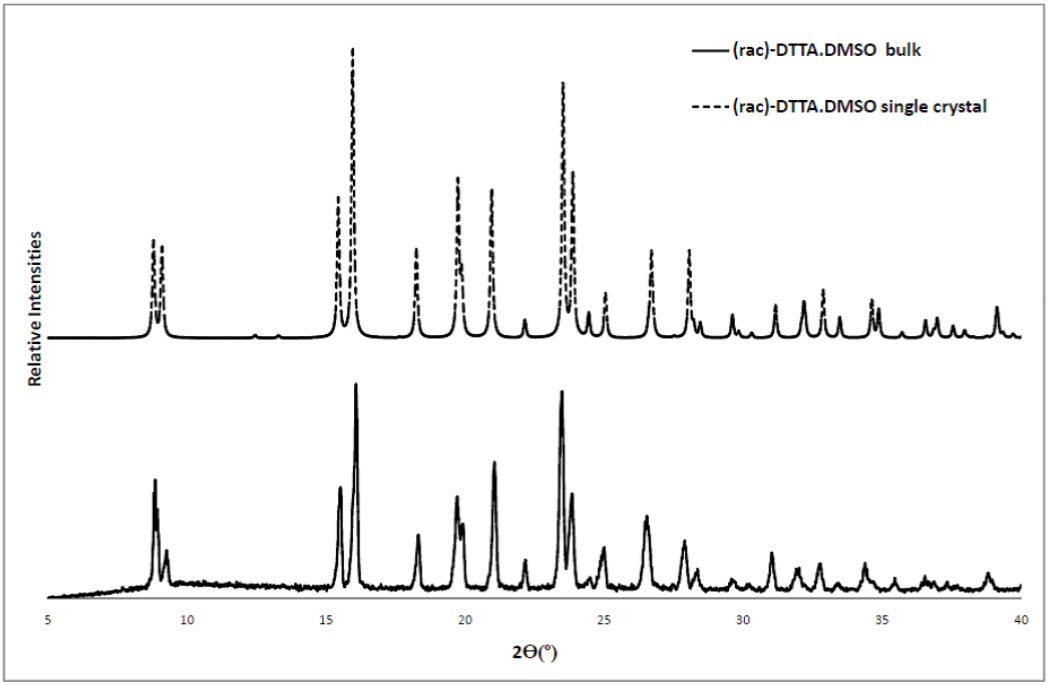

Figure A 24 PXRD patterns for the acid crystalline bulk material ((rac)-DTTA·DMSO, bulk-continuous line), and the single crystal structure (rac)-DTTA·DMSO dotted line)

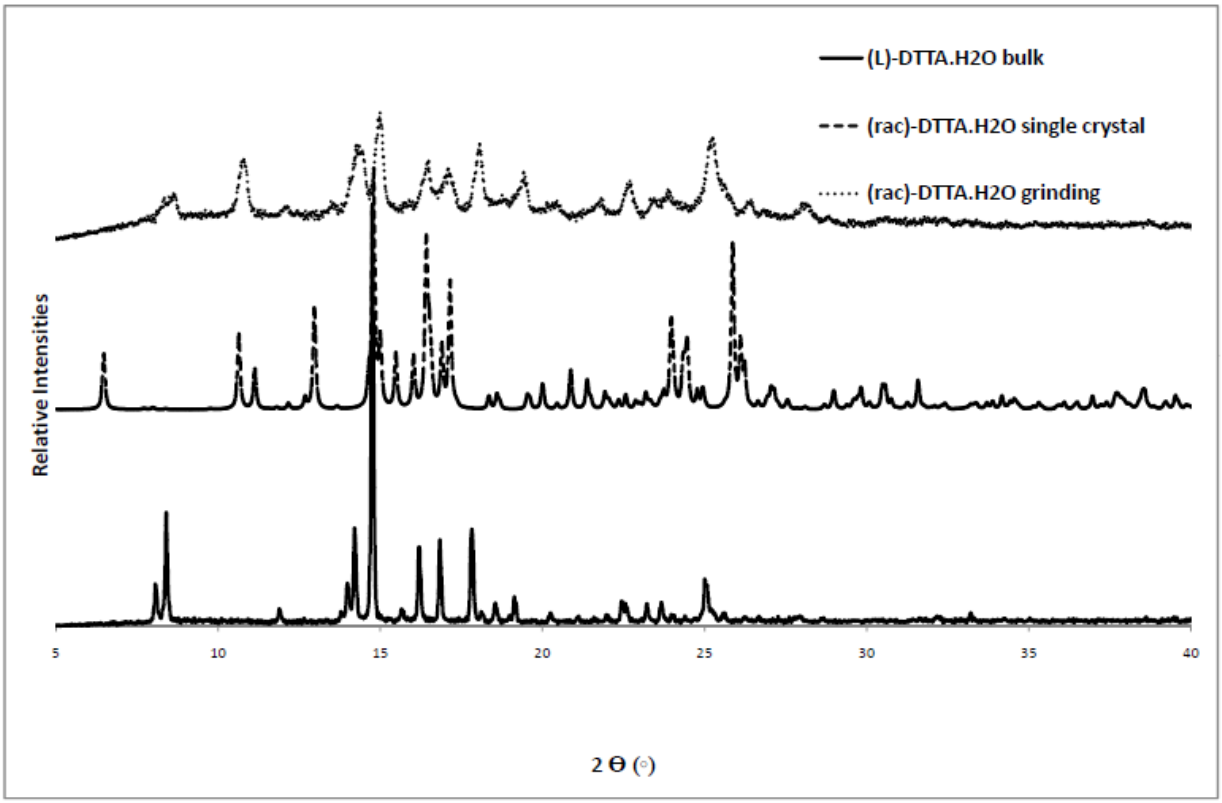

Figure A 25 PXRD patterns for the acid crystalline bulk material (L-DTTA.H_2O,bulk- continuous line), (rac)-DTTA·H_2O single crystal dashed line and ((rac)-DTTA ·H_2O, dotted line).

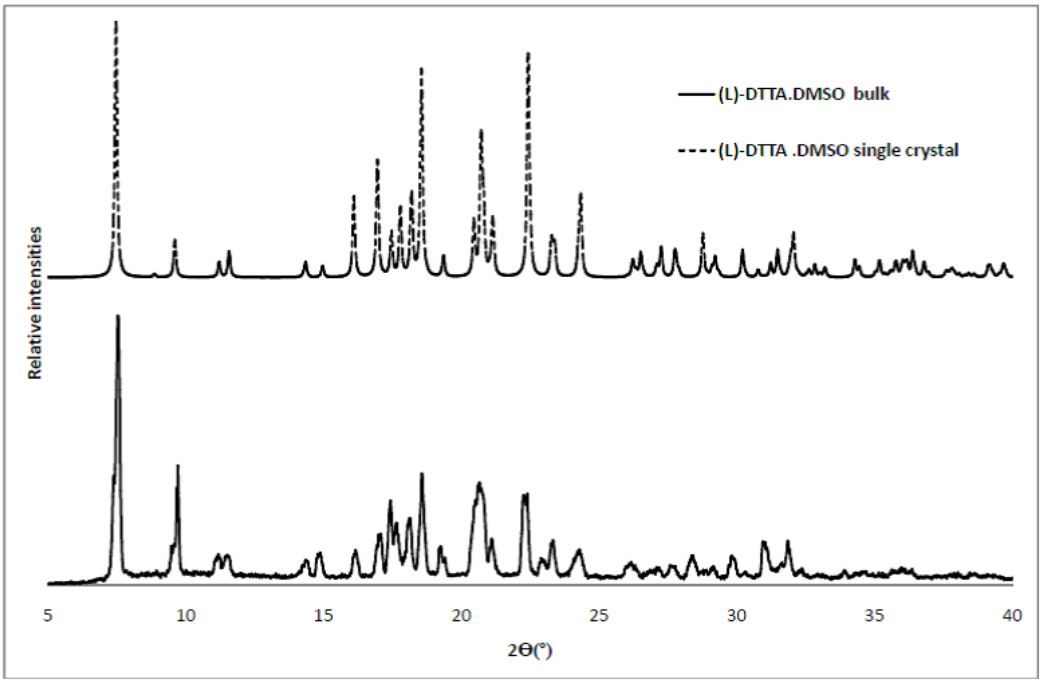

Figure A 26 PXRD patterns for the acid crystalline bulk material (L-DTTA· DMSO, bulk-continuous line), and the single crystal structure L-DTTA ·DMSO, dotted line)

1.2 Analytical results of diastereomeric salts

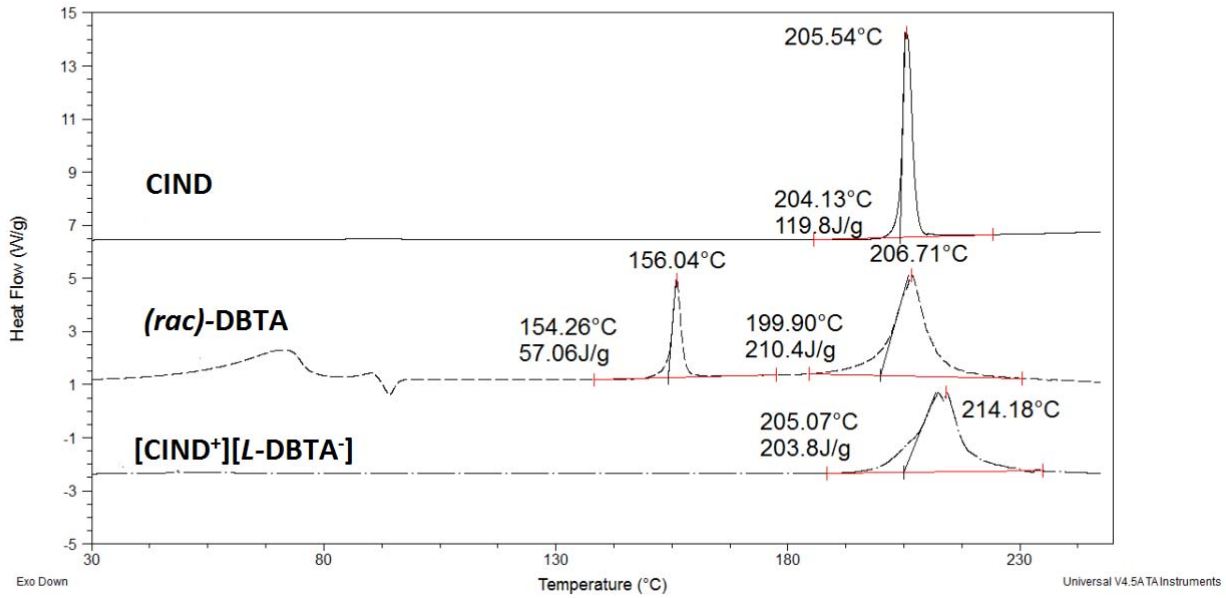

Figure A 27 DSC curve of CIND, (rac)-DBTA starting materials and [CIND$^+$][L-DBTA$^-$].

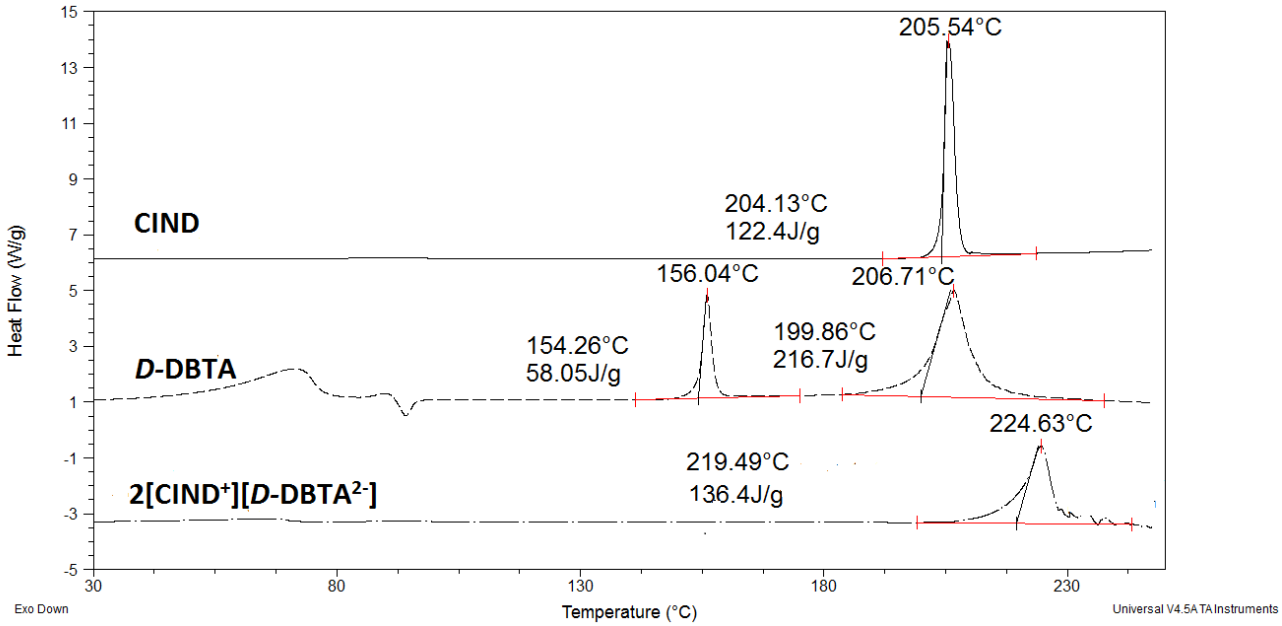

Figure A 28 DSC curve of CIND, D-DBTA starting materials and 2[CIND$^+$][D-DBTA^{2-}].

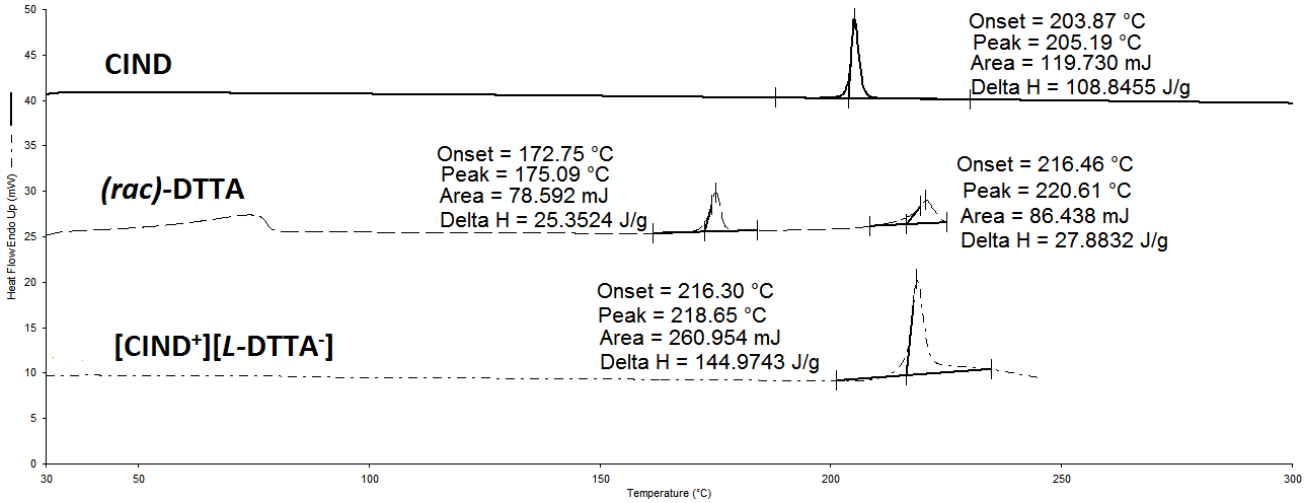

Figure A 29 DSC curve of CIND, (rac)-DTTA starting material and [CIND⁺][L-DTTA⁻].

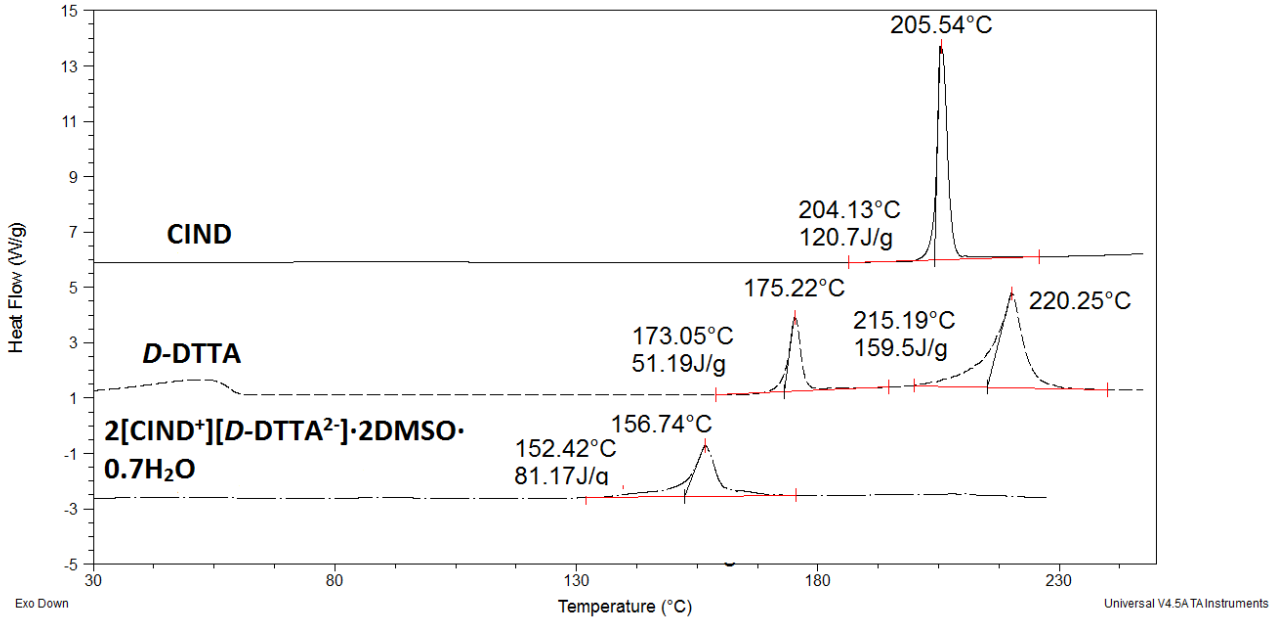

Figure A 30 DSC curve of CIND, D-DTTA starting materials and 2[CIND⁺][D-DTTA²⁻]·2DMSO·0.7H₂O.

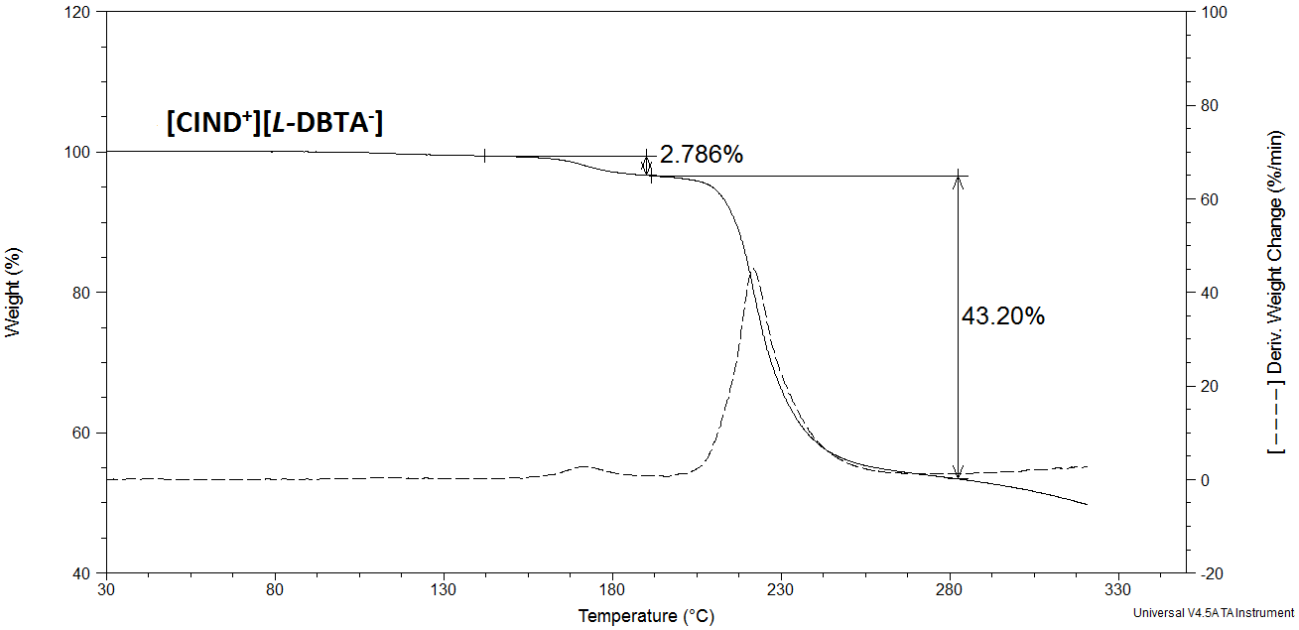

Figure A 31 TG curve of [CIND$^+$][L-DBTA$^-$].

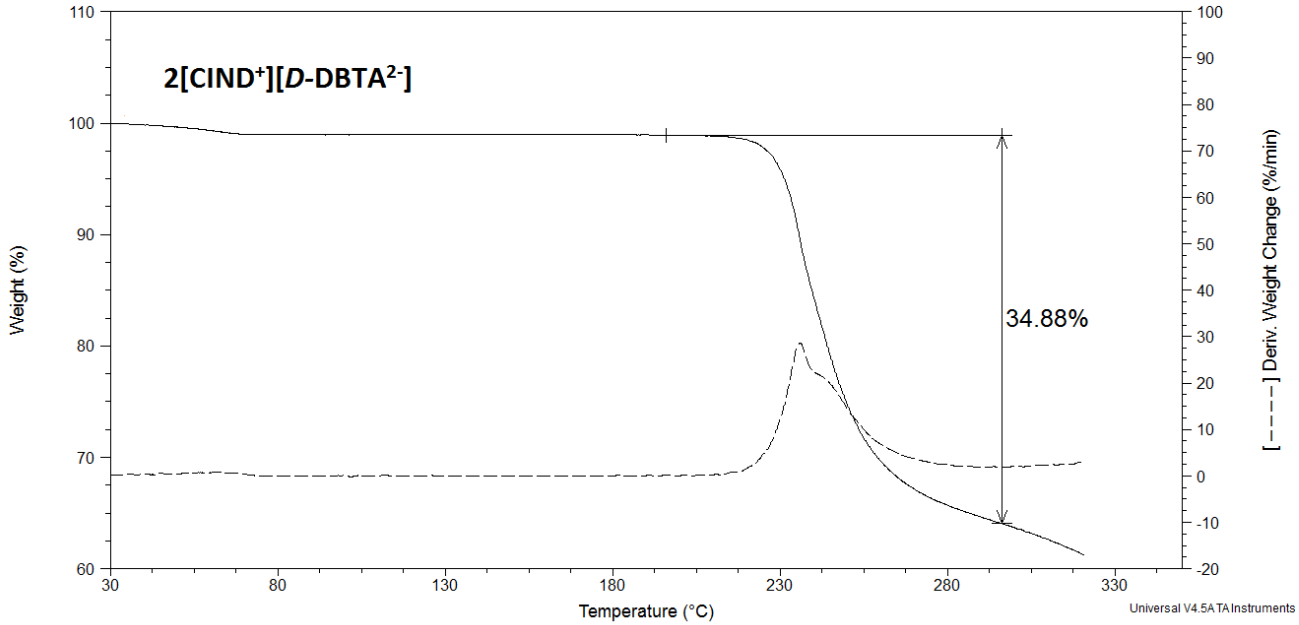

Figure A 32 TG curve of 2[CIND$^+$][D-DBTA^{2-}].

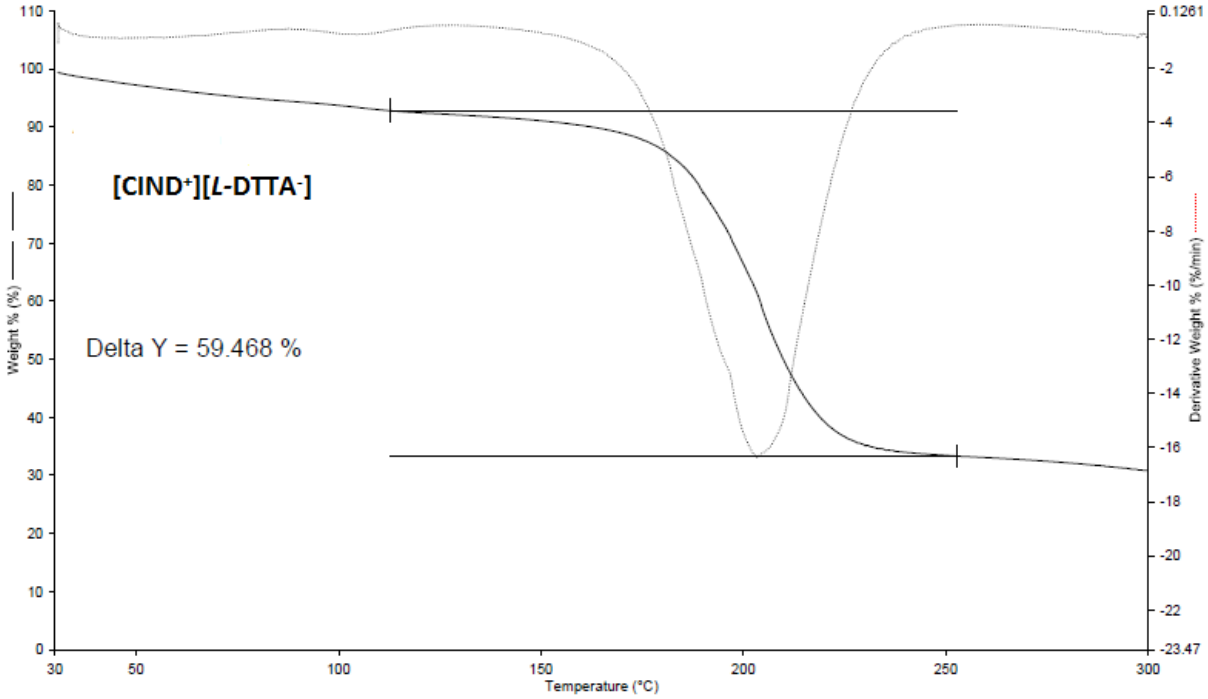

Figure A 33 TG curve of [CIND$^+$][L-DTTA$^-$].

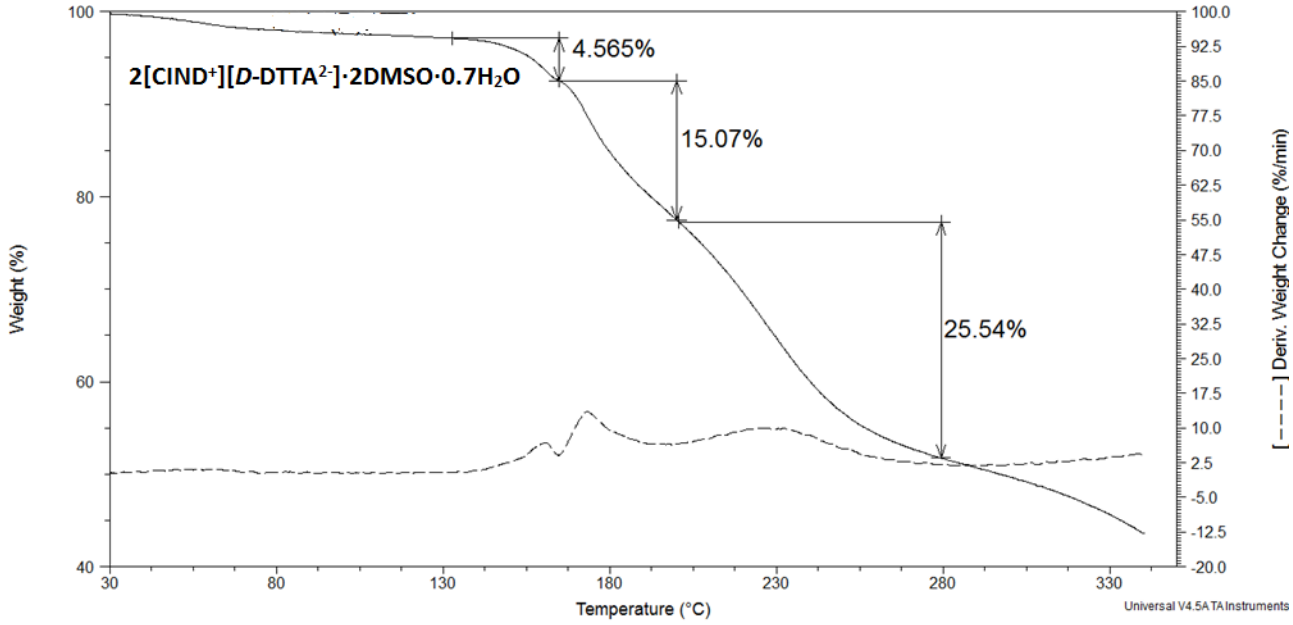

Figure A 34 TG curve of 2[CIND$^+$][D-DTTA^{2-}]·2DMSO·0.7H_2O.

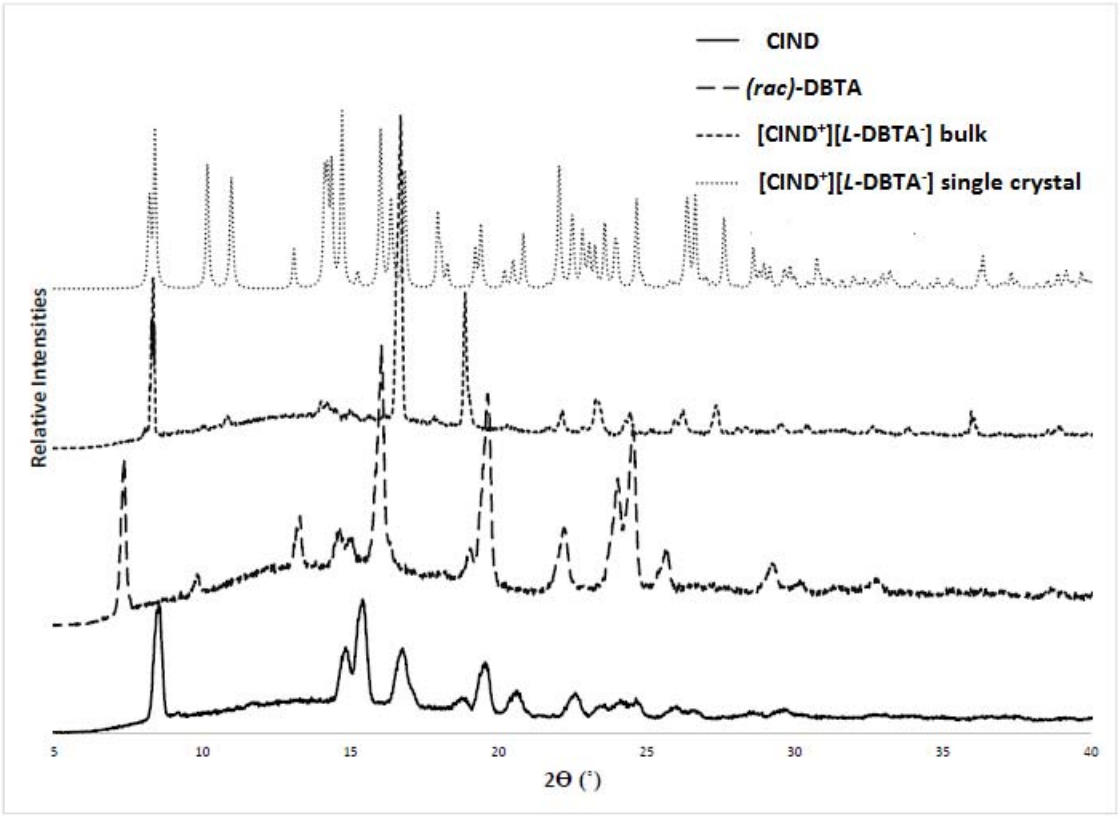

Figure A 35 PXRD patterns for the pure Cinchona alkaloid, the pure acid ((CIND , continuous line) (rac)-DBTA, dashed line, [CIND+][L-DBTA-] (bulk-ded line) and the generated single crystal [CIND+][L-DBTA-]. (fine dotted line)).

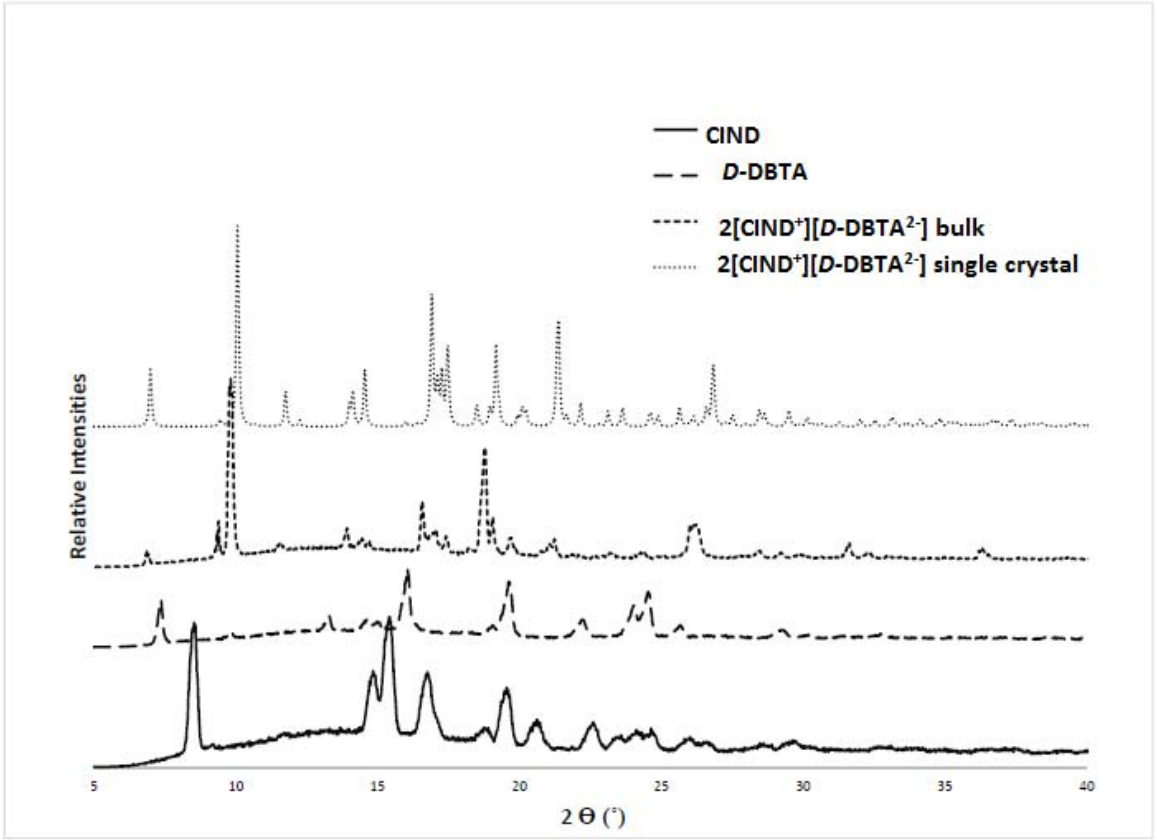

Figure A 36 PXRD patterns for the pure Cinchona alkaloid, the pure acid ((CIND , continuous line) D-DBTA, dashed line, 2[CIND$^+$][D-DBTA^{2-}] (bulk -dotted line) and the generated single crystal 2[CIND$^+$][D-DBTA^{2-}]. (fine dotted line)).

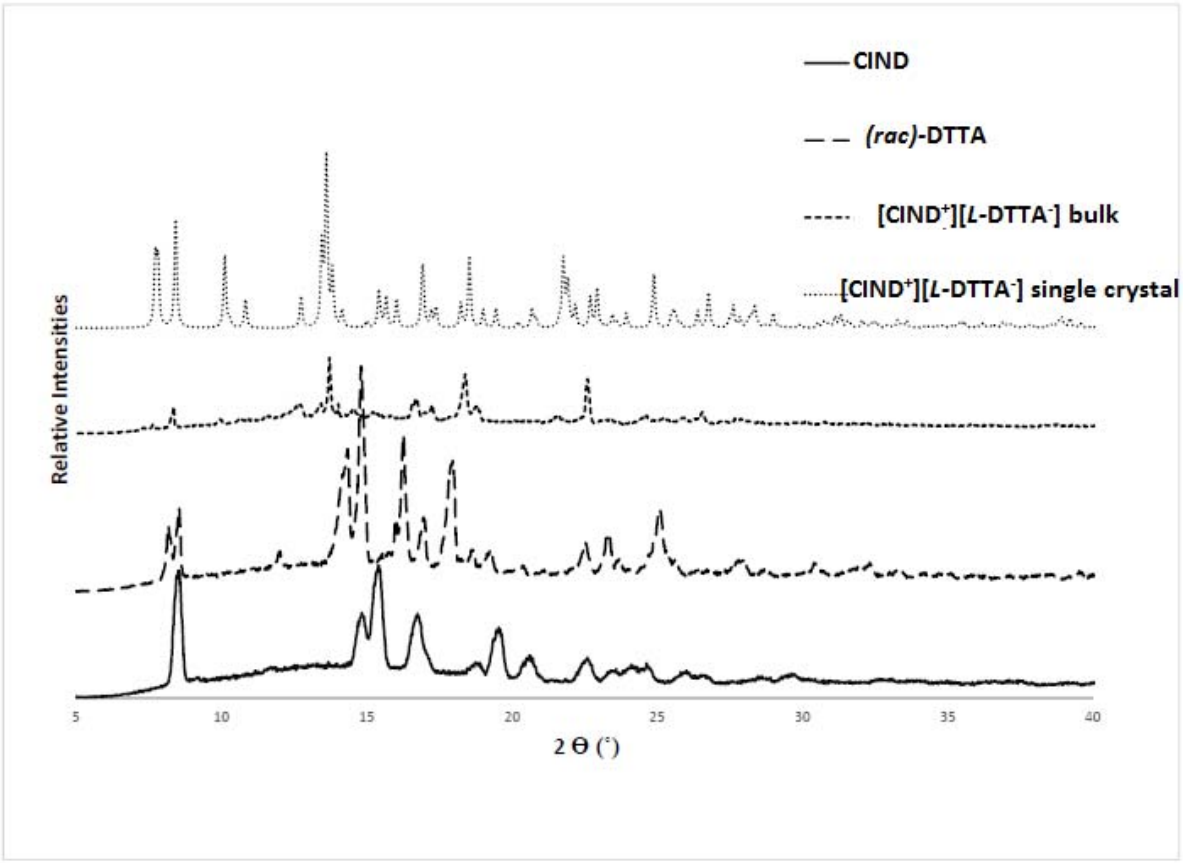

Figure A 37 PXRD patterns for the pure Cinchona alkaloid, the pure acid ((CIND ,continuous line) D-DTTA, dashed line, [CIND$^+$][L-DTTA$^-$] (bulk-dotted line) and the generated single crystal [CIND$^+$][L-DTTA$^-$] (fine dotted line)).

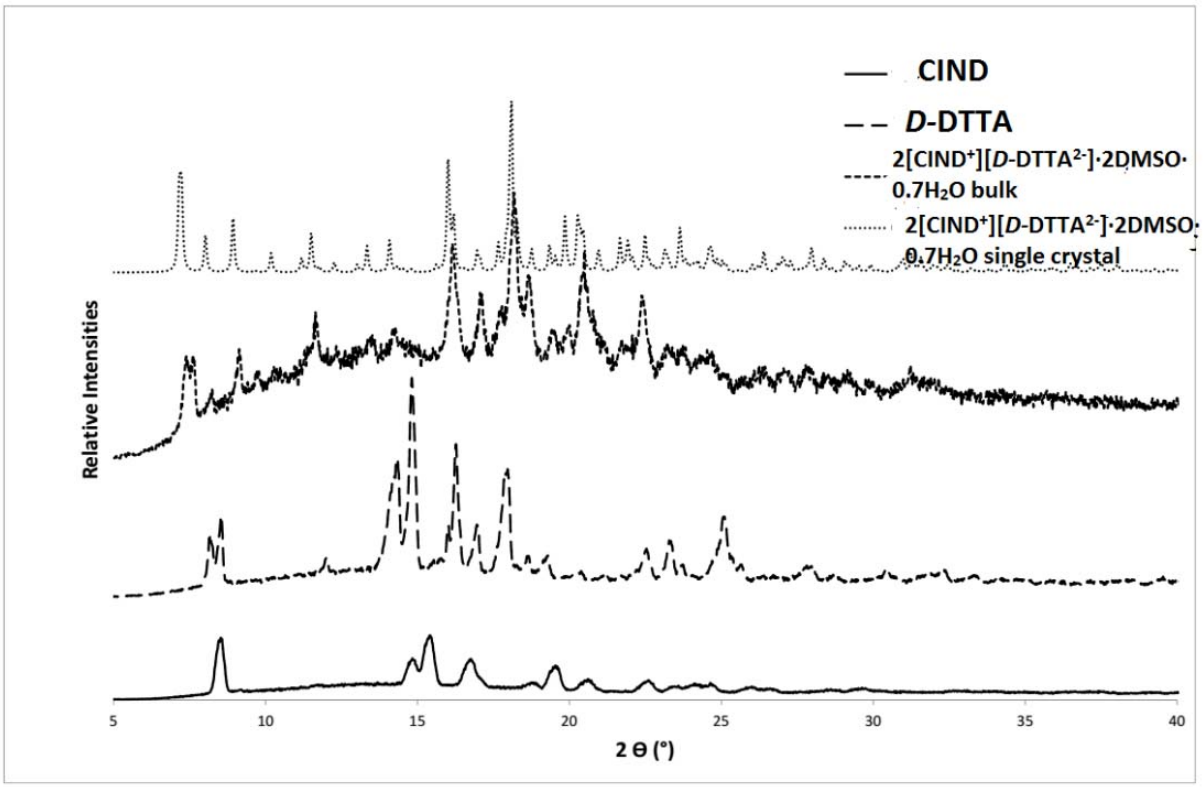

Figure A 38:PXRD patterns for the pure Cinchona alkaloid, the pure acid ((CIND ,continuous line) D-DTTA, dashed line, 2[CIND$^+$][D-DTTA^{2-}]·2DMSO·0.7H_2O (bulk-dotted line) and the generated single crystal 2[CIND$^+$][D-DTTA^{2-}]·2DMSO·0.7H_2O (fine dotted line))